informa
healthcare

Abstract Sessions I–VII

Friday, February 2, 2007
Oral Abstracts: Clinical-Session I

101. RAPID DETECTION OF MYOCARDIAL INFARCTION BY SUB-SECOND, FREE-BREATHING DELAYED CONTRAST-ENHANCEMENT CARDIOVASCULAR MAGNETIC RESONANCE

Burkhard Sievers, MD,[1] Michael Elliott, MD,[1] Lynne Hurwitz, MD,[2] Timothy Albert, MD,[1] Igor Klem, MD,[1] Wolfgang Rehwald, PhD,[1] Michele Parker, MS,[1] Robert Judd, PhD,[1] Raymond Kim, MD.[1] [1] *Duke Cardiovascular MRI Center, Duke University, Durham, NC, USA,* [2] *Department of Radiology, Duke University, Durham, NC, USA.*

Background: An ultrafast, delayed contrast-enhancement cardiovascular magnetic resonance (DE-CMR) technique that can acquire sub-second, 'snap-shot' images during free-breathing (SUB-SECOND) is becoming widely available. This technique provides myocardial infarction (MI) imaging with complete left-ventricular (LV) coverage in under 30 seconds. However, the accuracy of this technique is unknown.

Methods and Results: We prospectively compared SUB-SECOND imaging to routine breath-hold DE-CMR (STANDARD) in consecutive patients. Two cohorts with unambiguous standards-of-truth were prespecified: 1) patients with documented prior MI (n = 135); and 2) patients without MI and with low likelihood for coronary disease (lowest Framingham risk category, n = 103). Scans were scored masked to identity and clinical information. Sensitivity, specificity and accuracy of SUB-SECOND imaging for MI diagnosis was 87%, 96%, and 91%, respectively. Compared with STANDARD (98%, 100%, 99%), SUB-SECOND had modestly reduced sensitivity (p = 0.0001), but specificity was excellent (Fig. 1A). Missed infarcts were generally small or subendocardial (87%) (Fig. 1B). Overall, regional transmural extent of infarction (TEI) scores were highly concordant (2083/2294, 91%);however, 51 of 337 regions (15%) considered predominantly infarcted (>50% TEI) by STANDARD were considered viable (≤25% TEI) by SUB-SECOND. Quantitative analysis demonstrated moderately reduced contrast-to-noise ratios for SUB-SECOND imaging between infarct and remote myocardium (12.0 ± 7.2 versus 20.1 ± 6.6, $p < 0.0001$) and infarct and LV cavity (-2.5 ± 2.7 versus 3.6 ± 3.7, $p < 0.0001$).

Conclusions: Myocardial infarction can be rapidly detected by SUB-SECOND DE-CMR during free-breathing with high accuracy. This technique could be considered the preferred
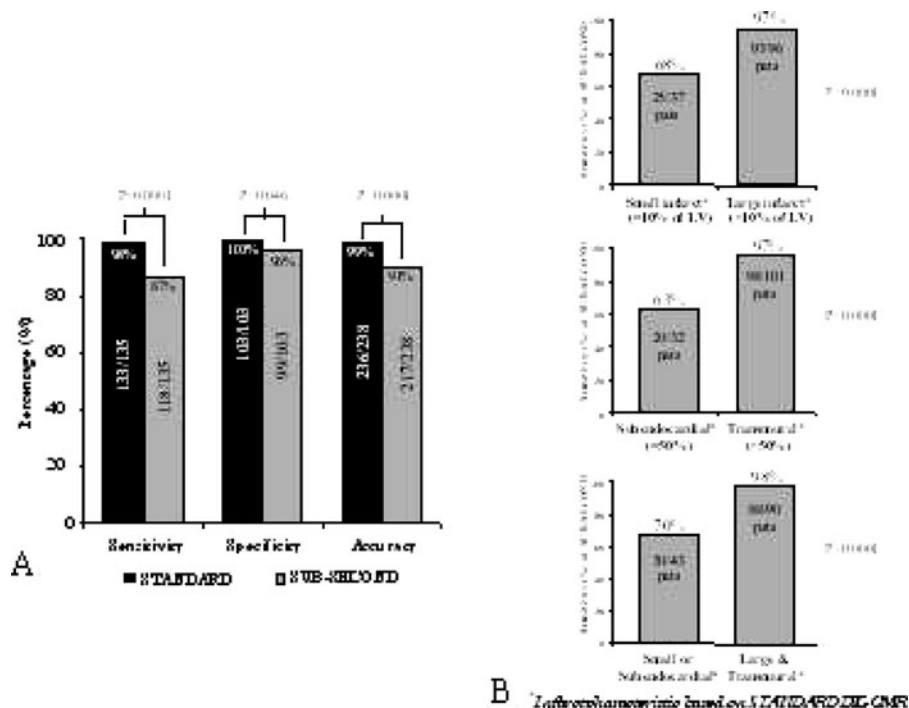

FIG. 1.

approach in patients more acutely ill or unable to breath-hold. However, compared with STANDARD imaging, sensitivity may be reduced and the transmural extent of infarction underestimated.

102.   EFFECTS OF RESPIRATORY MOTION AND CARDIAC ARRHYTHMIA ON THE DIAGNOSTIC ACCURACY OF MYOCARDIAL DELAYED CONTRAST-ENHANCED MAGNETIC RESONANCE IMAGING

Burkhard Sievers, MD, Wolfgang Rehwald, PhD, Timothy Albert, MD, Manesh Patel, MD, Michele Parker, MS, Raymond Kim, MD, Robert Judd, PhD. *Duke Cardiovascular MRI Center, Duke University, Durham, NC, USA.*

Purpose: To determine the optimal delayed contrast-enhanced magnetic resonance imaging (DE-MRI) technique for myocardial infarct detection when breath-holding is not possible and/or arrhythmia is present.
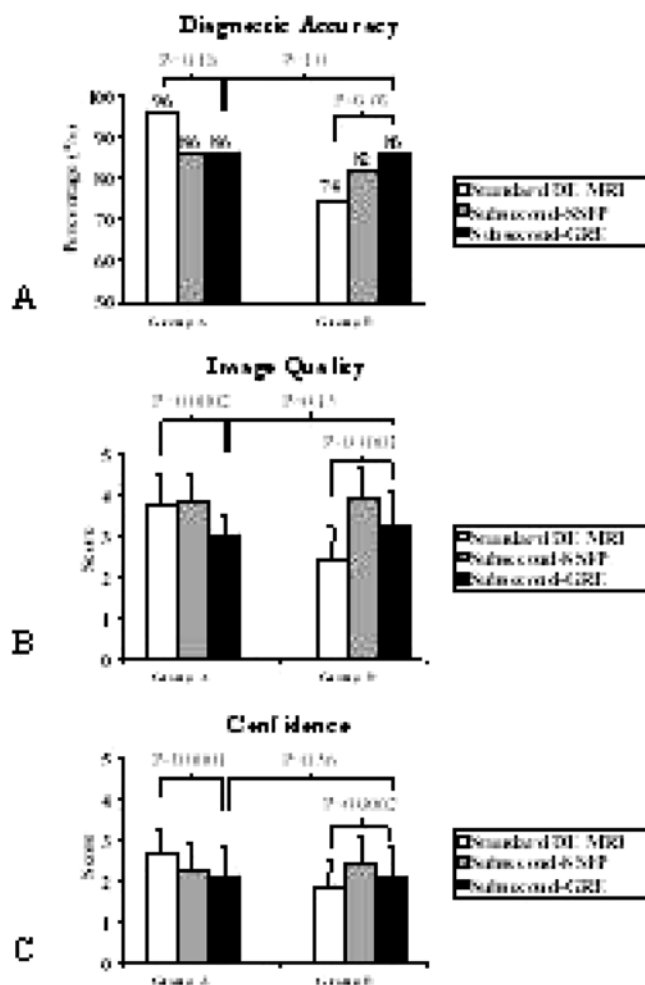

FIG. 1.

Materials and Methods: Images were acquired with Standard DE-MRI and two Subsecond techniques (Subsecond-SSFP and Subsecond-GRE) in the setting of myocardial infarction. All sequences were performed under two conditions: 1) Breath-holding and steady cardiac gating (Group A); and 2) non breath-holding and/or arrhythmia (Group B). For analysis, images were placed in random order and scored for presence or absence of infarction, image quality and confidence for infarct detection.

Results: The diagnostic accuracy, image quality, and confidence for Standard DE-MRI were 96%, 3.7 ± 0.8, and 2.7 ± 0.6 in group A but only 74%, 2.4 ± 0.8, and 1.8 ± 0.7 in group B ($p \leq 0.004$ for each), underscoring the need for a different imaging technique when breath-holding and steady cardiac gating are not possible. Under these non-ideal conditions (Group B), Subsecond-SSFP and Subsecond-GRE produced higher accuracy (82% and 86% versus 74%), image quality (3.9 ± 0.7 and 3.2 ± 0.8 versus 2.4 ± 0.8), and confidence (2.4 ± 0.7 and 2.1 ± 0.7 versus 1.8 ± 0.7) than Standard ($p \leq 0.0002$ for each) (Fig. 1). When breath-holding and steady cardiac gating were possible (Group A), however, Standard performed better than the Subsecond techniques.

Conclusions: Standard DE-MRI is the preferred technique for infarct detection during breath-holding and regular heart rhythm. When breath-holding and/or steady-gating is not possible, however, Subsecond techniques should be employed.

103.   DETECTION AND DISTRIBUTION PATTERN OF MYOCARDIAL INFARCTIONS AFTER HEART TRANSPLANTATION DETECTED BY CONTRAST ENHANCED MRI

Henning Steen, Sonja Refle, Constanze Merten, MD, Hugo A. Katus, MD, Evangelos Giannitsis, MD. *University Heidelberg, Heidelberg, Germany.*

Background: Transplant coronary artery disease (TCAD) is a prognostic factor of long-term survival after heart transplantation (HTX). From literature it is well established that X-ray angiography tends to underestimate the degree of TCAD and often underdiagnoses occluded small coronary arteries leading to myocardial infarctions (MI). Infarct-specific contrast enhanced MRI (CEMRI) is a sensitive non-invasive imaging technique to detect even small myocardial infarctions and fibrotic tissue.

Purpose: We hypothesized that CEMRI would detect chronic TCAD-related MI even in patients with Xray classified mild TCAD. Moreover, we present the distribution patterns of detected CEMRI areas in the AHA 17 Segment Model to further exclude annually recommended right ventricular (RV) biopsies as assignable cause for CEMRI areas.

TCAD	1 (20 pts.)	2 (11 pts.)	3 (4 pts.)	4 (6 pts.)
Myocardial Infarct Transmurality (%)	4	3	2	6
I (?50%)	0	0	1	2
II (50–75%)	1			1
III (75–100%)	3	3	1	3

Methods: CEMRI (Gadolinium: 0.2 mmol/kg bw) was performed in 41 HTX patients on a 1.5T Whole Body MRI scanner (Philips Medical Systems). On a workstation images were analysed blindly by two experienced observers. Areas of MI were classified as I = ≤50%, II = 50–75%, III = 75–100%. Segments adjacent to the RV were named a-e (Fig. 1). Selective coronary angiography was conducted by using standard Judkins technique. Results were reviewed qualitatively using the TCAD score (TCAD1 = no TCAD; 2 = wall irregularities; 3 = 50% stenosis; 4 ≥ 50% stenosis). Groups were compared using ANOVA. P values ≤ 0.05 were considered statitistically significant.

Results: TVP1-4 donor age (34.6/37.6/39.7/39.3 ys.) and time after HTX (5.7/6.5/8.8/11.6 ys.) were not significantly different. MI was prevalent in all four TCAD grades in cumulative percentage (I = 20%; II = 27%; III = 50%; IV = 100%, Table). Mean infarct size for groups I/II/III was $3.3 \pm 2.3/4.1 \pm 2.1/9.9 \pm 6.1$ ($p \leq 0.05$). The distribution pattern of CEMRI is shown in Fig. 1. Only 8 of 25 CEMRI were adjacent to the RV (Figure 1, a–e)
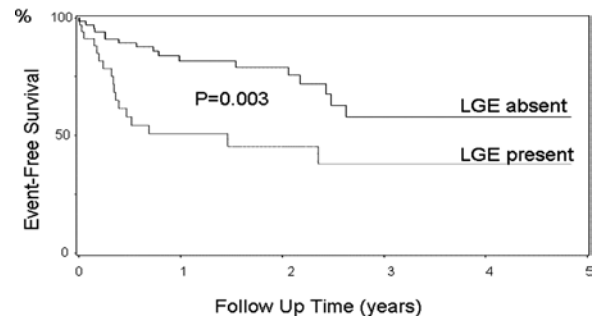
Conclusions: CEMRI is a novel and sensitive imaging technique to detect MI in TCAD. Unexpectedly, even in angiographically classified low grades of TCAD there is a prevalence of transmural MI which could have potential impact for future treatment and modified risk stratification for HTX patients. The potential confounder 'RV biopsy' for MI in TCAD pts. could not be responsible for 17 non-RV adjacent areas of CEMRI.

104. LATE GADOLINIUM ENHANCEMENT CMR IMAGING DETECTS SILENT MYOCARDIAL INFARCTION IN DIABETIC PATIENTS AND MAY IMPROVE THEIR RISK STRATIFICATION FOR MAJOR ADVERSE CARDIAC EVENTS

Hamid Sattar, MD, Vijay Gandla, MD, Sui Tsang, BSc, Raymond Y. Kwong, MD, MPH. *Brigham and Women's Hospital, Boston, MA, USA.*

Introduction: Silent myocardial infarctions (MI) are prevalent among diabetic patients and inflict significant morbidity and mortality. Late gadolinium enhancement (LGE) imaging by CMR can provide sensitive characterization of the myocardium but its prognostic significance in diabetic patients without prior history of infarction is unknown.

Kaplan Meier Survival Distribution of Diabetics Without History of MI:Stratified by Late Gadolinium Enhancement

Purpose: We tested the hypothesis that evidence of silent MI by LGE imaging portends to elevated hazards for major adverse cardiovascular events (MACE) in diabetic patients.

Methods: We performed clinically indicated CMR in 105 diabetic patients without known history of MI. Clinical indications included stress CMR for myocardial ischemia (n = 56, 53%) and assessment of left ventricular function (n = 49, 47%). Another 54 diabetic patients with a history of MI were selected as controls. CMR imaging performed on a 1.5T scanner included cine function with SSFP imaging and LGE imaging using a T1W inversion recovery fast-gradient echo technique (after cumulative gadolinium of 0.15 mmol/kg). In addition to assessing for the presence of LGE, we quantified left ventricular ejection fraction (LVEF), LV mass, and LV systolic and diastolic volumes. We collected clinical information regarding MACE, which included death, acute MI, new congestive heart failure or unstable angina, stroke, and significant ventricular arrhythmias. We performed Cox proportional hazards regression analyses to model the association of LGE with MACE, and assessed such association with respect to history of MI.

Results: The study cohort consists of 105 patients (65 M) at an average age of 61 ± 12 years. In this study cohort, 35 patients (33%) had abnormal LGE by CMR. At a median follow-up of 11 months (6 months to 4.6 years), 39 patients experienced MACE including 17 deaths, 1 acute MI, 10 new heart failure cases, 8 unstable angina, 2 strokes, and 1 ventricular arrhythmia. Presence of LGE portended to an elevated hazard for MACE (HR: 2.64, 95% CI 1.35–5.15, p = 0.004). Adjusted to LVEF, LV end-diastolic volume, and LV end-systolic volume, LGE maintained a strong association with MACE (adjusted HR: 2.56, 95% CI 1.11–5.89, p = 0.03). Including diabetic patients with known MI as control, the prognostic association of LGE with MACE remained strong independent of clinical status of prior MI (adjusted HR: 2.21, 95% CI 1.19–4.10, p = 0.01).

Conclusions: CMR can characterize evidence of MI in diabetics without a known history of MI. LGE by CMR is associated with MACE beyond markers of LV systolic function, and can potentially improve the risk stratification of diabetic patients.

105. ASSESSMENT OF RIGHT VENTRICULAR INVOLVEMENT IN PATIENTS WITH ACUTE MYOCARDIAL INFARCTION BY MAGNETIC RESONANCE IMAGING

Christoph Jensen. *Department of Cardiology, Elisabeth Hospital, Essen, Germany.*

Background: Right ventricular (RV) involvement in patients with left ventricular infarction affects complications during hospitalization and influences mortality post infarction. It can be identified on the basis clinical findings such as ST-segment-elevation in the right precordial leads on early ECG and by RV dysfunction on transthoracic echocardiography. Echocardiography of the right ventricle, however, is technically challenging. On the other hand, CMR is suitable for cine imaging of the RV and for detection of minor myocardial infarcts by means of delayed enhancement imaging.

Objectives: Aim of this study was to investigate the prevalence of right ventricular involvement in patients with acute myocardial infarction using delayed enhancement CMR.

Methods: Fifty consecutive patients (43 males; mean age, 58.3 ± 11.2 years) with first acute ST-segment elevating myocardial infarction underwent cardiac MRI within 5 days after symptom onset using a 1.5 Tesla MR System (Magnetom Sonata, Siemens Medical Solutions, Erlangen, Germany). The imaging protocol included SSFP cine sequences (TrueFISP, TR 3 ms, TE 1.5 ms, FA 60°) in contiguous short-axis views covering the entire left ventricle. During 3 minutes after injection of 0.2 mmol/kg of gadodiamide (Omniscan, GE Healthcare Buchler, Munich, Germany), an inversion-recovery single-shot steady-state free precession (IR-SSFP) sequence (TR 2.4 ms, TE 1.1 ms, FA 50°) rapidly covering the complete left ventricle in a single breath-hold was performed for detection of myocardial no reflow areas. Delayed enhancement imaging was performed in corresponding slices using a segmented 2D inversion-recovery fast low angle shot (IR-FLASH) sequence (TR 8 ms, TE 4 ms, FA 25°). TI was adjusted manually between 200 and 260 ms. All images were analyzed by two blinded observers (radiologist/cardiologist) in consensus using the AHA/ACC recommended 17-segment model. No-reflow volumes (NRV) were calculated from the IR-SSFP images taken within the first few minutes following gadodiamide infusion. Total delayed enhancement volumes (DEV) were calculated from manual planimetry of the IR-FLASH images taken 5 minutes or later after contrast administration by summation of discs. The RV was divided into 9 segments (basal anterior, basal lateral, basal inferior, midventricular anterior, midventricular lateral, midventricular inferior, apical anterior, apical lateral, apical inferior), and the presence of delayed enhancement was evaluated for each segment. ECG with right precordial leads were routinely performed in patients with acute inferior myocardial infraction. Transthoracic echocardiography was performed in all patients.

Results: Among these 50 patients, 30 patients (60%) had inferior wall myocardial infarction and 20 patients (40%), had anterior wall myocardial infarction. Transthoracic echocardiography showed no hints of right ventricular involvement. In the subgroup of inferior left ventricular myocardial infarction, ECG with right precordial leads indicated RV involvement in 3/30 patients (10%). In MRI, 15/30 patients (50%) showed RV involvement. In the subgroup of anterior left ventricular myocardial infarction, 12/20 patients (60%) showed RV involvement. Patients with RV inferior infarction and regional wall motion abnormalities showed increased mean RV enddiastolic volume 157 ± 45 mL in comparison to patients without RV involvement with an RV enddiastolic volume of 150 ± 41.3 mL.

Conclusion: Our study group showed a higher incidence of RV involvement in patients with anterior left ventricular infarction then known from literature. In patients with acute inferior myocardial infarction, ECG with right precordial leads showed RV involvement in 10%, whereas delayed enhancement MRI detected RV involvement in 60%. So, delayed enhancement MRI is more sensitive in detecting RV involvement in acute myocardial infarction than ECG.

106. RISK STRATIFICATION AFTER REPERFUSED ACUTE MYOCARDIAL INFARCTION USING CONTRAST-ENHANCED CARDIOVASCULAR MAGNETIC RESONANCE: COMPARISON OF FIRST-PASS AND DELAYED ENHANCEMENT IMAGING

Matthias Regenfus,[1] Carolin Stingl,[1] Christian Schlundt,[1] Johannes von Erffa,[1] Michaela Schmidt,[2] Werner Adler,[1] Werner Daniel.[1] *[1] FAU Erlangen-Nürnberg, Erlangen, Germany, [2] Siemens Medical Solutions, Erlangen, Germany.*

The established parameter for risk stratification after reperfused acute myocardial infarction (MI) is left ventricular (LV) ejection fraction (EF). With the use of contrast-enhanced cardiovascular magnetic resonance (CMR) further parameters for characterization of MI can be determined and related to the occurence of major adverse cardiac events (MACE).

Methods: One hundred forty-twopatients (pts) with left ventricular (LV) dysfunction (EF $39 \pm 8\%$) were examined on a 1.5T scanner within 3 ± 2 (2–6) days of an reperfused acute MI. Cine, first-pass (FP) perfusion and delayed enhancement (DE) CMR was acquired and scored for regional wall thickening and DE using a 17-segment model. Additionally, LV EF, infarct size (from DE imaging) and the extent of microvascular obstruction (MO) (from FP imaging) were quantified. Serial clinical follow-up was obtained in all patients (mean follow-up 3.7 ± 1.8 years) regarding occurrence of MACE. Patient-related and CMR data were analyzed by Cox proportional hazard regression.

Results: Among the 142 patients, there were 18 cardiac deaths and reinfarctions in the follow-up period. Additionally, there were 48 patients with further myocardial revascularization or

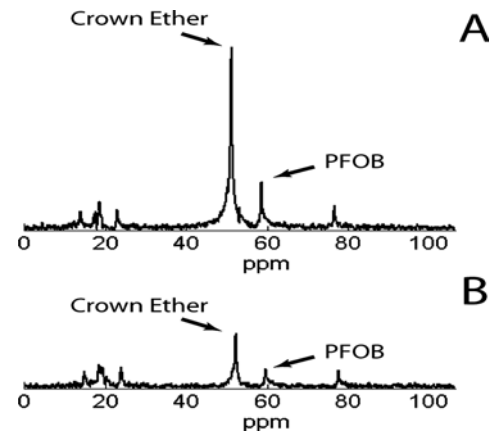|	Hazard ratio	Low. limit 95% CI	Up. limit 95% CI	P
EF	3.2	1.5	5.0	<0.0001
Extent of MO	3.7	1.6	5.1	<0.0001
Infarct size	1.9	0.9	3.3	0.02

FIG. 1. Sample spectra of valves (A) pretreated with targeted oil particles invisible to spectroscopy; (B) treated with targeted particles only. Significantly lower signal in the pretreated valve demonstrates competitive inhibition of binding.

hospitalization due to unstable angina or congestive heart failure. Patients with events at follow-up showed significantly lower EF ($32 \pm 10\%$ vs. $46 \pm 10\%$, $p = 0.001$), and larger extent of MO ($18 \pm 9\%$ vs. $5 \pm 4\%$, $p < 0.001$) than patients without events. By univariate analysis, EF, extent of MO, and, infarct size by CMR were related to occurence of MACE (Table 1). By multivariable analysis, extent of MO remained the strongest predictor after adjustement for LV EF.

Conclusions: In patients after reperfused acute MI, contrast-enhanced CMR can be used to predict major adverse cardiac events. Next to the established parameter for risk stratification- ejection fraction -, the extent of MO determined from FP imaging prooved highly predictive.

Friday, February 2, 2007
Oral Abstracts: Basic-Session II

107. DETECTION OF INFLAMMATORY COMPONENTS OF INCIPIENT AORTIC VALVE DISEASE IN THE CHOLESTERO-FED RABBIT WITH 19F MAGNETIC RESONANCE SPECTROSCOPY OF AVB3-INTEGRIN TARGETED PERFLUOROCARBON NANOPARTICLES

Emily A. Waters, Junjie Chen, Gregory M. Lanza, Samuel A. Wickline. *Washington University in St. Louis, St. Louis, MO, USA.*

Introduction: Cholesterol-fed rabbits are a well characterized model of atherosclerosis; they also develop plaques on the aortic valve leaflets, resulting in a disease state similar to human aortic valve sclerosis, the precursor to calcific aortic stenosis. An inflammatory angiogenic component is a precursor to both aortic and valvular lesions, and upregulation of $\alpha_V \beta_3$ integrins is associated with early angiogenic vessels (but not mature vasculature). Magnetic resonance spectroscopy of targeted perfluorocarbon-core nanoparticles can be used to detect and quantify the presence of angiogenesis on valve leaflets. In this study, we used $\alpha_v \beta_3$ integrin-targeted fluorinated nanoparticles to bind to aortic valve angiogenesis in cholesterol-fed rabbits, and then performed *ex vivo* fluorine spectroscopy of valve leaflets at 11.7 Tesla. We obtained a unique signature of inflammatory components of early valve disease and were able to confirm specific binding of targeted nanoparticles to pathological angiogenesis.

Methods: Twelve New Zealand White rabbits were maintained on a 0.25% cholesterol diet for 5 months. In one study group, four rabbits were treated intravenously with 2.2 mL/kg of $\alpha_v \beta_3$ integrin-targeted perfluorocarbon nanoparticles containing 15-crown-5 ether. Four controls were treated with untargeted nanoparticles. In these rabbits, nanoparticles were allowed to circulate and bind for two hours. A competition study was performed in a second group. Two rabbits were treated with 2.2 mL/kg of $\alpha_v \beta_3$-targeted nanoparticles containing safflower oil instead of perfluorocarbon, rendering these particles invisible to fluorine spectroscopy. Two hours later, they received a second treatment of 2.2 mL/kg of $\alpha_v \beta_3$-targeted crown ether nanoparticles. Two controls received 2.2 mL/kg of $\alpha_v \beta_3$-targeted
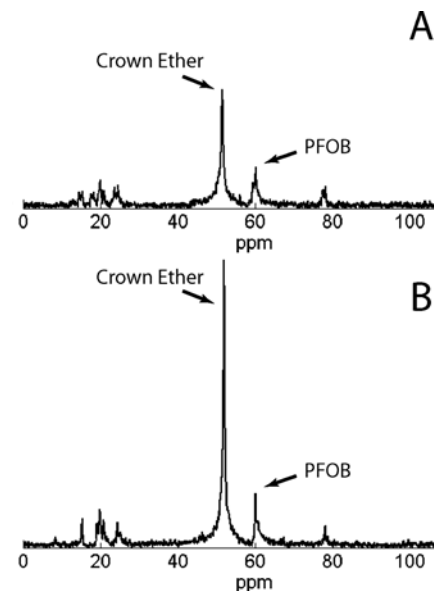

FIG. 2. Sample spectra of valves treated with (A) targeted and (B) nontargeted particles, showing ~3x greater signal in the valve treated with targeted particles, confirming specific binding.

crown ether nanoparticles, which were allowed to circulate for two hours.

At the end of the circulation time, rabbits were euthanized and aortic valve leaflets excised and preserved in formalin. *Ex vivo* ^{19}F spectroscopy was performed using an 11.7T Varian magnet and a custom-built 4-turn solenoid coil. A reference standard of a known quantity of nanoparticles containing perfluoro-octyl-bromide (PFOB) was included to allow quantitative comparison of spectra between animals. Spectra were acquired using a spin echo pulse sequence with 512 signal averages. Quantitative comparison of spectra was achieved by computing the ratio between the crown ether peak and the PFOB peak located 8 ppm away. These ratios were then normalized to the average value for control animals.
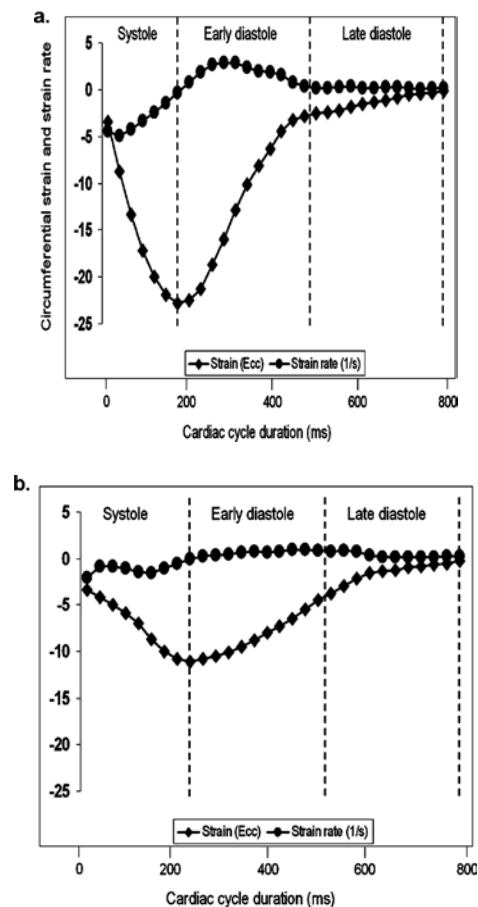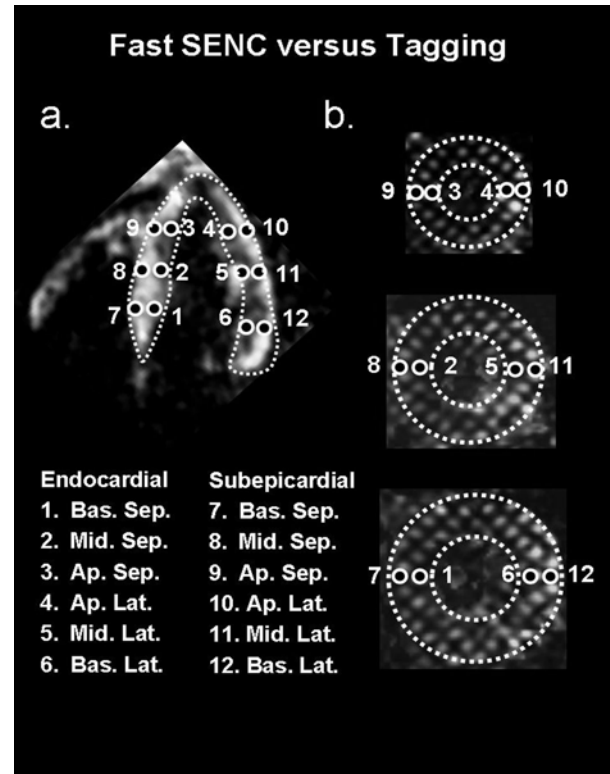
Results: The spin echo pulse sequence enabled detection of the single crown ether fluorine peak with excellent signal-to-noise ratio (7.3 ± 0.8). Aortic valves of rabbits receiving targeted particles exhibited an average $190\% \pm 60\%$ ($p < 0.05$) increase in CE signal compared to those of rabbits receiving untargeted particles (Fig. 1). In the competition study, the aortic valves of rabbits pretreated with targeted, but undetectable particles, manifested a significant decrease ($30\% \pm 4\%$; $p < 0.05$) in the CE signal compared to the valves of rabbits receiving only targeted particles (Fig. 2). These results confirm specific binding of nanoparticles to $\alpha_v\beta_3$ integrin in angiogenic vasculature.
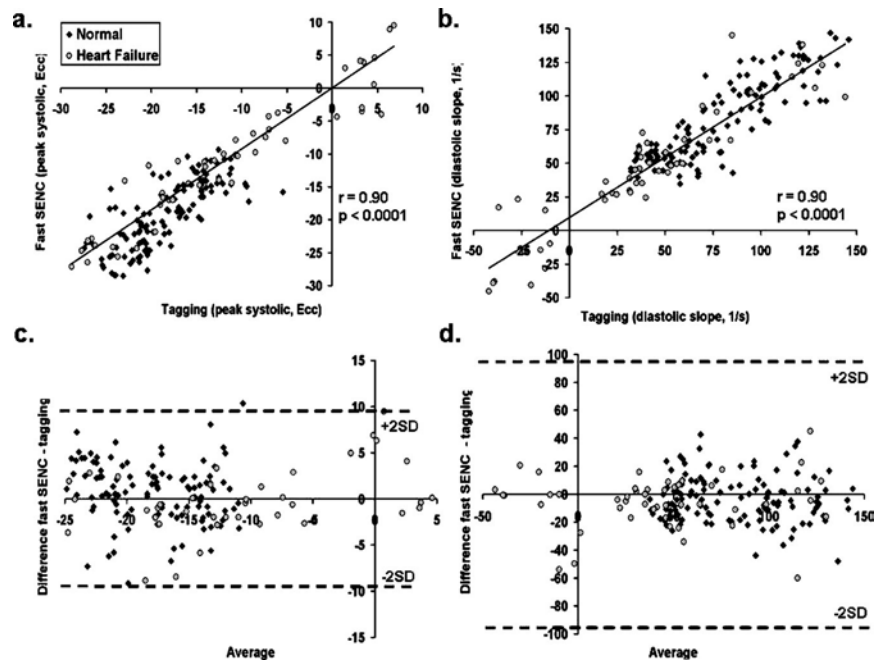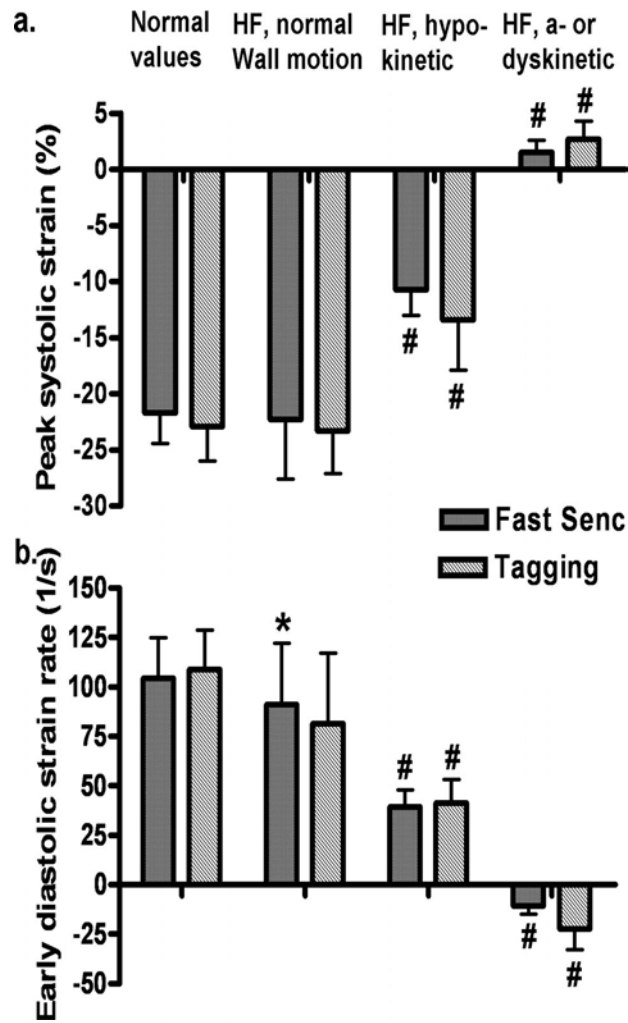
Discussion: MRS of targeted perfluorocarbon-core nanoparticles offers a specific and quantifiable method for detecting angiogenesis in an animal model of early aortic valve disease. Because fluorine is not naturally present in living tissue, targeted perfluorocarbon nanoparticles appear useful for molecular detection of inflammatory components of developing disease. They offer the potential of definitive detection due to the unique ^{19}F signature, which might facilitate early identification and medical therapy of valve disease, possibly forestalling clinical sequelae.

108. REAL TIME FAST STRAIN-ENCODED MAGNETIC RESONANCE IMAGING TO EVALUATE REGIONAL LEFT VENTRICULAR FUNCTION. COMPARISON TO CONVENTIONAL TAGGING

Grigorios Korosoglou, MD, Amr A. Youssef, MD, Albert C. Lardo, PhD, Shenghan Lai, PhD, Matthias Stuber, PhD, Nael F. Osman, PhD. *Johns Hopkins University Medical School, Baltimore, MD, USA.*

Introduction: Tagged magnetic resonance imaging (MRI) of the heart provides direct measures of regional myocardial function (1). However, tagging requires long series of breath holds so that real-time imaging techniques, as fast Strain-Encoded Magnetic Resonance Imaging (fast SENC). Recently, fast Strain-Encoded Magnetic Resonance Imaging (fast SENC) has been proposed for the evaluation of regional myocardial function in real-time

Fast SENC versus Tagging

Endocardial
1. Bas. Sep.
2. Mid. Sep.
3. Ap. Sep.
4. Ap. Lat.
5. Mid. Lat.
6. Bas. Lat.

Subepicardial
7. Bas. Sep.
8. Mid. Sep.
9. Ap. Sep.
10. Ap. Lat.
11. Mid. Lat.
12. Bas. Lat.

(2). This novel method allows the acquisition of regional function during a single heart beat and may therefore provide a valuable alternative in patients who cannot perform prolonged breath holds. Similarly to myocardial tagging, the measurement of myocardial strain using fast SENC occurs during the whole heart cycle providing valuable information on both regional systolic and diastolic function.

Purpose: To investigate the feasibility of fast SENC for quantification of regional myocardial function.

Methods: Healthy volunteers (n = 12) and patients with heart failure (n = 4) were examined using tagged MRI and fast SENC at 3.0 Tesla. Circumferential strain was measured using fast SENC in 6 endo- and 6 subepicardial points in the basal-, mid- and apical-septal and lateral wall from the 4-chamber view. These measurements were plotted to conventional tagging, using corresponding anatomical points in basal-, mid- and apical-short axis images as shown in Fig. 1. For each segment the temporal course of regional strain was registered throughout the whole cardiac cycle as demonstrated in Fig. 2. From every strain curve, the peak systolic strain (Ecc) and the mean strain rate over the duration from peak systole to 50% of the (early diastolic strain rate, Ecc/s) were calculated (3). Less negative Ecc values and less positive Ecc/s indicate diminished regional LV function as it can be appreciated in a dysfunctional hypokinetic segment of a patient with heart failure compared (Fig. 2b) compared with a segment with normal wall motion in a healthy volunteer (Fig. 2a).

Results: Both tagging and fast SENC detected significantly higher Ecc values for systolic strain and significantly lower values for diastolic strain rate between normal and dysfunctional segments ($^{#}p < 0.001$, Fig. 3). In contrast to conventional tagging fast SENC was also able to detect significantly diminished diastolic function within segments with normal wall motion in patients with heart failure ($^{*}p < 0.05$, Fig. 3). Peak systolic strain and early diastolic strain rate acquired by fast SENC correlated closely to strain measurements using tagged MRI (r = 0.9 for both systolic and early diastolic strain rate, p < 0.001 for both, Fig. 4a–b). Good agreement could be demonstrated between the 2 techniques by Bland-Altman plots (Fig. 4 c–d). Furthermore, both fast SENC and tagging allowed the accurate and reproducible assessment of regional systolic and diastolic LV-function showing low intraobserver variability (4.1% for fast SENC and 6.7% for tagging). Analysis of tagged MRI proved to be more time consuming than the analysis of fast SENC images (time spent of 3.8 ± 0.7 minute versus 9.5 ± 0.7 minute per patient, p < 0.001).

Conclusions: Fast SENC allows the rapid and reproducible quantification of regional systolic and diastolic LV-function. This real time imaging modality of the heart could offer significant advantages for the rapid and quantitative evaluation of regional myocardial function in patients unable to perform prolonged breath holds and during stress testing. Thus, multi center studies are now necessary to validate the feasibility of this attractive technique in more selected populations.

REFERENCES

1. Fischer SE, et al. MRM 1993;30:191–200.
2. Pan L, et al. MRM. 2006;55:386–95.
3. Ennis DB, et al. MRM. 2003;50:638–42.

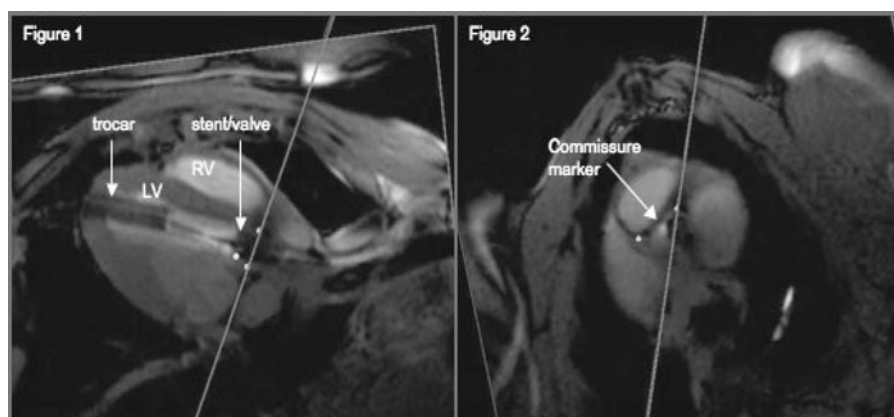## 109.   REAL-TIME, INTERACTIVE MRI FOR GUIDING MINIMALLY INVASIVE AORTIC VALVE REPLACEMENT

Michael A. Guttman, MS, Dumitru Mazilu, PhD, Ming Li, PhD, Tim Hunt, Shawn Kozlov, Robert J. Lederman, MD, Keith A. Horvath, MD, Elliot R. McVeigh, PhD. *National Institutes of Health, Bethesda, MD, USA.*

Introduction: Minimally invasive approaches to cardiac surgical therapies are under active investigation to reduce trauma and recovery time. Therapies traditionally requiring open-chest access are now being carried out through small incisions, using fiber optics for visual guidance. However, current methods still require emptying the heart of blood to allow unobstructed visualization, and the heart is arrested to operate on a stationary target. Real-time magnetic resonance imaging (rtMRI) provides views of anatomy and invasive devices in a natively beating heart with circulating blood, and can be used to guide the procedure and monitor the results.

Purpose: To perform feasibility experiments using interactive rtMRI with active (signal receiving) guide wires for aortic valve implantation using minimally invasive surgical approach.

Methods: Experimental aortic valve implantation was performed on swine in a short bore 1.5T scanner (Espree, Siemens Medical Solutions). SSFP imaging parameters were: 108×192 matrix, TR/TE = 3.84/1.92 ms, 1000 Hz/pixel bandwidth, 45 degree RF pulse, even/odd echo view sharing. A custom designed platform was used for real-time multiple slice imaging with a variety of features designed for interventional procedures. A conventional bioprosthetic valve was sewn to a platinum stent and compressed onto a balloon catheter. An active guide wire was temporarily affixed to the outside of the stent, along one of the valve commissures.

The minimally invasive surgical procedure involved making a 6 cm subxiphoid incision to expose the apex of the heart, through which a trocar was inserted into the left ventricle. An active guide wire was used to cross the native valve. Three oblique imaging slices were prescribed: 1) Axial view of the aortic valve; 2) Long axis image containing the LAD ostium, aortic valve and trocar; 3) Long axis image containing the RCA ostium, aortic valve and trocar. The axial image was interactively translated above the valve to show the ostia of the LAD and RCA, which were then marked for reference. The aortic valve annulus level was similarly marked on one of the long-axis images. Multiple-slice imaging with color-highlighted active guide-wires and anatomical reference markers were then used to guide the delivery trajectory and positioning of the prosthetic valve.

After implantation, device and heart function were monitored by cine, 1st pass perfusion, and phase-contrast imaging, as well as standard hemodynamic monitoring.

Results: Figures 1 and 2 show long-axis and short-axis views of biplanar imaging as seen by the surgeon during implantation. All images are given cyan borders to indicate their orientations. The green represents the sensitivity field of the active guide wire fastened alongside a valve commissure. The prosthetic valve is seen as a dark region, due to shielding by the stent. The cyan marks denote the coronary ostia and the yellow mark depicts the level of the native aortic valve annulus. The view of Fig. 1 was used to position the prosthetic valve longitudinally, and the view in Fig. 2 was used to position the commissure between the coronary ostia by rotating the catheter. Active devices and stent positions were clearly seen next to relevant anatomy and markers in the 3D rendering.

Post implantation, blood flow through the valve was monitored in real-time, cine and phase-contrast MRI. Myocardial function was monitored with cine MRI. First pass perfusion imaging confirmed adequate blood flow to myocardium. Most often used interactive features during deployment were on-demand switching between short and long axis views, and adjustments to imaging planes.

Conclusion: Interactive rtMRI provided excellent visual guidance during minimally invasive surgical deployment of aortic prosthetic valve in a swine model. Other MRI techniques provided monitoring of valve patency and heart function. Our initial experiences suggest that valve positioning and deployment may be performed entirely under rtMRI guidance.
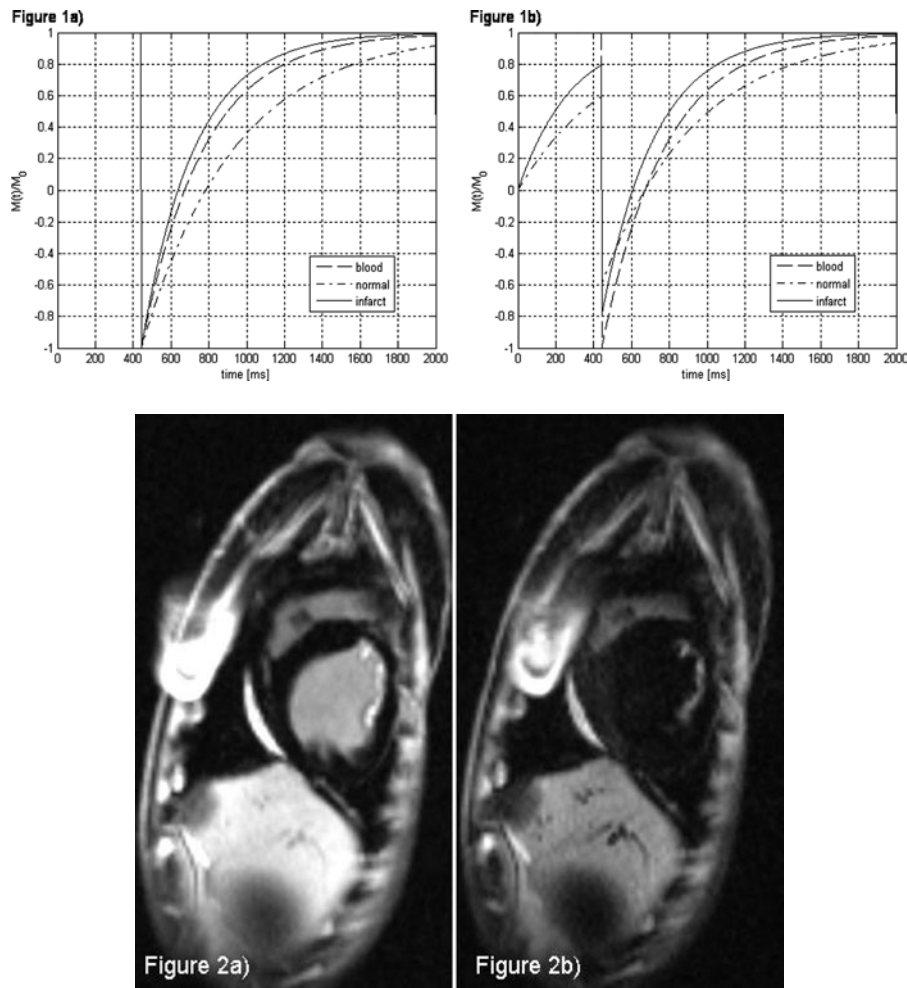
110. DARK BLOOD DELAYED ENHANCEMENT MRI FOR THE ASSESSMENT OF SUBENDOCARDIAL INFARCTS

Wolfgang G. Rehwald, PhD,[1] **Michael Salerno, MD, PhD,**[2] **Sven Zuehlsdorff, PhD,**[3] **Raymond J. Kim, MD,**[2] **Robert M. Judd, PhD.**[2] [1]*Duke University and Siemens Medical Solutions, Durham, NC, USA,* [2]*Duke University, Durham, NC, USA,* [3]*Siemens Medical Solutions, Chicago, IL, USA.*

Introduction: The introduction of the delayed enhancement technique employing the segmented IR-TurboFlash sequence has drastically improved the detection of myocardial infarctions (1). It has become the gold standard for imaging myocardial viability (2). However, small subendocardial infarcts are sometimes difficult to detect as they may have a similar signal intensity as the blood pool. The standard double-inversion "dark blood" approach (3) does not work in conjunction with delayed enhancement as the contrast agent unfavorably alters the required timing. A dark blood delayed enhancement technique has not been described, but would be clinically useful.

Purpose: To develop a technique that renders blood and non-infarcted myocardium dark and infarct bright.

Methods: To make blood and non-infarcted myocardium appear black in the image, the relaxation curves of both T1-species need to simultaneously cross the zero-line ("be nulled"). A single inversion used in standard delayed enhancement nulls only one species at a time (Fig. 1a) shows the relaxation curves for normal myocardium, infarct, and blood about 15 minutes after IV injection of 0.125 mmol/Kg Gd-DTPA ($T1_{blood} = 330$ ms, $T1_{normal} = 490$, $T1_{infarct} = 280$ ms) (4, 5). When normal myocardium is nulled, blood exhibits nearly the same signal as infarct resulting in poor infarct/blood contrast of the standard technique. Nulling two T1-species can be achieved by a timed combination of two non-selective inversion pulses, but for the given T1 values contrast between infarct and blood is small. We designed a double-preparation scheme consisting of a slice-selective saturation (SSSR) followed by a non-selective inversion (NSIR). Timing and relaxation curves are shown in (Fig. 1b). The timed combination of slice-selective and non-selective preparation decouples the infarct- from the blood-curve and enables greater image contrast than is possible with two non-selective preparations. The time from the NSIR to the center of k-space is chosen to null blood and only depends on its T1. The time between the SSSR and NSIR pulse is set to null normal myocardium when blood is nulled. The technique was tested in patients and dogs with chronic infarcts using a clinical MR scanner (Magnetom Sonata, Siemens Medical Solutions). Parameters used were field of view 300 mm, matrix 256×114, TE 3.85 ms, spatial resolution $1.6 \times 1.6 \times 6$ mm, lines per

Figure 1a)

Figure 1b)

Figure 2a)

Figure 2b)

segment 19, bandwidth 160 Hz/pixel, acquisition duration 18 heartbeats.

Results: Figure 2 shows a short-axis slice of a canine heart acquired with the standard technique (2a) and the new technique (2b). Due to the dark blood the conspicuity of the infarcted regions was improved with the new technique. The contrast-to-noise ratio between infarct and blood was 3.1 for the standard, but 18.2 for the new technique (nearly six-fold improvement). Infarct SNR was 43.2 for the standard, and 22.8 for the new technique. In the simulation of the standard technique, the signal of infarct was 0.43 M_0, and that of blood 0.28 M_0 corresponding to a 43% increased signal relative to blood. In the simulation of the new technique the infarct signal was 0.21 M_0 yielding a very large increase relative to blood.

Conclusions: We have developed a dark blood delayed enhancement technique that improves the visualization of subendocardial infarcts that may otherwise be disguised by the bright blood pool. The timed combination of a slice-selective and a non-selective preparation improves the infarct/blood contrast by decoupling their relaxation curves, but results in lower infarct SNR. The slice-selective preparation occurs early enough in the cardiac cycle so that fresh blood can enter the imaged slice.

REFERENCES

1. Radiology 2001;218:215–223.
2. Nat Clin Pract Cardiovasc Med 2005;2:150–8.
3. MAGMA. 1996;4:231–40.
4. Radiology. 2006;238:1004–12.
5. Radiology. 2005;236:1041–6.

111.   MRI-GUIDED MAPPING AND PULMONARY-VEIN ABLATION IN SWINE MODELS USING MRI-TRACKING

Ehud J. Schmidt, PhD,[1] Andre d'Avila, MD,[2] Godtfred Holmvang, MD,[3] Aravinda Thiagalingam, MD,[2] Renee Guhde, MS,[4] Robert D. Darrow, MS,[4] Richard P. Mallozzi, PhD,[4] Charles L. Dumoulin, PhD,[4] Jeremy D. Dando, BS,[5] Zachary Malchano, MS,[2] Vivek Y. Reddy, MD.[2] *[1] GE Medical Systems ASL East, Newton, MA, USA, [2] Cardiac Arrhythmia Service, Massachusetts General Hospital, Boston, MA, USA, [3] Cardiology, Massachusetts General Hospital, Boston, MA, USA, [4] GE Global Research, Niskayuna, NY, USA, [5] Saint Jude Medical, Minnetonka, MN, USA.*
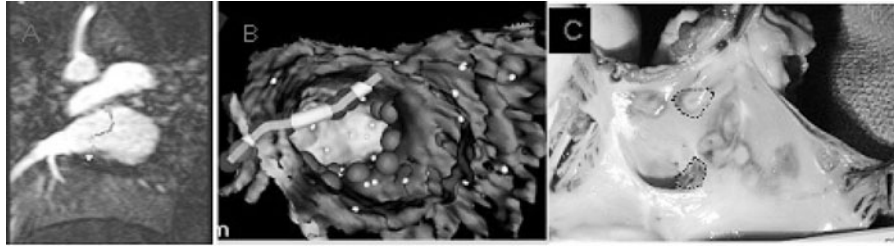
FIG. 1. (A) Coronal MRA slice with overlaid deflectable sheath (lower yellow and green points) and protruding EP catheter (upper blue, yellow, and green points, connected by a purple line) during LA mapping, (B) 3D voltage-colored luminal view of LA/PA junction after EP-voltage mapping (actual mapped locations marked with white dots), with EP catheter position overlaid (connected blue points) during circumferential RFA (ablation point positions marked with large red spheres), (C) Gross pathology showing RFA lesions (2 lesions highlighted by dashed black lines).

Introduction: MRI-guided navigation and Electro-Physiological (EP) mapping of scar in swine Left Ventricles was previously reported (1, 2). This study is an extension of the MRI-tracked technique, using an enhanced system, to EP mapping and Radio-Frequency Ablation (RFA) of the Left-Atrium (LA)/Pulmonary-Vein (PV) junction.

Purpose: To perform EP mapping and RFA at the LA/PV junction, utilizing a set of MR-tracked catheters, and to demonstrate CMRI-guidance advantages in navigation, administration of RFA, and monitoring of ablation damage.

Methods: Intubated swines (N = 4) were used. A trans-septal puncture, followed by insertion of an MR-tracked sheath into the LA, was performed under X-ray guidance. The animals were then transferred to the MRI suite. Pre-procedural MRI included 3D ECG-gated MR Angiography and 3D wall motion Cine. The images were then reformatted and 3D rendered for use as navigational roadmaps, which were displayed inside the scanner room. Under MR-Tracking guidance (2), a 5-microcoil MRI-tracked deflectable catheter, equipped with a 4 mm ablation tip and an integrated thermocouple heat sensor, was advanced through the deflectable sheath, which had 4 tracking micro-coils at its distal end. The sheath and the catheter were used synergistically in navigation within the LA and in EP mapping (Fig. 1A, B). Circumferential RFA (20–40 W for 2 minutes) was performed using an MRI-noise-filtered RFA generator, utilizing a 3D endo-luminal display of the PV/LA junction, with the overlaid catheter positions updated at 10–15 frames-per-second. Following RFA, invivo contrast-enhanced navigated 3D Myocardium Delayed Enhancement (3DMDE) was performed. Gross patholigcal exam was performed following sacrifice.

Results: MRI-guided navigation in the small swine LA required improvement in the deflection capabilites of the EP catheter. Change in local electrogram voltage post-ablation were observed at all lesion locations. Near circumferential ablation was accomplished in 2 swines, while in 2 swine only part of the LA/PV junction could be accessed. Gross pathology (Fig. 1C) verified ablation lesions at all induced locations. Three dimensionalMDE was only partially successful in finding the ablation lesions.

Conclusions: MRI-guided atrial mapping and RFA, with independent multiple-catheter control, as well as ablation monitoring, similar to that available in the conventional EP lab, is feasible using the prototype MRI-tracked system. MR image verification of ablation lesion size and position at the LA/PV junction requires further improvement.

REFERENCES

1. Dukkipati S R, et al. AHA Conference Proceedings. Circulation 2005;112:
2. Schmidt E.J. et al. SCMR 2006;8:177–178.

112. STRAIN-ENCODED MAGNETIC RESONANCE IMAGING PROVIDES REPRODUCIBLE ASSESSMENT OF RIGHT VENTRICULAR REGIONAL FUNCTION

Amr A. Youssef, MD, El-Sayed Ibrahim, MSE, Grigorios Korosoglou, MD, Shenghan Lai, MD, MPH, M. Roselle Abraham, MD, Robert G. Weiss, MD, Nael F. Osman, PhD. *Johns Hopkins University, Baltimore, MD, USA.*

Background: Regional right ventricular function assessment is important in patients with heart failure and arrhythmogenic right ventricular dysplasia. Currently, there is no easily reproducible method for accurate assessment of regional right ventricular (RV) function. To date, the application of MRI with tissue tagging provides the most comprehensive method for assessment of left ventricular and right ventricular regional function. However, regional RV function assessment is often compromised due to incomplete tags resulting from the thin walled RV.

Hypothesis: We hypothesize that the use of through-plane tags in strain encoding (SENC) MRI would permit an easy and reproducible method for assessment of regional RV function; in SENC, signal intensity is directly dependent on the degree of tissue contraction allowing direct quantification of strain values.
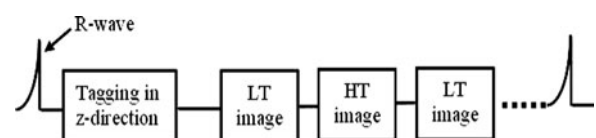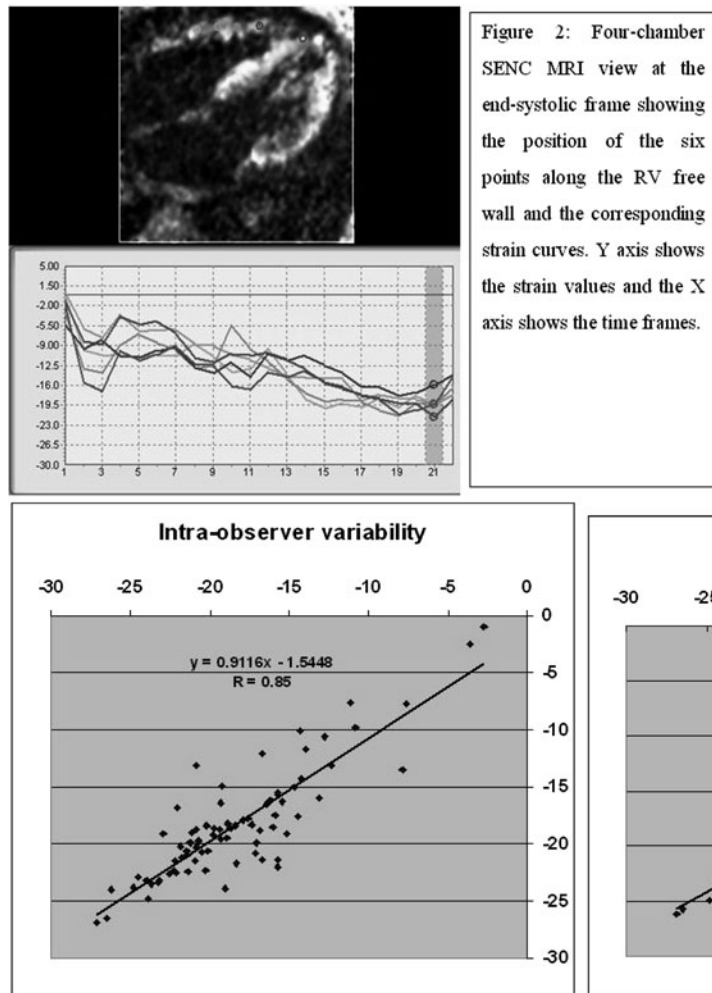

FIG. 1. SENC pulse sequence

Figure 2: Four-chamber SENC MRI view at the end-systolic frame showing the position of the six points along the RV free wall and the corresponding strain curves. Y axis shows the strain values and the X axis shows the time frames.

Intra-observer variability

$y = 0.9116x - 1.5448$
$R = 0.85$

Inter-observer variability

$y = 0.7921x - 4.3958$
$R = 0.82$

Aim: We aim to test the reproducibility of SENC MRI for assessment of regional RV function in normal human subjects.

Methods: Normal human volunteers (n = 16) were imaged on Philips Achieva 3 Tesla XMR scanner (Philips Medical Systems, Best, The Netherlands) with a 6-element cardiac phased array coil. After initial scouting and obtaining gradient echo cine images in four chamber view, four-chamber SENC images were acquired during a single breath hold throughout 13 heart beats using prospective ECG gating. SENC MRI is based on the acquisition of two images with different phase-encodings, or tunings, in the slice-selection direction. We call these images the low-tuning (LT) and high-tuning (HT) images. Bright regions in the LT and HT images represent static and contracting tissues, respectively. The two images are then combined as described in reference 1 to result in a strain image, where signal intensity is proportional to the strain value. Strain measurements calculated from SENC images have recently been validated against standard Spatial Modulation of Magnetization (SPAMM) tagging images (2). Figure 1 shows a schematic diagram of the SENC pulse sequence. Imaging parameters are: TR = 14.4 ms; TE = 0.8 ms; flip angle = 40°; and slice thickness = 8 mm.

Data Analysis: Images were analyzed using the SENC software package (Diagnosoft Inc., Palo Alto, California, USA). Circumferential systolic strain of the RV was calculated from the SENC CMRI four-chamber view. Circumferential myocardial strain was measured during systole at six equidistant points along the RV free wall, starting from base to apex (Fig. 2). In order to detect the timing of end-systole from the cine SENC images in the absence of corresponding ECG, peak contraction of the RV free wall was defined as the maximum value of the averaged circumferential strain from the six points. Regional function was defined as the strain value of each point at the time of peak contraction. Intra-observer and inter-observer variability were calculated by using the intra-class correlation coefficient (R).

Results: The SENC MRI measured myocardial strains for the basal, mid and apical regions of the RV free wall were (mean ± standard deviation): -20.4 ± 2.9, -18.8 ± 3.9 and -16.5 ± 5.7, respectively. Regional myocardial strain measurements demonstrated low intra- and inter-observer variability (r = 0.85/0.85, 0.79/0.78 and 0.93/0.84 for the basal, mid and apical regions, respectively). The overall intra- and inter-observer variability were r = 0.85 and 0.82, respectively.

Conclusion: SENC MRI allows rapid and reproducible quantification of regional RV function in healthy volunteers and has the potential for objective assessment of regional strain in patients with RV dysfunction.

REFERENCES

1. Osman NF, et al. Magn Reson Med 46:324–334.
2. Garot J, et al. Circulation 101:981–988.

Friday, February 2, 2007
Oral Abstracts: Congenital-Session III

113. UNDIAGNOSED CAUSE OF RIGHT VENTRICULAR ENLARGEMENT: VALUE OF CARDIOVASCULAR MAGNETIC RESONANCE FOR THE DETECTION OF SINUS VENOSUS DEFECT AND PARTIAL ANOMALOUS PULMONARY VENOUS CONNECTION

Henryk Kafka, MD, FRCPC, FACC,[1] Raad H. Mohiaddin, MD, FRCR, FRCP, FESC.[2] [1]*Queens University, Kingston, ON, Canada,* [2]*Cardiovascular Magnetic Resonance Unit, Royal Brompton Hospital, London, United Kingdom.*

Introduction: Patients are often referred for cardiology assessment because of an enlarged right ventricle (RV) but no cause apparent by echocardiography (TTE), computerized tomography or cardiac catheterization. Before a diagnosis of RV cardiomyopathy or primary pulmonary hypertension is made in these cases, sinus venosus defect (SVD) or partial anomalous pulmonary venous connection (PAPVC) must be considered.

Purpose: To provide a systematic analysis of CMR for the detection and quantification of SVD in the patient with undiagnosed cause of RV enlargement.

Methods: All first CMR scans performed over a 4 year period at the Royal Brompton Hospital (RBH) were searched for the CMR diagnosis of SVD or PAPVC. Only those patients for whom there had been no definite pre-scan diagnosis were included in the study. Clinical notes and previous investigations were reviewed and correlated with the CMR findings. Comparison with surgical findings was made when available.

Results: Thirty-seven patients (25 women and 12 men, aged 16 to 75, median age 40) met the study criteria. All patients had TTE prior to referral for CMR, and 15 had transesophageal echocardiography (TEE). TTE or TEE reported PAPVC or possible PAPVC in 5 patients. No SVD was reported by TTE prior to referral, but TEE reported SVD or possible SVD in 4 patients. In these cases, CMR had been requested to rule out associated PAPVC.

SVD: A total of 19 patients (10 women) had a CMR diagnosis of SVD. PAPVC was the commonest associated defect, present in 95% (18/19) of patients with SVD. All PAPVC associated

FIG. 1. Left. Magnetic resonance angiogram showing right PAPVC (arrow) into SVC(*). Right. Turbo spin echo axial image demonstrating SVD (arrow) between the left atrium (LA) and SVC(*).

with SVD were from the right side. No patient with SVD had anomalous left connection or scimitar vein. Two patients also had CMR diagnosis of secundum ASD. Qp:Qs ratios were determined for all 19 patients using CMR pulmonary and aortic flow mapping and ranged from 1.5 to 4.

Eleven of 19 patients with SVD underwent surgery at RBH and SVD was confirmed in all 11 cases, as were all CMR identified PAPVC. In the one case of SVD with no PAPVC identified by CMR, there was no PAPVC at surgery. No patient had additional PAPVC discovered at surgery. The 2 secundum ASD diagnosed in addition to the SVD, were confirmed at surgery.

PAPVC: A total of 60 PAPVC were demonstrated in 36 patients. PAPVC were right-sided in 27 patients (75%), left-sided in 7 patients (19.4%) and bilateral in 2 patients (5.6%). Three patients with right-sided connections had scimitar veins. There was a single anomalous pulmonary vein connection in 18 (50%), two anomalous connections in 12 (33.3%) and three anomalous connections in 6 patients (16.6%). Of the 60 abnormal connections, 31 (51.7%) were to SVC, 4 (6.7%) were to SVC/RA junction, 10 (16.6%) were to RA, 6 (10%) were to IVC and 9 (15%) were to a vertical vein on the left that communicated with the brachiocephalic vein. The commonest associated defect was SVD in 18 (50%) of these patients. Secundum ASD was present in 6 patients, including 2 who already had SVD. Of the other four patients with ASD, one had an anomalous LUPV connection and three had right PAPVC. Intact septum was present in 14/36 (38.8%), including 8 of 9 patients with a left connection and all 3 patients with a scimitar vein.

Conclusions: CMR can reliably detect, delineate and quantify SVD and PAPVC in patients for whom other diagnostic methods have failed to provide a complete diagnosis for the cause of right heart enlargement.

114. DYNAMIC CONTRAST ENHANCED MRI IN PATIENTS BEFORE AND AFTER TRANSCATHETER CLOSURE OF PATENT FORAMEN OVALE

Oliver K. Mohrs,[1] Steffen E. Petersen,[2] Thomas Schulze,[3] Damir Erkapic,[4] Bernd Nowak,[5] Hans-Ulrich Kauczor,[6]

Thomas Voigtlaender.[5] [1] *Darmstadt Radiology, Darmstadt, Germany,* [2] *University of Oxford (OCMR), Oxford, United Kingdom,* [3] *Siemens Medical Solutions, Erlangen, Germany,* [4] *Kerckhoff Heart Clinic, Bad Nauheim, Germany,* [5] *Cardiovascular Center Bethanien, Frankfurt/Main, Germany,* [6] *German Cancer Research Center (DKFZ), Heidelberg, Germany.*

Introduction: Due to paradoxical embolism even in young patients, patent foramen ovale (PFO) is a known cause of cerebral strokes or transient ischemic attacks. Percutaneous transcatheter occlusion offers an attractive, less invasive treatment compared to surgical approaches. Diagnosis and follow-up assessment is important to prevent further cerebral events.

Purpose: The purpose of this study was threefold: To evaluate the diagnostic accuracy of dynamic contrast-enhanced magnetic resonance imaging (ceMRI) to detect patent foramen ovale (PFO) or residual shunts after occlusion of PFO compared to transesophageal echocardiography (TEE), to define cut-off values for semi-quantitative analysis of signal-to-time curves and to compare diagnostic accuracy of visual detection with semi-quantitative analysis.

Methods: We examined 43 patients (18 women, 25 men; mean age 51 $\pm$ 14 years) who underwent TEE for suspicion of PFO (n = 19 with and n = 7 without PFO) or routine assessment for residual shunts after transcatheter PFO occlusion (n = 9 with and n = 8 without residual shunt) were enrolled to undergo ceMRI (saturaton-recovery steady-state free precession sequence) which was analyzed both visually and semi-quantitatively for arrival of contrast agent in the left atrium prior to the arrival in the pulmonary veins during a valsalva maneuver. TEE results were used as the reference standard in all cases.

Results: The maximum height of the first initial peak in signal intensity in the left atrium proved to be the best discriminator for right-to-left shunt detection with an area under the curve of 0.85. For a cut of value of 129% (from baseline signal) for this parameter sensitivity, specificity was 17/19 and 7/7, respectively, in patients without PFO devices and 5/9 and 7/8, respectively, in patients with PFO devices. Diagnostic accuracy is better for visual than semi-quantitative shunt assessment in patients with (sensitivity 6/9 correctly diagnosed - specificity 7/8) and without PFO occluders (sensitivity 18/29 - specificity 7/7). Diagnostic accuracy is consistently superior in patients prior to PFO device implantation both for visual assessment and for semi-quantitative analysis compared to after device implantation.

Conclusions: MRI provides an attractive, alternative non-invasive technique, if TEE is technically impossible or is declined by patients. Diagnostic accuracy is better for visual shunt assessment in patients both with and without PFO occluders. However, less experienced observers may wish to confirm the visual assessment by semi-quantitative assessment. We suggest the use of a cut of value of 129% for this first initial peak in the left atrium to detect right to left shunts through a PFO.

115. CARDIAC MRI COMBINED WITH LOW-DOSE DOBUTAMINE STRESS REVEALS AN ABNORMAL STRESS RESPONSE IN CHILDREN AND YOUNG ADULTS AFTER FONTAN OPERATION AT YOUNG AGE

Danielle Robbers-Visser, MD,[1] Derk-Jan ten Harkel, MD, PhD,[1] Jan L. M. Strengers, MD, PhD,[2] Livia Kapusta, MD, PhD,[3] Folkert J. Meijboom, MD, PhD,[4] Peter M. T. Pattynama, MD, PhD,[4] Ad J. J. C. Bogers, MD, PhD,[4] Willem A. Helbing, MD, PhD.[1] [1] *Erasmus MC—Sophia, Rotterdam, The Netherlands,* [2] *University MC Utrecht—Wilhelmina Children's Hospital, Utrecht, The Netherlands,* [3] *UMC St Radboud, Nijmegen, The Netherlands,* [4] *Erasmus MC, Rotterdam, The Netherlands.*

Introduction: Assessment of stress response is an important tool in detecting clinical and subclinical signs of ventricular dysfunction. After Fontan operation, this response of the functionally univentricular heart is unknown. In patients with complex congenital heart disease, stress response can be assessed with cardiovascular magnetic resonance (CMR) imaging combined with low-dose dobutamine stress.

Purpose: To assess the stress resonse of functionally univentricular hearts with low-dose dobutamine stress CMR imaging.

Methods: Patients with an atriopulmonary (APC) or total cavopulmonary connection (TCPC), completed before the age of 7 and at least 5 years after completion were included. A CMR study was done at rest and during low-dose dobutamine stress (7.5 microgr/kg/min maximal). A multiphase short axis stack of twelve contiguous slices of the systemic ventricle was obtained during rest and stress (SSFP, flip angle = 45°, TE set at min full, TR = 3.4–3.6 ms, 7–10 mm slice thickness, 0 mm interslice gap, 12 views/segment, scanning matrix 160 * 128, 3 signal averages). For stroke volume validation, flow measurements in the aorta or through the atrioventricular valve plane were obtained with velocity-encoded phase-contrast imaging (2D FSPGR, TR = 5–6 ms, TE = 3 ms, flip angle = 20°, 7 mm slice thickness, 6 views/segment, scanning matrix 256 * 128, 3 signal averages).

Results: Twenty-four patients with a TCPC and 4 patients with an APC were included (20 boys, mean age 13.1 $\pm$ 4 (SD) years, mean follow-up after Fontan operation 9.6 $\pm$ 4 years). In 3 patients, the MRI was discontinued after localizers because of patient discomfort. Dobutamine was administered safely to the remaining 25 subjects. Results are summarized in the following Table:

Indices of ventricular function

Parameter	Rest	Dobutamine stress	p value
Heart rate (/min)	70 $\pm$ 11	93 $\pm$ 17	p < 0.001
End-diastolic volume (mL/m^2)	78 $\pm$ 16	64 $\pm$ 14	p < 0.001
End-systolic volume (mL/m^2)	35 $\pm$ 15	21 $\pm$ 12	p < 0.001
Stroke volume (mL/m^2)	43 $\pm$ 11	43 $\pm$ 11	P = 0.502
Ejection fraction (%)	56 $\pm$ 12	67 $\pm$ 12	p < 0.001
Cardiac index (L/min/m^2)	2.9 $\pm$ 0.6	3.8 $\pm$ 0.7	p < 0.001

Linear regression analysis showed an excellent correlation of both aortic and atrioventricular stroke volume with ventricular stroke volume (r = 0.98 and r = 0.97 respectively).

Conclusions: With beta-adrenergic stimulation, the functionally univentricular heart after Fontan completion at young age has an adequate increase in ejection fraction. However, as a result of impaired preload with stress, cardiac output can be increased only by increasing heart rate.

116. IMPACT OF TRANSVERSE AORTIC ARCH HYPOPLASIA AFTER SURGICAL REPAIR OF AORTIC COARCTATION: AN EXERCISE ECHO AND MAGNETIC RESONANCE IMAGING STUDY

Giardini Alessandro, MD,[1] Luigi Lovato, MD,[2] Maurizio Montalti, MD,[2] Valentina Gostoli,[2] Cesare La Palombara, MD,[2] Katia Buttazzi, MD,[2] Vincenzo Russo, MD,[2] Fernando M. Picchio, MD,[3] Rossella Fattori, MD.[2] [1] *University of Bologna, Bologna, Italy,* [2] *University of Bologna, Cardiovascular Radiology, Italy,* [3] *University of Bologna, Pediatric Cardiology and Adult Congenital Unit, Italy.*

Introduction: Patients with repaired aortic coarctation (AoC) may show an abnormal blood pressure response to exercise even in the absence of recoarctation. The mechanisms responsible for exercise-induced systemic hypertension are poorly understood.

Background: We sought to assess the impact of persistent hypoplasia of the transverse aortic arch (TAA) after repair of AoC, on blood pressure response to exercise, left ventricular (LV) hypertrophy, and presence of collateral circulation.

Methods: Thirty-four consecutive patients with end-to-end repair of AoC (age at repair 3.2 ± 2.5 years) underwent exercise echocardiography and magnetic resonance imaging (MRI) at 24 ± 7 years of age (range 11.3 to 44.6 years). Systolic Doppler pressure gradient (SPG) across the descending aorta and blood pressure at the right arm were measured at baseline and every minute throughout all exercise. Magnetic resonance imaging was used to measure LV mass index, presence and amount of collateral flow, and the diameters of the aortic isthmus and TAA indexed to the diameter of the diaphragmatic.

Results: Aortic isthmus index was higher than that of the TAA (p = 0.006). We observed LV hypertrophy in 15 patients (45%) and presence of collateral circulation in 14 (41%). Eighteen patients (53%) had an abnormal blood pressure response to exercise. Patients with abnormal pressure response to exercise had smaller TAA index (p = 0.0005), but similar aortic isthmus index (p = 0.09). They also had higher exercise SPG (p < 0.0001), higher LV mass index (p < 0.0001) and prevalence of LV hypertrophy (p = 0.007), higher prevalence of collateral circulation (p < 0.0001), and a higher amount of collateral flow (p < 0.0001). TAA index, but not aortic isthmus index, correlated with exercise blood pressure (r = −0.59, p = 0.003), exercise

SPG (r = −0.70, p = 0.0005), amount of collateral flow (r = −0.74, p = 0.0002), and LV mass index (r = −0.68, p = 0.0007).

Conclusions: After repair of AoC, hypoplasia of the TAA may be responsible for abnormal blood pressure response to exercise, persistence of collateral circulation and LV hypertrophy.
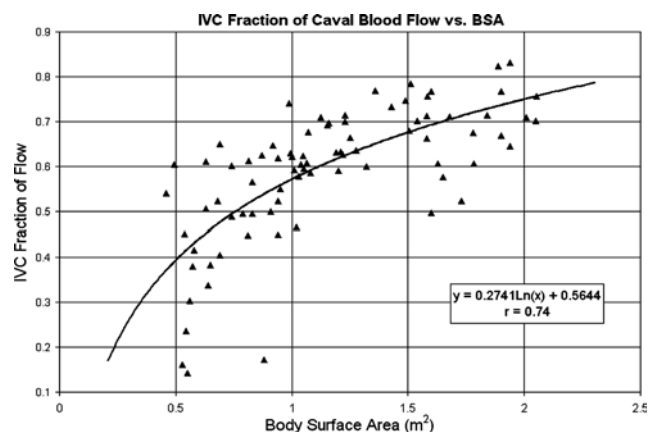
117. IMPACT OF FONTAN TYPE IN A LARGE SERIES OF SINGLE VENTRICLE PATIENTS—A CARDIAC MAGNETIC RESONANCE VELOCITY MAPPING STUDY

Kevin K. Whitehead, MD, PhD,[1] Kartik S. Sundareswaran, BS,[2] Resmi A. Krishnankutty, BS,[2] William J. Parks, MD,[3] Shiva Sharma, MD,[4] William B. Hyslop, MD,[5] Ajit P. Yoganathan, PhD,[6] Mark A. Fogel, MD.[1] [1] *Children's Hospital of Philadelphia, Philadlephia, PA, USA,* [2] *Georgia Institute of Technology, Atlanta, GA, USA,* [3] *Children's Healthcare of Atlanta, Sibley Heart Center, Atlanta, GA, USA,* [4] *Pediatric Cardiology Services, Atlanta, GA, USA,* [5] *University of North Carolina, Chapel Hill, NC, USA,* [6] *Georgia Institute of Technology and Emory University, Atlanta, GA, USA.*

Introduction: No large series exists that establishes the flow distributions in Fontan patients, which would be an important resource for everyday clinical use and may impact future surgical reconstruction. In addition, the impact of Fontan type and cavopulmonary connection on flow distributions in a large series of Fontan pts is unknown. Cardiac magnetic resonance (CMR) is an ideal tool for evaluating these patients because of its non-invasive nature and the accuracy at which it can quantitate blood flow with cine phase contrast MRI (PC-MRI).

Purpose: The goal of this study is to determine flow distribution in the cavopulmonary connections of Fontan patients with and without bilateral superior vena cavae (SVC). In addition, we evaluated the utility and internal consistency of CMR in measuring these flows.

Methods: We studied 81 Fontan patients (ages 2–24 years) with through-plane PC-MRI to determine flow rates in the

IVC Fraction of Caval Blood Flow vs. BSA

$y = 0.2741 \mathrm{Ln}(x) + 0.5644$
$r = 0.74$

Summary of flows and flow splits and comparisons between +/− LSVC and Fontan type.

Flows in (L/min/m^2) Ratios as fraction	All pts Mean ± S.D.	With LSVC Mean ± S.D.	LSVC vs. no LSVC p value	Intracardiac Fontan Mean ± S.D.	Extracardiac Fontan Mean ± S.D.	Intra- vs. Extracardiac p value
(IVC + SVC)/BSA	2.8 ± 0.8	2.9 ± 0.7	0.69	2.8 ± 0.8	3.0 ± 0.8	0.31
(LPA + RPA)/BSA	2.4 ± 0.7	2.2 ± 0.5	0.43	2.3 ± 0.7	2.7 ± 0.9	0.06
IVC/(IVC + SVC)	0.59 ± 0.15	0.58 ± 0.11	0.89	0.60 ± 0.16	0.56 ± 0.11	0.38
RPA/(LPA + RPA)	0.53 ± 0.16	0.47 ± 0.18	0.14	0.55 ± 0.14	0.49 ± 0.14	0.06
Aortic Flow/BSA	3.7 ± 1.6	4.0 ± 1.1	0.45	3.4 ± 1.4	4.2 ± 1.9	0.13

inferior and right and left (if present) superior vena cavae, and left and right pulmonary arteries. Eleven patients had bilateral superior vena cavae.

Results: Total caval flow was 2.8 ± 1.3 L/min/m^2, with an inferior vena cava contribution of 59% ± 15%. Total pulmonary blood flow was 2.4 ± 0.7 L/min/m^2. The right pulmonary artery contribution was 53% ± 16%, which was not statistically different from left pulmonary artery flow. In 10 patients with bilateral superior cavae, the right superior vena cava accounted for 49% ± 15% of the flow. No difference was noted in the pulmonary flow splits for patients with bilateral superior cavae, with 49% ± 15% to the right lung. Age and body surface area were correlated with inferior vena cava contribution (r = 0.60 and 0.74 respectively). Type of superior vena cava anastomosis or Fontan did not significantly affect pulmonary flow splits.

Conclusions: Total cardiac output was 2.8 L/min/m^2, with equal flows to both lungs regardless of Fontan type or presence of bilateral superior cavae. Inferior vena cava contribution to total flow increases with body surface area and age, consistent with data from healthy children.

118. MRI GUIDED CARDIAC CATHETERIZATION TO ASSESS PULMONARY VASCULAR RESISTANCE IN THE CONTEXT OF A LEFT TO RIGHT SHUNT: AN ILLUSTRATION OF CLINICAL UTILITY

Aaron J. Bell, MbChB, MRCPCH,[1] Vivek Muthurangu, MbChB, MRCPCH,[2] Sanjeet Hegde, MBBS, MRCPCH,[1] Tobias Schaeffter, PhD,[1] Reza Razavi, MD, MRCP, MRCPCH.[1] [1]*Kings Collge London, London, United Kingdom,* [2]*University Collge London, London, United Kingdom.*

For the majority of patients with a large left to right shunt it is clear that closure of the defect is the correct management. However, the presence of pulmonary vascular disease increases risk and may render some patients inoperable. This group of patients include those who present late, those with significant respiratory co-morbidity, or those with no clinical evidence of high pulmonary blood flow in the presence of a large defect. Accurately determining the presence of pulmonary vascular disease is a clinical challenge in this group.

We have described a technique for cardiac catheterization in a MRI suite equipped with X-Ray facilities (XMR). We have shown that MRI catheter with direct pressure measurement and phase contrast MRI can accurately determine pulmonary vascular resistance (PVR) (1). Here, we describe the results of this technique when applied to a group of patients with a left to right shunt in whom assessment of PVR was required to determine whether surgery was indicated.

Methods: MRI guided cardiac catheterisation was performed in an Interventional XMR suite with a 1.5T Philips Intera MR scanner and a single plane Pulsera Cardiac X-ray Unit (Philips Medical Systems, Best, Netherlands). Informed consent was obtained from all patients or their parents/legal guardians for patients under 16 years. All procedures were undertaken with a general anaesthetic and patients ventilated to normocarbia. Cardiac catheter was undertaken with a 4Fr or 6Fr angiographic catheter with a carbon dioxide filled balloon which was manipulated under the guidance of either X-ray, MRI or combined. Direct pressure measurement was performed using fluid filled catheters. Phase contrast flow was performed simultaneously with direct pressure measurement in 3 conditions (30% Oxygen, 30% Oxygen and 20ppm nitric oxide, 100% oxygen and 20 ppm nitric oxide).

Results: Results are summarized in Table 1. Data is expressed as mean ± SD unless stated. Twelve CMRI catheters were performed in 11 patients, mean age years 4.28 years (range 0.25 to 42.3), 6 female, 5 male. The mean left to right shunt at baseline (Qp:Qs) was 2.59 ± 1.08 . The mean PVR was 4.56 ± 2.98 WU.m2.

Six patients had Downs' syndrome, all had an AVSD, 1 of whom had 2 studies. These patients exhibited a non-significant tendency towards higher PVR (p = 0.12) and lower shunt (p = 0.4).

Seven Patients demonstrated a significant left to right shunt (3.29:1 ± 0.81) with low PVR (2.97 WU·m^2 ± 0.71) and underwent surgical correction. This group had a lower PVR (p = 0.04) and greater shunt (p = 0.005) than those not repaired. All patients with a PVR < 4.0 WU·m^2 underwent corrective surgery, except patient 10 who also had restrictive lung disease.

In the remaining 4 patients, the PVR was deemed too high for surgical correction. One of these patients had severe pulmonary vein stenosis, which was repaired. Another had previous surgical correction of AVSD but had a residual VSD with

TABLE 1
Patient demographics, diagnosis, baseline hemodynamics and outcome

	Diagnosis	Age (years)	Co-morbidity	Downs syndrome	Shunt	PVR (WU.m^2)	Outcome
1	TAPVD with residual ascending vein	0.66	—	—	3: 1	2.6	Ligation of ascending vein
2	Unbalanced AVSD, Pulmonary artery band	0.75	Pulmonary vein stenosis	—	1:1	6.2	Repair of pulmonary vein stenosis
3	AVSD	0.5	Chronic lung disease	Yes	3.2:1	3.5	AVSD Repair
4*	AVSD	0.75	Chronic lung disease, residual VSD	Yes	1.8:1	4.1	Conservative treatment
5	VSD	0.25	Diaphragmatic hernia repair	—	4.6:1	3.3	VSD Repair
6	AVSD	0.33	—	Yes	2.1:1	3.9	AVSD Repair
7	AVSD	2.5	Late presentation	Yes	3.7:1	2.1	AVSD Repair
8	AVSD	0.83	—	Yes	1.3:1	12	Conservative treatment
9	AVSD	1.08	Late presentation	Yes	2:1	8.6	Conservative treatment
10	VSD	42.4	Restrictive lung disease	—	2.5:1	3.0	Conservative treatment
11	AVSD	0.52	—	Yes	4.4:1	3.0	AVSD Repair
12	VSD	0.78	Late presentation	—	2.7:1	2.1	VSD Repair

*Second study in patient 3.

TAPVD = Total anomalous pulmonary venous drainage, AVSD = atrio-ventricular septal defect, VSD = ventricular septal defect.

elevated PVR post operatively and was subsequently treated conservatively.

Conclusion: There are a group of patients with left to right shunt who develop pulmonary vascular disease. In these patients assessment of the PVR and shunt can prove invaluable in determining whether closure of the defect is the correct course of management. CMRI catheter provides accurate assessment of the shunt and PVR and can be confidently used to plan management in this patient group.

REFERENCE

1. Muthurangu V, et al. Novel method of quantifying pulmonary vascular resistance by use of simultaneous invasive pressure monitoring and phase-contrast magnetic resonance flow. Circulation 2004;110:826–34.

Friday, February 2, 2007
Oral Abstracts: Clinical-Session IV

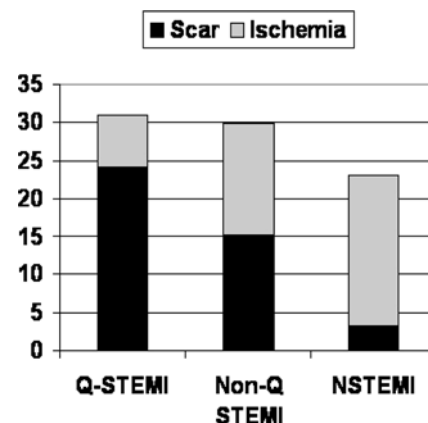**119. ISCHEMIA AND SCAR BURDEN AFTER ACUTE MYOCARDIAL INFARCTION—INSIGHTS FROM CARDIAC MRI**

Sven Plein, MD, PhD,[1] John Younger, MD,[1] Patrick Sparrow, MD,[1] John P. Ridgway, PhD,[1] Mohan Sivananthan, MD,[2] Stephen G. Ball, PhD,[1] John P. Greenwood, PhD.[1] [1]*University of Leeds, Leeds, United Kingdom,* [2]*Leeds General Infirmary, Leeds, United Kingdom.*

Introduction: Despite a common underlying pathophysiological substrate (the vulnerable plaque), different types of myocardial infarction have diverse morphological consequences as well as different early and late outcomes. These differences are likely to occur as a consequence of the different ratio of permanently damaged (scar) tissue and myocardium remaining at ischemic risk after the acute event.

Purpose: In this study we measured ischemia and scar burden in patients with Q-wave ST-elevation myocardial infarction (Q-STEMI), non-Q-wave ST-elevation myocardial infarction (NQ-STEMI) and Non-ST-elevation myocardial infarction (NSTEMI) to test the hypothesis that the ratio of scar and ischemia burden differs between these different types of myocardial infarction.

Methods: Seventy-five subjects presenting with acute coronary syndromes were recruited: 25 consecutive patients with NSTEMI, 25 with thrombolysed Q-STEMI and 25 with NQ-STEMI. All patients underwent CMR imaging of myocardial function, perfusion (rest and adenosine-stress) and viability (by late gadolinium enhancement) 2–7 days after presentation and before any invasive procedures.

Results: By analysis of variance, scar burden was highest in Q-STEMI, followed by NQ-STEMI and NSTEMI (24.1%, 15.2% and 3.3% of LV mass, respectively; $p < 0.0001$). Ischemia burden showed a reverse correlation and was lowest in Q-STEMI, followed by NQ-STEMI and NSTEMI (6.9%, 14.7% and 19.9% of LV mass, respectively; $p < 0.012$). The combined burden of scar plus ischemia was similar between the three groups. Left ventricular ejection fraction was lowest in Q-STEMI and highest in NSTEMI ($p < 0.001$).

Conclusions: The ratio of scar versus ischemia burden differs significantly between NSTEMI and STEMI as well as between NQ-STEMI and Q-STEMI. These morphological differences in the various sub-types of acute myocardial infarction may relate to their diverse early and late prognosis. The higher scar mass in STEMI is a probable substrate for early haemodynamic complications while the ischemia burden in NSTEMI may be responsible for delayed events in this group.

120.   COMBINING FIRST-PASS PERFUSION AND CINE WALL MOTION ASSESSMENT BY CARDIAC MAGNETIC RESONANCE DURING HIGH-DOSE DOBUTAMINE STRESS CAN PROVIDE STRONG LONG TERM PATIENT PROGNOSIS FROM CORONARY ARTERY DISEASE

Raymond Y. Kwong, MD, MPH, Matthew Kaminski, MD, Maung M. Khin, MD, Kenneth Brown, MD, Sui Tsang, BSc, H. Glenn Reynolds, MSc, E. Kent Yucel, MD. *Brigham and Women's Hospital, Boston, MA, USA.*

Introduction: Assessment of myocardial perfusion and regional function during dobutamine cardiac MRI (CMR) can characterize the cascade of demand ischemia.

Purpose: We tested the hypothesis that ischemia by perfusion (PERF) or regional function (CINE) by dobutamine CMR can provide independent prognostic association with adverse cardiac events (MACE) in patients.

Methods: One hundred fourteen patients (74 M, age 60 ± 14 years) with suspected ischemia underwent dobutamine stress CMR with combined perfusion and cine imaging. Logistic regression assessed the association with subsequent diagnosis of

significant ($>70\%$) coronary stenosis (CATHCAD) or MACE at 12 months after CMR. CATHCAD within 1 month after CMR was excluded to minimize the impact by CMR on angiographic referral. We also performed Cox regression to model the event-free survival of patients in the follow-up period.

Results: At 12 months after CMR, 28 patients were diagnosed to have CATHCAD and 8 experienced MACE. At study end, 25 patients experienced MACE including 13 deaths. For new CATHCAD within 12 months after CMR, CINE, PERF, and combined CINE/PERF had sensitivities of 75%, 96%, and 96%, and specificities of 86%, 71%, and 58%, respectively. By multivariable logistic regression, CINE and PERF provided independent and complementary association with CATHCAD or MACE at 12 months after CMR (adjusted OR: 7.33, $p = 0.001$ and 4.18, $p = 0.02$, respectively). Abnormal CINE and PERF were both associated with reduced event-free survival over the study period (median 18 months, range 6-48) (Fig. 1).

Conclusions: CINE and PERF provide complementary assessment of coronary artery disease and long-term patient prognosis.

121.   THE ROLE OF CARDIOVASCULAR MAGNETIC RESONANCE IN PATIENTS PRESENTING WITH CHEST PAIN, RAISED TROPONIN AND UNOBSTRUCTED CORONARY ARTERIES

Ravi Assomull, Jonathan C. Lyne, MRCP, Niall G. Keenan, MRCP, Ankur Gulati, MRCP, Nicholas H. Bunce, MD, MRCP, Simon W. Davies, FRCP, Dudley J. Pennell, MD, FRCP, FACC, FESC, Sanjay K. Prasad, MD, MRCP. *Royal Brompton Hospital, London, United Kingdom.*

Introduction: Troponin measurement is used in the assessment and risk stratification of patients presenting acutely with chest pain when the main cause of elevation is coronary artery disease. However, some patients have no coronary obstruction on angiography leading to diagnostic uncertainty. Defining the underlying cause of the clinical presentation is important and further investigation is justified as lack of an accurate diagnosis is likely to result in patients not receiving appropriate treatment and/or
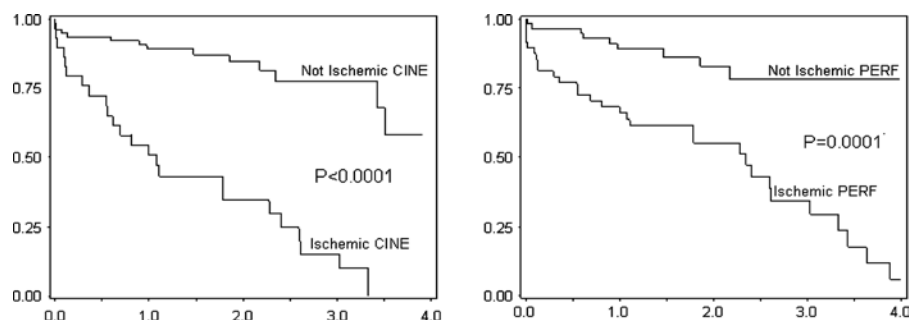

FIG. 1.   Event-free Survival Distribution of the Study Cohort Over the Study Follow-up Period.
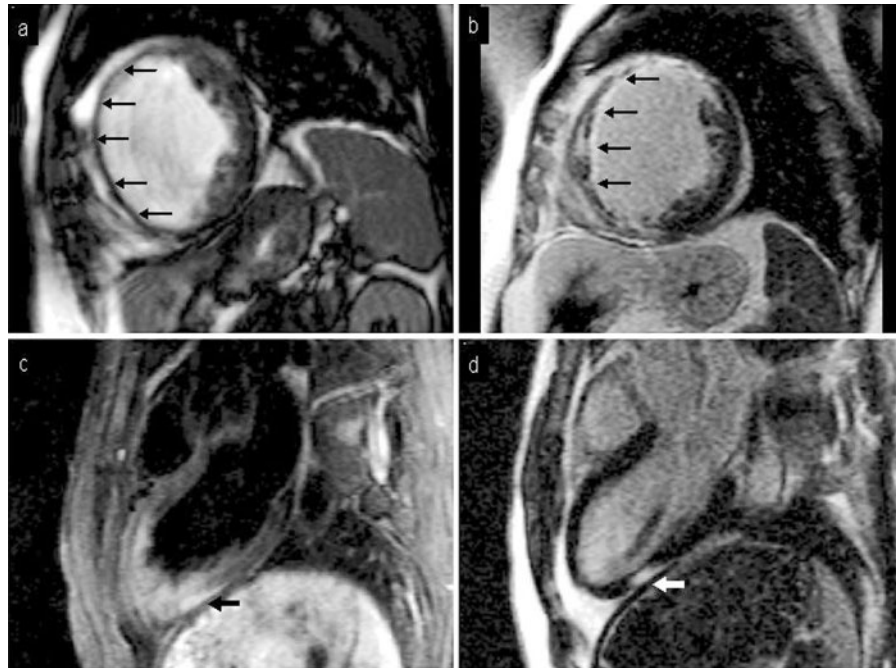
FIG. 1.

follow up. This current lack of diagnostic uncertainty may in turn explain why this cohort of patients has been shown to have a poorer prognosis.

Purpose: There are a number of potential causes of this scenario, including non-cardiac aetiologies, myocardial infarction with a recanalized coronary artery (Fig. 1a, 1b) and acute myocarditis (Fig. 1c, 1d). We therefore evaluated the incremental diagnostic value of cardiovascular magnetic resonance (CMR) in a consecutively referred cohort of patients with chest pain, raised troponin and normal coronary angiography.

Methods: Sixty consecutive patients (mean age 44 years, 72% male) with a troponin-positive episode of chest pain and unobstructed coronary arteries were recruited within 3 months of initial presentation. All patients underwent CMR (Siemens Sonata 1.5T, Erlangen, Germany) with cine imaging, T2 weighted imaging for detection of inflammation, and late gadolinium enhancement imaging (Schering, 0.1 mmol/kg) for detection of infarction/fibrosis.

Results: An identifiable basis for troponin elevation was established in 65% of patients. The commonest underlying cause was myocarditis (50%) followed by myocardial infarction (11.6%) and cardiomyopathy (3.4%). In the 35% of patients where no clear diagnosis was identified by CMR (non-diagnostic group), significant myocardial infarction/fibrosis was excluded. Additionally, there was a larger proportion of patients with single small troponin rise (<5 ULN) in the non-diagnostic group vs the patients with a CMR-ascribed diagnosis (52% vs 8%, p =< 0.01).

Conclusions: CMR is a valuable adjunct to conventional investigations in a diagnostically challenging and important group of patients with troponin-positive chest pain and unobstructed coronary arteries. In patients where CMR was unable to ascribe a diagnosis, myocardial infarction was excluded. Additionally, this "non-diagnostic" group of patients also presented with a single small rise in troponin suggesting that the raised level of troponin seen here was a biochemical false positive. Further studies are required to evaluate the prognostic implications of CMR abnormalities in this cohort of patients.
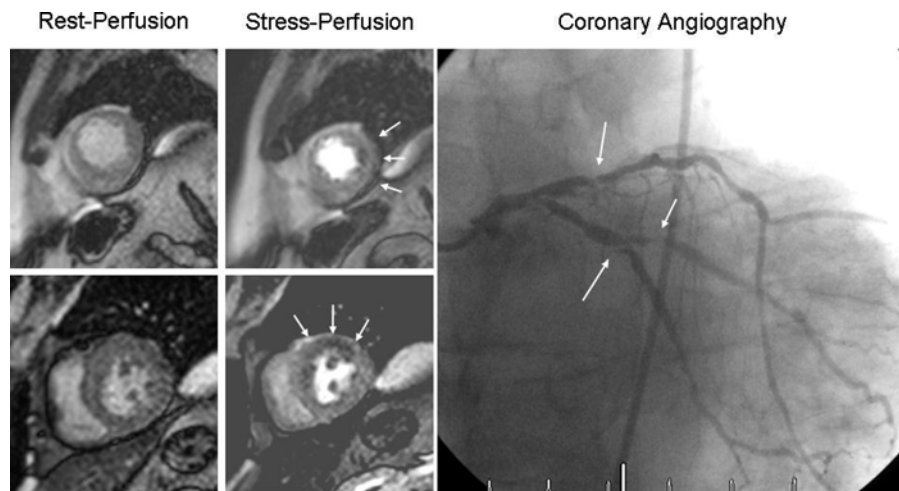
122. NONINVASIVE DIAGNOSIS OF CORONARY ARTERY DISEASE BY DOBUTAMINE STRESS MYOCARDIAL PERFUSION IMAGING WITH MRI

Rolf Gebker, Ingo Paetsch, Cosima Jahnke, Thomas Kokocinski, Eckart Fleck, Eike Nagel. *German Heart Institute Berlin, Berlin, Germany.*

Introduction: Several studies have demonstrated the diagnostic value of wall motion during dobutamine stress magnetic resonance imaging. At the same time high dose dobutamine has been applied as a stress agent in myocardial perfusion studies for echocardiography and nuclear imaging techniques.

Purpose: The aim of this study was to assess the feasibility and accuracy of high dose dobutamine stress myocardial perfusion imaging (DSMPI) with MRI in the diagnosis and localization of coronary artery disease (CAD).

Methods: Eighty consecutive patients (suspected and known CAD) scheduled for coronary angiography underwent cardiac MR (1.5 T). After a standard wall motion

examination rest perfusion was imaged, followed by standard DSMR/atropine stress CMR. During maximum stress DSMPI was performed. After a 10 minute break delayed enhancement imaging was carried out. For perfusion imaging we used a balanced steady state free precession (bSSFP) sequence (TE: 1.4 ms, TR: 2.8 ms, α: 50°), acquiring 4 slices (3 short axis views and 1 long axis view, spatial resolution: $2.8 \times 3 \times 10$ mm) every second heart beat. The sequence allowed imaging up to a heart rate of 160 beats per minute. A bolus of Gd-DTPA (0.05 mmol/kg bw) was injected both at rest and during maximum dobutamine-atropine stress when patients had reached their age-adjusted submaximal heart rate. CAD was defined as $\geq 50\%$ stenosis in major coronary arteries or their major branches. DSMPI was considered diagnostic of CAD in the presence of reversible perfusion abnormalities.

Results: CAD was detected in 53 (66%) patients by angiography. Reversible perfusion abnormalities were detected in 47 patients with and 9 patients without CAD. The overall sensitivity of DSMPI was 89%, specificity 67% and accuracy 84%. All patients with multivessel CAD were identified correctly. Regional sensitivity of CAD was 78% for left anterior descending, 61% for left circumflex and 75% for right coronary artery. Overall image quality was good. No patients had to be excluded due to non-diagnostic image quality.

Conclusions: DSMPI is a feasible and useful technique for the diagnosis of CAD and might respresent an alternative modality for stress perfusion imaging in patients with contraindications to adenosine.

123. CARDIOVASCULAR MAGNETIC RESONANCE PERFUSION IMAGING AT 3 TESLA FOR THE DETECTION OF CORONARY ARTERY DISEASE: A COMPARISON WITH 1.5 TESLA

Adrian S. H. Cheng, MBBS, MRCP,[1] Tammy J. Pegg, MBChB, MRCP,[1] Thedoros D. Karamitsos, MD,[1] Matthew D. Robson, PhD,[1] Nick Searle, DCR(R),[2] Michael Jerosch-Herold, PhD,[3] Robin P. Choudhury, DM, MRCP,[1] Adrian P. Banning, MD, FRCP, FESC,[1] Stefan Neubauer, MD, FRCP,[1] Joseph B. Selvanayagam, Dphil, FRACP, FESC.[1] [1] *University of Oxford, Oxford, United Kingdom,* [2] *Department of Radiology, John Radcliffe Hospital, Oxford, United Kingdom,* [3] *Advanced Imaging Research Center, Oregon Health & Science University, Portland, OR, USA.*

Introduction: Myocardial perfusion imaging is considered one of the most compelling applications for CMR at 3T. 3T systems provide increased signal-to-noise ratio (SNR) and contrast-to-noise ratio (CNR), compared with 1.5T, which may potentially improve spatial resolution and image quality.

Purpose: To compare the diagnostic performance of cardiovascular magnetic resonance (CMR) perfusion imaging at 3 Tesla (T) against 1.5 Tesla in patients with suspected coronary artery disease (CAD).

Methods: Sixty-one patients (age 64 ± 8 years) referred for elective diagnostic coronary angiography for investigation of exertional chest pain were studied (pre-angiogram) with first-pass perfusion CMR at both 1.5T (Sonata, Siemens Medical Solutions, Erlangen, Germany) and 3T (Trio, Siemens Medical Solutions) and at stress (140 mcg/kg/min intravenous adenosine) and rest. Perfusion imaging on each system was performed at least an hour apart and in randomised order. Four short axis images were acquired during every heartbeat using a saturation recovery fast gradient echo sequence (echo time 1.04 ms, repetition time 2 ms, voxel size $2.1 \times 2.6 \times 8$ mm^3) and 0.04 mmol/kg contrast agent (Gadodiamide, Omniscan, GE Healthcare) bolus injection, while patients held their breath for as long as possible in end-inspiration. Quantitative coronary angiography served as the reference standard. Perfusion of each myocardial segment (except the apex) was interpreted visually by 2 blinded observers. Significant CAD was defined angiographically as the presence of at least 1 stenosis of at least 50% diameter in any of the main epicardial
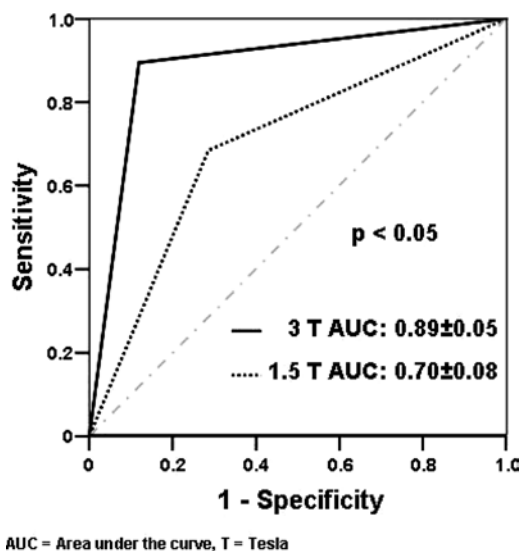
FIG. 1. Receiver operating characteristic curves for visual assessment of 1.5 and 3 Tesla perfusion imaging for the correct identification of single vessel disease. The diagnostic performance of 3 Tesla perfusion imaging was significantly greater (p < 0.05).

coronary arteries or their branches with a diameter of at least 2 mm.

Results: The prevalence of significant CAD was 66%. All perfusion images were found to be visually interpretable for diagnosis. 3T CMR perfusion imaging provided a higher diagnostic accuracy (90% vs. 82%), sensitivity (98% vs. 90%), specificity (76% vs. 67%), positive predictive value (89% vs. 84%) and negative predictive value (94% vs. 78%) for detection of significant CAD, compared to 1.5T. The diagnostic perfor-

mance of 3T perfusion imaging was significantly greater than that of 1.5T in identifying both single vessel disease (area under receiver operating characteristic (ROC) curve: 0.89 ± 0.05 vs. 0.70 ± 0.08; p < 0.05) and multi-vessel disease (area under ROC curve: 0.95 ± 0.03 vs. 0.82 ± 0.06; p < 0.05) (Figs. 1 and 2). For the LAD coronary artery, there was a strong trend to improved diagnostic performance at 3T for detection of LAD stenoses, compared to 1.5T (area under ROC curve: 0.92 ± 0.04 vs. 0.79 ± 0.06 respectively; p = 0.05). Diagnostic performance of 3T imaging for detection of circumflex stenoses was significantly greater than that at 1.5T (area under ROC curve: 0.84 ± 0.06 vs. 0.64 ± 0.08 respectively; p < 0.05). There was no significant difference in diagnostic performance of 3T and 1.5T for detection of RCA stenoses (area under ROC curve: 0.90 ± 0.04 vs. 0.91 ± 0.04 respectively; p = 0.98). 'Susceptibility artifacts' (hypoenhanced zone in the subendocardial layer before contrast material arrival) were observed more commonly at 1.5T compared to 3T (23% of patients vs. 8% of patients respectively, p < 0.01). 3T perfusion imaging provided a significant increase in both SNR (17 ± 6 vs. 11 ± 2 respectively; p < 0.01) and CNR (17 ± 10 vs. 11 ± 4 respectively; p < 0.01), compared to 1.5T.

Conclusion: 3T CMR perfusion imaging provided greater diagnostic performance than at 1.5T in identifying both significant single vessel and multi-vessel disease, and identified the anatomical location of coronary disease with high accuracy. 3T may become the preferred CMR field strength for myocardial perfusion assessment in clinical practice.

124. ABSOLUTE QUANTIFICATION OF MYOCARDIAL BLOOD FLOW USING FIRST-PASS PERFUSION MRI: EXTRACTION FRACTION OF GD-DTPA VARIES WITH MYOCARDIAL BLOOD FLOW IN HUMAN MYOCARDIUM

Masaki Ishida, MD,[1] Hajime Sakuma, MD,[1] Kakuya Kitagawa, MD,[1] Takashi Ichihara, PhD,[1] Hisato Maeda, PhD,[2] Yasuaki Goko,[3] Tairo Kurita, MD,[1] Kan Takeda, MD.[1] [1]*Mie University Hospital, Tsu, Mie, Japan,* [2]*Fujita Health University, Toyoake, Aichi, Japan,* [3]*AZE Ltd., Chiyoda-ku, Tokyo, Japan.*

Introduction: Quantitative analysis of blood input function and myocardial output function using deconvolution method or Patlak plot method can provide absolute quantification of unidirectional transfer constant (K1) of gadolinium contrast medium in the myocardium, which represents product of myocardial blood flow (MBF) and the extraction fraction (EF) of gadolinium contrast medium. Previous studies using animal models demonstrated that the EF of Gd-DTPA is approximately 0.5 in the resting state (1–3). However, the EF of Gd-DTPA has not been determined in human hearts. Another point of importance in quantifying MBF is that the EF of perfusion indicators is generally expressed as EF = 1-exp(-PS/MBF), where PS is a
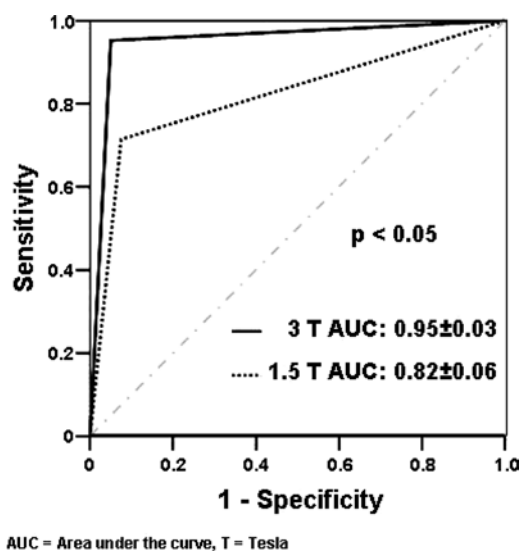

FIG. 2. Receiver operating characteristic curves for visual assessment of 1.5 and 3 Tesla perfusion imaging for the correct identification of multi-vessel disease. The diagnostic performance of 3 Tesla perfusion imaging was significantly greater (p < 0.05).
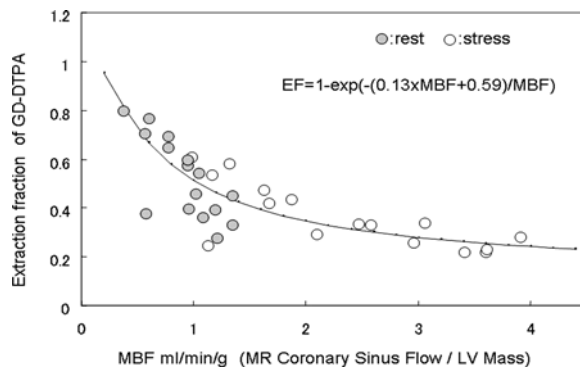
FIG. 1. Relationship between extraction fraction of Gd-DTPA and myocardial blood flow in human myocardium.

permeability-surface area product. This equation indicates that the EF of Gd-DTPA may be significantly reduced with pharmacological stress.

Purpose: The purpose of this study was to evaluate the relation between the EF of Gd-DTPA and MBF in human heart.

Methods: Sixteen subjects (9 men, mean age of 64 ± 12 years) with normal coronary arteries were evaluated with a 1.5 T MR system (Achieva, Philips Medical Systems). First-pass perfusion MR images were obtained with a saturation recovery balanced TFE sequence (TR 3.0 ms, TE 1.5 ms, TI 150 ms). In order to perform saturation correction of the blood signal, we initially obtained first-pass MR images by administrating diluted Gd-DTPA injection (0.005 mmol/kg). Then first-pass MR images were acquired at rest and during ATP stress with a dose of 0.05 mmol/kg. After correcting saturation of the blood signal and coil sensitivity profile, arterial input and myocardial output time-intensity curves were analyzed with a Patlak plot method to quantify myocardial K1. In addition to myocardial perfusion MRI, phase contrast cine MR images at rest and during stress were acquired to measure coronary sinus flow, and balanced TFE cine MR images were obtained to calculate LV mass. Mean MBF was determined as coronary sinus flow divided by LV mass. The EF of Gd-DTPA was quantified as the mean K1 (by quantitative perfusion MRI)/mean MBF (by coronary sinus flow/LV mass).

Results: The averaged EF of Gd-DTPA in the resting state was 0.52 ± 0.16 in 16 subjects, which showed a good agreement with the rest EF values previously reported in animal studies. The EF of Gd-DTPA during stress (0.36 ± 0.13) was significantly lower than the EF at rest ($p < 0.001$). Fig. 1 demonstrates the relationship between the EF and mean MBF in human myocardium. The fitted curve was expressed as $EF = 1 - \exp(-[0.13 \times MBF + 0.59]/MBF)$. This approximation formula is consistent with the Renkin/Crone equation, $EF = 1 - \exp(-PS/MBF)$, with an indication of slightly increased PS during hyperemia in human heart.

Conclusions: The EF of Gd-DTPA in human myocardium is approximately 0.5 in the resting state, which corresponds well with the rest EF reported in previous animal studies. The EF of

Gd-DTPA varies with the MBF. The current results indicate that the absolute MBF in the resting state and during stress can be accurately quantified from first-pass contrast enhanced MRI by performing a correction using the EF versus MBF curve determined in this study.

REFERENCES

1. Svendsen JH, et al. Cardiology 1992;80:18.
2. Diesbourg LD, et al. MRM 1992;23:239.
3. Tong CY, et al. MRM 1993;30:337.

125. STRONG LONG-TERM PROGNOSTIC VALUE OF VASODILATOR STRESS CMR MYOCARDIAL PERFUSION IMAGING IN PATIENTS WITH AN INTERMEDIATE PRE-TEST SUSPICION OF CORONARY ARTERY DISEASE

Kevin E. Steel, DO, Ryan J. Broderick, MD, Vijay Gandla, MD, Zelmira Curillova, MD, Sui Tsang, BSc, Raymond Y. Kwong, MD, MPH. *Brigham and Women's Hospital, Boston, MA, USA.*

Introduction: Vasodilator stress CMR myocardial perfusion (CMR_MP) can sensitively assess myocardial ischemia from flow-limiting coronary stenosis in patients with chest pain syndrome. However, knowledge regarding the long-term prognostic impact of CMR_MP remains limited.

Purpose: We tested the hypothesis that myocardial ischemia characterized by CMR_MP has strong prognostic association with major adverse cardiovascular events (MACE) in a patient cohort referred for suspected coronary artery disease (CAD).

Methods: CMR_MP was performed on 253 patients (149 males, mean age 58 ± 14 years) for evaluation of myocardial ischemia. Rest and stress first-pass CMR_MP were obtained on a 1.5T scanner using a T1-weighted notched-saturated fast gradient-echo sequence, with 0.05 to 0.1 mmol/Kg of gadolinium bolus, followed by late gadolinium enhancement imaging. All images were qualitatively interpreted for myocardial ischemia using the AHA/ACC 17-segment nomenclature, blinded to any clinical outcome. Any segmental reversible perfusion defect in absence of infarct by late enhancement was considered positive for myocardial ischemia. We used Cox proportional hazards regression to model the association of CMR_MP with MACE which includes new episodes of unstable angina, acute myocardial infarction, congestive heart failure, or death.

Results: The study cohort consisted of patients with intermediate cardiovascular risk (history of MI in 22% and diabetes in 25%). Eighty-two studies (32%) demonstrated abnormal stress perfusion of which 73 were consistent with myocardial ischemia. At a median follow up of 10 months (range 6 months–4.5 years), 18 fatal and 34 nonfatal events occurred (3 acute myocardial infarctions, 19 unstable angina, and 12 congestive heart failure). Event-free survival was significantly reduced in those with ischemia by CMR_MP (Fig. 1). Presence of ischemia was
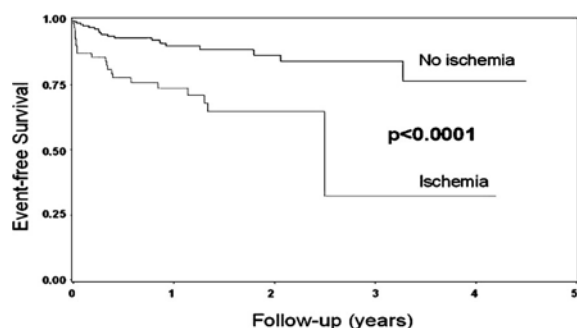
FIG. 1. CMR Stress Perfusion and MACE.

associated with a >3-fold hazard increase to MACE (HR 3.4, CI 1.8–6.4, p = 0.002) and when adjusted to patient age, number of coronary risk factors, history of myocardial infarction, and an abnormal baseline ECG the negative association of ischemia CMR_MP was still seen (adjusted HR 2.12, 95% CI: 1.03-4.38, p < 0.05). At 12 months after CMR, absence of CMR_MP evidence for ischemia demonstrated a favorable outcome (OR = 0.24, 95% CI:0.11–0.53, p = 0.0002).

Conclusions: CMR_MP provides strong long-term prognostic value for MACE in patients suspected of significant coronary stenosis, beyond common clinical risk assessment strategy.

Friday, February 2, 2007
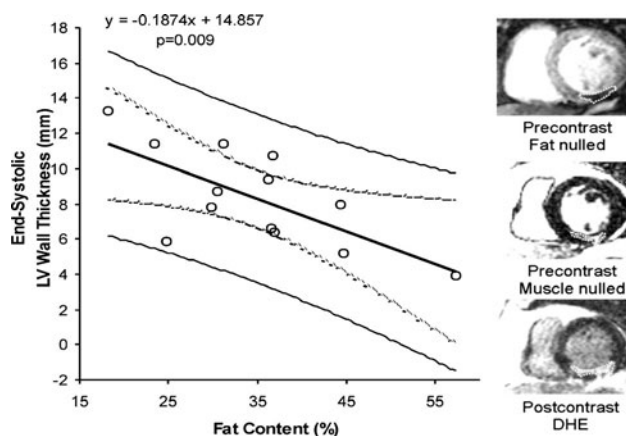## Oral Abstracts: Clinical-Session V

126. DECREASED POST-INFARCTION LV WALL THICKNESS IS ASSOCIATED WITH INCREASED MYOCARDIAL FAT CONTENT

James W. Goldfarb, Sheeba Arnold, Marguerite Roth, Jing Han. *St. Francis Hospital, Roslyn, New York, USA.*

Introduction: Improvements in the clinical and pathological characterization of myocardial infarction (MI) have led to better risk stratification, treatments and patient outcomes. Advances in the electrocardiographic and biochemical diagnosis of acute MI have affected not only the clinical care of patients, but also the tracking of epidemiological trends, public policy and clinical trials. After the acute stage, the description of infarct expansion and ventricular remodeling has led to an understanding of ventricular function changes and prognosis.

Pathology has provided excellent post-mortem descriptions of MI, but does not have the capability of showing the serial changes of human MI as non-invasive imaging can. As a result of its flexibility, CMR imaging has recently become a research tool and a clinical aid in the diagnosis and functional assessment of MI.

Older pathologic literature makes no reference to fat deposition in infarction. In 1997, an autopsy study reported that mature adipose tissue was often found within LV myocardial segments having MI. A second study in 2004 histologically confirmed the high prevalence (84%) of adipose tissue in healed myocardial infarcts. These studies provide complementary evidence that fatty tissue is present in myocardial scars where the normal architectural arrangement has been completely destroyed.

Purpose: Several autopsy studies indicate that myocardial fat deposition is common after infarction. MR imaging can quantify the amount of fatty tissue within myocardial infarction and measure functional and structural variables of the infarcted heart. We sought to determine the relationship between the two.

Methods: Thirteen patients (mean age: 63 ± 9 yrs) with prior infarctions (age of infarcts: 14 ± 7 yrs; range: 0.7–31 years) underwent functional CINE imaging, precontrast inversion recovery (IR) MR imaging using a TrueFISP IR CINE technique and delayed hyperenhancement (DHE) infarct imaging. T1 relaxation times of the infarct, adjacent myocardium and epicardial fat were measured from the images. Using a biexponential fit, the fat content of the infarct was estimated. Associations of infarct T1 relaxation times and fat content with clinical variables and those measured from DHE and CINE imaging were investigated using correlation analysis.

Results: Precontrast infarct T1 relaxation times were significantly (p < 0.0001) less than those of adjacent myocardium. T1 (infarct) = 454 ± 75 ms (350–575 ms); T1 (adjacent) = 664 ± 90 ms (532–860 ms); T1 (fat) = 286 ± 35 ms (234–375 ms). Infarct fat content was 34% ± 10% (range: 18% to 57%). There was a significant negative correlation between the infarct T1 relaxation time, fat content and LV wall thickness at both end-diastole and end-systole (Fig.).

Conclusions: Fatty replacement after myocardial infarction is a common process that can be assessed using inversion recovery precontrast MR imaging. The fat content of infarcted areas increases as the end-diastolic and end-systolic wall thickness decreases.

127. AUTOMATIC MOTION CORRECTION OF FREE-BREATHING DELAYED ENHANCEMENT IMAGING USING NON-RIGID REGISTRATION

Maria J. Ledesma-Carbayo, PhD,[1] Peter Kellman, PhD,[2] Andrew E. Arai, MD,[2] Elliot R. McVeigh, PhD.[2]

FIG. 1. Average of 30 images acquired during free breathing. Rigid body motion correction uses a user defined bounding region around the LV to optimize image registration. Non-rigid body motion correction is automatically performed over the full FOV without any user defined input.

[1] *Universidad Politecnica Madrid, Madrid, Spain,* [2] *NIH, Bethesda, MD, USA.*

Introduction: Single-shot imaging with inversion recovery true-FISP readout may be conducted during free-breathing (1–2). This provides an alternative to segmented, breath-held turbo-FLASH for cases where patients cannot tolerate breath-holding and is also an attractive protocol for reducing scan time. Single-shot true-FISP inversion recovery has been validated against conventional inversion recovery segmented turbo-FLASH for assessment of myocardial infarction (MI).

Respiratory motion corrected averaging of multiple images acquired while free-breathing may be used to substantially improve the image SNR. Fully automatic, non-rigid registration was compared with previously validated rigid body registration that required user interaction (2). The proposed technique provides improved performance across the full field-of-view as compared to the rigid body method.

Purpose: To develop and test an automatic free-breathing, delayed enhancement imaging method with improved image signal-to-noise ratio.

Methods: Free-breathing infarct images were acquired for multiple repetitions of a single-shot IR trueFISP sequence and averaged to enhance SNR following respiratory motion correction based on non-rigid body image registration. The performance between rigid (3) and non-rigid (4) methods was compared using the measured variance of edge positions in intensity profiles through the MI enhanced region and through the RV wall.

The imaging sequence (2) was ECG triggered, with 2 R-R intervals between inversions. Typical parameters were: bandwidth $= 977$ Hz/pixel, TE/TR $= 1.2/2.7$ ms, flip angle $= 50°$, image matrix $= 256 \times 128$. Parallel imaging (rate $= 2$) was used to obtain the full resolution with 64 phase encodes acquired in a single heartbeat. A phase-sensitive reconstruction (PSIR) method was used. Images were acquired on a Siemens Sonata 1.5T scanner.

Results: Short-axis images (Fig. 1) of the heart for a patient with anteroseptal MI were compared with and without motion corrected averaging. The non-rigid registration compensated the motion over the full field of view resulting in a sharper definition of the right ventricular wall and the MI compared with non-registered or rigid body registered images. Signal intensity profiles (Fig. 2) through each image in the free-breathing dataset allow assessment of the adequacy of registration for different parts of the heart. The left ventricle and myocardial infarction area are correctly aligned when either registration method is used; however, alignment is better through the full heart area using non-rigid registration, and a great improvement is achieved in the right ventricular area.

Measured variation of edge positions (N $=$ 6 patients) in intensity profiles showed significant improvement ($p < 0.005$) at the RV edge where the standard deviation was 2.06 ± 0.56 mm (mean $\pm$ SD) for rigid body and 0.59 ± 0.22 mm for non-rigid registration. Improvement in MI region was observed in 2 cases (Fig. 2c) but was not statistically significant; measured variation of MI was 1.16 ± 0.71 mm for rigid body and 1.08 ± 0.76 mm for non-rigid registration.
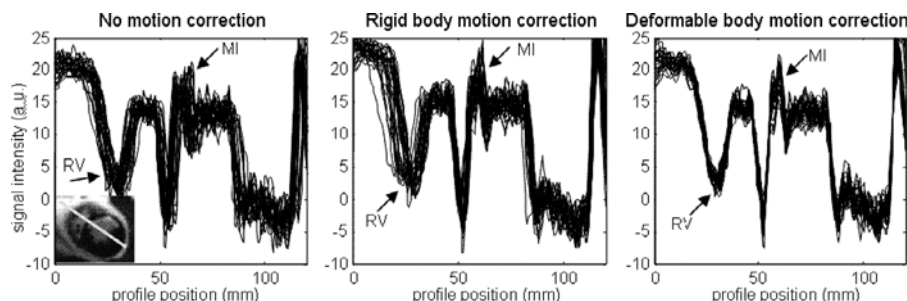

FIG. 2. Signal intensity profiles through the heart along line shown in inset image. Profiles for 30 images acquired during free-breathing are shown overlayed. The intensity profiles are well aligned across the full heart using non-rigid motion correction but have significant motion in RV using rigid body correction.

Conclusions: The proposed approach achieved delayed enhancement images with high resolution and SNR without requiring a breath-hold. Motion correction of free-breathing delayed enhancement imaging using non-rigid image registration was implemented in a fully automatic fashion and performed uniformly well across the full FOV.

REFERENCES

1. Chung Y, et al. JCMR 2002;4:12–13.
2. Kellman P, et al. MRM 2005;53:194–200.
3. Thevenaz P, et al. IEEE TIP 1998;7:27–41.
4. Kybic J, et al. IEEE TIP 2003;12:1427–1442.

128. MECHANISTIC INSIGHTS FROM SERIAL CARDIAC MAGNETIC RESONANCE AT 3 AND 15 MONTHS AFTER APPLICATION OF BLOOD-DERIVED PROGENITOR CELLS IN RECANALIZED CHRONIC CORONARY TOTAL OCCLUSIONS (CTO)

Holger Thiele, Andreas Schuster, Dietmar Kivelitz, Sandra Erbs, Volker Adams, Axel Linke, Rainer Hambrecht, Gerhard Schuler. *University of Leipzig—Heart Center, Leipzig, Germany.*

Introduction: Transplantation of circulating progenitor cells (CPC) was shown to improve left ventricular (LV) function after successful recanalization of CTO at short-term to mid-term follow-up. Cardiac magnetic resonance (CMR) is an excellent diagnostic tool for serial assessment of changes in left ventricular function and might uncover underlying mechanisms by assessment of myocardial perfusion and infarct size at mid-term and long-term follow-up.

Purpose: To assess the effects of CPC on infarct size, perfusion and left ventricular function at mid-term and long-term follow-up.

Methods and results: Twenty-eight patients with reperfused CTO were randomized to either CPC's or inactive serum (control) infused into the target vessel. Serial CMR performed at baseline, after 3 and 15 months revealed a significant increase in left ventricular (LV) ejection fraction in the CPC group (from 51 ± 14 to $58 \pm 13\%$ and $60 \pm 10\%$; $p < 0.01$ versus baseline), a decrease in endsystolic volume (from 68 ± 33 to 60 ± 33 mL and 60 ± 31 mL; $p < 0.05$ versus baseline) and unchanged enddiastolic volumes (136 ± 37 vs. 133 ± 33 and 147 ± 45, $p =$ n.s. vs. baseline). Infarct size decreased significantly from 10.3 ± 7.7 to 9.0 ± 7.2 and 9.5 ± 8.5 mL, $p < 0.05$ vs. baseline. First-pass myocardial perfusion at rest and stress using adenosine revealed significant improvement of the myocardial perfusion reserve index in affected segments by 1.50 ± 0.17 to 1.76 ± 0.16 ($p < 0.001$) and 1.82 ± 0.20 ($p < 0.001$) at 3 and 15 months, respectively. In control ejection fraction showed no increase at 3 ($p = 0.99$) but delayed improvement at 15 months ($p = 0.04$), whereas myocardial perfusion was improved at 3 ($p = 0.01$) and 15 months ($p = 0.004$) follow-up. There was an inverse relationship between infarct transmurality and regional functional improvement in control, whereas this effect was attenuated in the CPC group.

Conclusions: Analysis of serial CMR suggests that intracoronary application of CPC post CTO recanalization is associated with improved myocardial perfusion, reduction in infarct size and subsequent improved recovery of LV function as compared to control at mid-term and long-term follow-up.

129. ROLE OF LOW-DOSE DOBUTAMINE AND CONTRAST ENHANCED CARDIAC MR TO PREDICT FUNCTIONAL RECOVERY IN PATIENT WITH SINGLE CHRONIC CORONARY ARTERY OCCLUSION. FOLLOW UP MRI 6 MONTHS AFTER PERCUTANEOUS ANGIOPLASTY

Guido Ligabue, Federica Fiocchi, Sonia Ferraresi, Andrea Di Girolamo, Fabio A. Sgura, Renato Romagnoli, Pietro Torricelli. *Università di Modena e Reggio Emilia, Modena, Italy.*

Introduction: Low dose dobutamine and delayed enhancement imaging are employed in identifying viable myocardium in chronic ischemic patients.

Purpose: Evaluate which MRI parameter predicts better the recovery after revascularization procedure in patients with chronic coronary artery occlusion (CCO).

Methods: Nineteen patients (mean age 64.7) with angiographic proven CCO underwent delayed enhanced (DE) and low-dose dobutamine stress MRI (LDMR). Diastolic-wall-thickness (DWT) and dobutamine induced systolic-thickening (SWT) were measured in each infarct region that was also assigned a DE score (0 = no enhancement; 4 = enhancement > 75%). Viable myocardium was defined as a combination of these parameters introducing a new parameter: Viability Index (VI) = (SWT × DE)/100. Patients with transmural enhancement were excluded from revascularization procedure. At 6 months follow-up MRI, functional recovery was defined as 2 mm increase in SWT.

Results: The chronically occluded coronaries were the right (10), anterior descending (5) and circumflex (4). Contractility stress induced improvement (defined as 2 mm increase SWT) was present in 16/19 (mean DWT and SWT were 7.1 ± 2.6 and 4.3 ± 2.2 mm). Transmural enhancement (DE score of 4) was present in 3 patients without significant DWT and SWT ($3,4\pm1,7$ e $2\pm1,3$ mm). Of the remaining 16 patients mean DWT, SWT and VI were 7.8 ± 2.1, 4.3 ± 2.2 mm and 3.3 ± 1.9; DE score was 1 in 10.5%, 2 in 31.5% and 3 in 42.1%. Interventive procedure was successful in 14/16. Functional recovery of the CCO area was achieved in 12 patient. Post-revascularization DWT, SWT were 8.2 ± 1.7 mm, 3.08 ± 1.7 mm. Functional recovery showed significant correlation not only with SWT (Pearson

$r = 0.76$; $p < 0.001$), but even higher with VI ($r = 0.82$; $p < 0,001$).

Conclusions: Viability index, that express the contribution of viable myocardium to systolic thickening, can be used as a more accurate parameter to predict post-revascularization contractile recovery respect the widely used SWT.
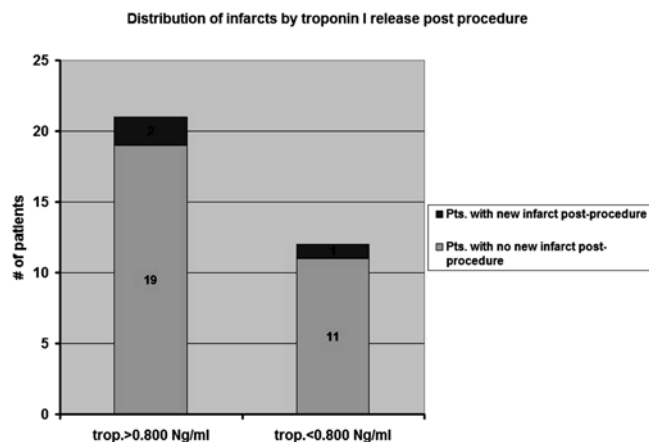
130. EVIDENCE OF PERI-PROCEDURAL MYOCARDIAL INFARCTION: INSIGHTS FROM TROPONIN I AND DELAYED HYPERENHANCEMENT

Nathan H. Calloway, Gaby Weissman, Anthon Fuisz. *Washington Hospital Center, Washington, DC, USA.*

Introduction: Delayed hyperenhancement (DHE) techniques are used to predict recovery of myocardial segments after revascularization. Peri-procedure Troponin-I measures are commonly used to assess for peri-procedure myocardial infarction. We hypothesized that DHE imaging before and after revascularization would offer unique information from peri-procedure cardiac enzymes.

Methods/Results: Thirty-three patients underwent functional and DHE imaging, pre and post-revascularization, and had peri-procedure troponin-I levels measured. Twenty-eight patients underwent CABG and five patients underwent PTCA. DHE images were acquired on a Philips Intera 1.5 T CV imaging platform using a SENSE 3D sequence, both short-axis and long-axis planes, 10 minutes following gadodiamide dosing 0.2 mmol/kg IV. Twenty-two patients had prior evidence of MI on pre-procedure DHE imaging. Of these infarcts, 10/22 (45%) were transmural. Peri-procedure troponin levels considered diagnostic of MI (> 0.800 Ng/mL) were seen in 21/33 (64%) of patients. DHE techniques showed new infarcts in new territories in 3/33 (9%) of patients.

Discussion: Peri-procedure Troponin-I may overestimate the incidence of peri-operative MI visible using DHE techniques. DHE imaging pre and post revascularization detects new infarcts in a new territories in a small group of patients.

131. THE PREDICTION OF VENTRICULAR TACHYARRHYTHMIA INDUCIBILITY BY QUANTIFICATION OF THE PERI-INFARCT BORDER ZONE BY DELAY-ENHANCEMENT CARDIAC MRI

Jason C. Rubenstein, MD, Daniel Lee, MD, Edwin Wu, MD, Alan Kadish, MD, Rod Passman, MD, Jeffrey Goldberger, MD. *Northwestern University, Chicago, IL, USA.*

Risk stratification for sudden cardiac death following a myocardial infarction remains a challenge. The peri-infarct border zone (BZ) as quantified by late gadolinium delayed-enhancement cardiac magnetic resonance (CMR) has been proposed as a risk stratification tool because it is associated with increased mortality in a human population (1). The postulated mechanism is that BZ identifies a potentially arrhythmic heterogeneous zone of viable and nonviable peri-infarct myocardium, but this has not been tested in humans. We had previously published the importance of infarct size in predicting electrophysiology study inducibility(2). We retrospectively assessed whether the additional determination of BZ predicted inducible arrhythmia during electrophysiological study (EPS).

Methods: CMR was performed in 48 patients with CAD who were referred for EPS to assess for inducibility of ventricular tachyarrhythmias (VT). CMR data was retrospectively re-analyzed for BZ quantification. Size of the BZ was identified as the area difference between 2 and 3 standard deviations above the mean signal intensity of remote myocardium surrounding the identified infarct zone, and expressed as a percent of total LV mass (Fig. 1). EPS results were classified as negative
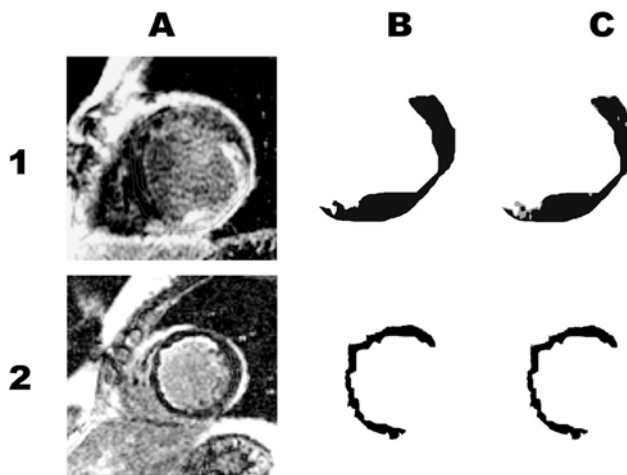

FIG. 1.   Example CMR images. Row 1 is a patient with a borderzone of 6.1%, infarct size of 19.3%, EF of 27.8%, and had MVT on EPS. Row 2 is a patient with a borderzone of 1.2%, infarct size of 22.1%, EF of 54.6%, and was non-inducible during EPS. Column A is the original short-axis delayed-enhancement CMR image with endocardial, epicardial, and remote myocardial ROI overlaid. Column B shows all pixels within the LV mass that are mean $+ \geq 2*$ SD of the remote ROI. Column C shows in grey all pixels with values between 2 and 3*SD over the mean of the remote ROI (borderzone), and all pixels $>3+$ mean in black.

(non-inducible) or positive (monomorphic VT). Patients with indeterminate EPS outcomes (VF or polymorphic VT), or those without a recoverable CMR were not included in this analysis.

Results: The study group consisted of 38 subjects with an average age of 60.2 ± 10.8 yrs and was 68% male. A total of ten patients were excluded from the analysis, nine for an indeterminate EPS and one for unrecoverable CMR. During EPS, 20 patients were non-inducible for ventricular arrhythmia and 18 had induced monomorphic VT (MVT). There was no significant difference between the two groups in terms of age, gender, history of MI, CHF, DM, HTN, β-blocker or ACE-I use. EF was also not significantly different between non-inducible patients and those with MVT (33.4 ± 11.9% vs. 28.1 ± 9.3, p=0.13). BZ was significantly different (1.4 ± 1.3% vs. 3.1 ± 1.5%, p = 0.001), as was infarct size (15.0 ± 11.6% vs. 26.4 ± 12.0%, p = 0.005). BZ was not well correlated to infarct size (Pearson = 0.467). Multivariate analysis demonstrated that BZ was the strongest independent predictor of EPS outcome after controlling for infarct size (OR 1.97 per % change, 95% CI 1.04 to 3.73, p = 0.04). Borderzone remained the strongest independent predictor when controlling for both infarct size and EF, (OR 2.12 per % change, 95% CI 1.06 to 34.22, p = 0.03).

Conclusion: This study demonstrates that large BZ size as measured by CMR is a stronger predictor of inducible MVT than either EF or infarct size. Furthermore, BZ is only weakly correlated to infarct size, and appears to give additional information beyond a geometric relation to larger infarcts. This data supports the hypothesis that ventricular arrhythmias may be responsible for the reported association between BZ and mortality and suggests that BZ may be another CMR marker of elevated risk of sudden cardiac death.

REFERENCES

1. Yan
2. Bello

132. CORRESPONDENCE BETWEEN CORONARY VASCULATURE AND THE 17-MYOCARDIAL SEGMENT MODEL

Jose T. Ortiz, MD, Jose F. Rodriguez, MD, Preeti Kansal, MD, Sheridan N. Meyers, MD, Daniel C. Lee, MD, Edwin Wu, MD. *Northwestern University, Chicago, IL, USA.*

Background: The American Heart Association suggests the use of a 17-myocardial segment model for reporting results in all cardiac imaging modalities. The information currently available regarding the correspondence between different coronary arteries and the area at risk is based on nuclear scintigraphy studies. Contrast-enhanced CMR (ce-CMR) yielding exquisite high spatial resolution images, is more accurate than nuclear perfusion techniques for detecting irreversible necrotic myocardium. Using ce-CMR, we studied the correspondence between the culprit lesion upon angiography and its dependent myocardium at risk in a model of patients with reperfused first ST-segment elevation acute myocardial infarction (STEMI).

Methods: A standard ce-CMR study was acutely performed in 93 patients presenting with their first STEMI and initial Thrombolysis In Myocardial Infarction (TIMI) flow ≤1 in the infarct related artery. Two experienced invasive cardiologists noted the location of the culprit lesion and the dominancy from the initial coronary angiogram. Two additional experienced CMR cardiologists observers blinded to the angiographic findings evaluated the basal, mid-ventricular and apical short axis ce-CMR slices as well as the long axis 2-chamber views. Segments with any hyperenhancement (HE) were scored on the 17-myocardial segment model.

Results: Forty-four subjects had occlusion of the left descending artery (LAD), 34 right coronary artery (RCA), and 15 had occlusion of the left circumflex (LCX) or ramus. The Fig. displays the individual specificities for each segment according to the infarct related artery. The presence of HE in the basal anteroseptal (Segment 2), mid-anterior (Segment 7), mid-anteroseptal (Segment 8) or apical anterior segments (Segment 13) was 100% specific for LAD occlusion. In patients with an anterior infarction, involvement of the basal anteroseptum (Segment 2) was also highly specific (85%) for *proximal* LAD occlusion. No single segment was specific for RCA or LCX occlusion. However, involvement of basal anterolateral segment (Segment 6) was highly specific (98%) of LCX or ramus occlusion. Specificity for LCX occlusion was further increased to 100% when accompanied by HE in the basal inferolateral (Segment 5), mid-inferolateral (Segment 11) or apical lateral (Segment 16). Combination of HE in the inferior and inferoseptal segment were related to either RCA or *left dominant* LCX occlusion.

Conclusion: The anteroseptal, mid and apical anterior segments are the only segments specific for LAD occlusion. No
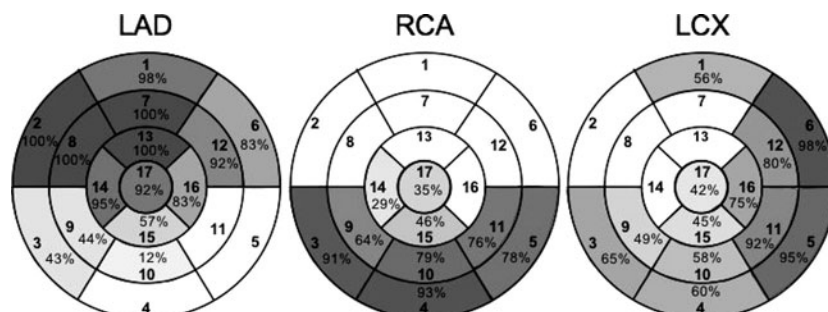

FIG. 1.   Specificity of segment involvement according to infarct realated artery.

segment can be exclusively attributed to the RCA or LCX occlusion. However, the combination of HE in adjacent segments increased the specificity for a given coronary artery occlusion. The results of this study reflect the wide anatomical variability of human coronary distribution and may be helpful when interpreting the coronary correspondence of stress perfusion CMR and viability studies.

Friday, February 2, 2007
Oral Abstracts: Experimental-Session VI

133.   ACTIVATABLE TARGETED MRI CONTRAST AGENT FOR MOLECULAR IMAGING OF FIBRIN

Patrick Winter,[1] Kejia Cai,[1] Junjie Chen,[1] Garry Kiefer,[2] Christopher Adair,[2] Phillip Athey,[3] Patrick Gaffney,[4] Shelton Caruthers,[5] Samuel Wickline,[1] Gregory Lanza.[1] [1]*Washington University, St. Louis, MO, USA,* [2]*Macrocyclics, Dallas, TX, USA,* [3]*Dow Chemical Co., Freeport, TX, USA,* [4]*St. Thomas' Hospital, London, United Kingdom,* [5]*Philips Medical Systems, Cleveland, OH, USA.*

Introduction: Fibrin is a hallmark of ruptured atherosclerotic plaques, which are the proximate cause of myocardial infarction and stroke. Fibrin in microthrombus cannot be detected with traditional MRI techniques, requiring the development of specifically targeted contrast agents. Typical MRI contrast agents alter the local relaxation times to produce observable contrast, but identification of early pathology may require imaging before and after contrast agent injection in order to recognize subtle changes in signal intensity. A new class of MRI contrast agents that do not require pre- and post-injection imaging are paramagnetic chemical exchange saturation transfer (PARACEST) chelates, which can be switched "on" or "off" at will with pre-saturation pulses. PARACEST agents have a slowly exchanging bound water signal at a resonant frequency far away from the bulk water. Saturation of the bound water can lead to transfer of magnetization into the bulk water pool. To detect PARACEST agents, saturation pulses are applied at the bound water frequency, which induces a decrease in the bulk water signal.

Purpose: This study demonstrates the use of a targeted PARACEST nanoparticle contrast agent to image fibrin in vitro.

Methods: A water-soluble PARACEST chelate, europium-methoxy-DOTA, was conjugated to a lipophilic tail, phosphotidylethanolamine, for incorporation onto perfluorocarbon nanoparticles. Phantoms (150 μL) containing PARACEST nanoparticles or the free chelate were prepared with identical europium concentrations, 2.1 mM. [1]H spectra were collected at 4.7 T from nanoparticles or the free chelate using a 5 second pre-saturation pulse at frequency offsets ranging from ±100 ppm in 1 ppm increments. The bulk water signal intensity was integrated and plotted against the saturation offset frequency. Plasma clots were formed by combining human plasma, thrombin and calcium chloride. Clots were suspended on a suture in individual vials of PBS. PARACEST (n = 5) or control (n = 4) nanoparticles were targeted to the clots utilizing anti-fibrin antibodies. Gradient echo images were collected of the clots at 4.7 T with a 2.5 second saturation pulse applied at either +52 ppm or −52 ppm (TR = 2.52 s, TE = 4.4 ms, slice thickness = 4 mm, 156 μm by 156 μm resolution). The 52 ppm images were subtracted from the -52 ppm images to detect PARACEST contrast.

Results: PARACEST nanoparticles displayed clear saturation transfer at a frequency offset of 52 ppm, producing a similar change in signal as the free PARACEST chelate. Fibrin-targeted PARACEST nanoparticles bound to the clot surface and produced a CNR >10 on the subtraction images (Fig. 1). Control nanoparticles, lacking the PARACEST chelate, did not generate any appreciable MRI contrast, CNR = 2.2.

Conclusions: This study demonstrates the first targeted PARACEST nanoparticle contrast agent. The unique ability to turn contrast on and off may allow detection of fibrin associated with unstable or disrupted plaques without imaging before and after contrast agent injection. These agents and techniques may have clinical advantages for localizing lesions responsible for unstable angina or transient ischemic attacks.
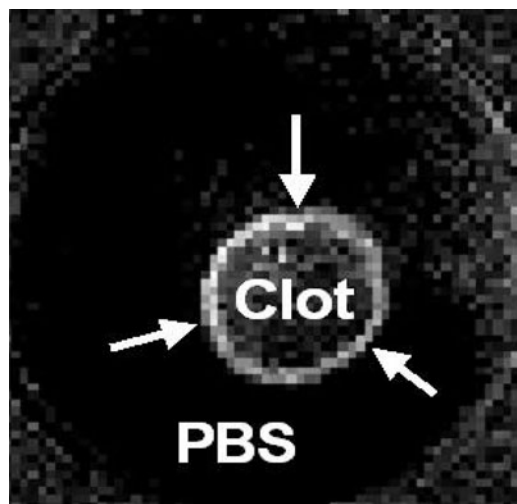

FIG. 1.   Subtraction image of clot treated with fibrin-targeted PARACEST nanoparticles demonstrating clear enhancement along clot surface (arrows).

134.   COULD MACROPHAGE INFILTRATION BE AN EARLY MARKER FOR GRAFT CORONARY ARTERY DISEASE (GCAD)? SINGLE MACROPHAGES DETECTED WITH IN VIVO MRI IN A GENETIC MIS-MATCHED CHRONIC CARDIAC ALLOGRAFT REJECTION TRANSPLANTATION MODEL

Yijen L. Wu, PhD,[1] Qing Ye, MD,[1] Lesley M. Foley, BS,[1] T. Kevin Hitchens, PhD,[1] Haval Shirwan, PhD,[2] Chien Ho, PhD.[1] [1]*Carnegie Mellon University, Pittsburgh, PA, USA,* [2]*University of Louisville, Louisville, KY, USA.*
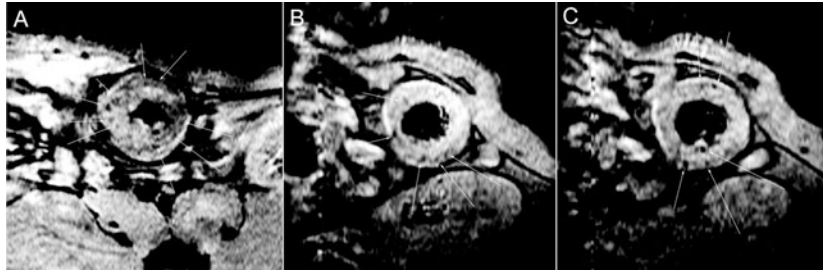
FIG. 1. T2*-weighted in vivo MRI, with in-plane resolution of 156 micrometer, for an allograft on POD 22 (A) and 37 (B, C) after MPIO labeling. Very sparse punctate and distinct contrast spots can be seen, as indicated with white arrowheads, which represent macrophages infiltrated at the graft, even though no detectable acute rejection is present at this stage.
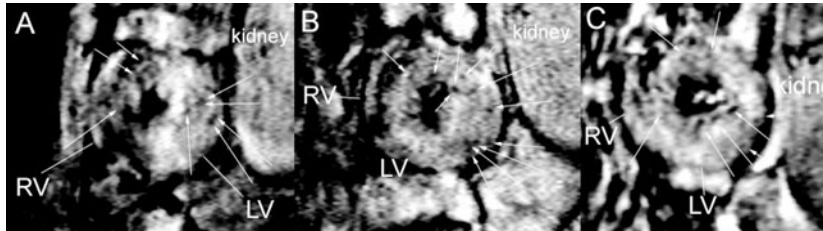

FIG. 2. Repetitive T2*-weighted in vivo MRI, with in-plane resolution of 156 micrometer, for an allograft on POD 21 (A), POD 29 (B), and POD 42 (C), after single MPIO administration on POD 20. White arrowheads point to individual macrophages infiltrated.

FIG. 3. MR microscopy, with 46 micrometer isotropic resolution, of an allograft heart at POD 22, showing both short-axis (left) and long-axis (right) views.
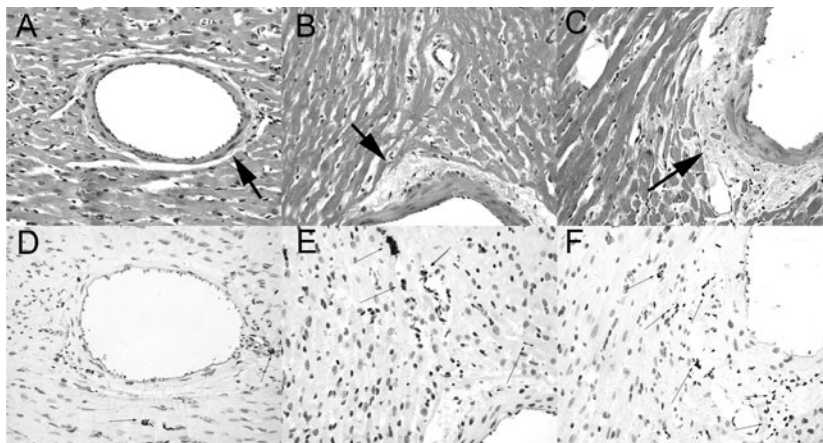Q5 Each dark spot is one single macrophage.

FIG. 4. H&E staining (A, B, C) and anti-rat ED1 macrophage staining (D, E, F) for allografts on POD 22 (A, D), POD 37 (B, E), and POD 77 (C, F). Thick arrowheads are pointing to the arterial intimal thickening, whereas thin arrowheads are pointing to ED1+ macrophages. The arterial intimal thickening comprising smooth muscle cell proliferation, fibrosis and mononuclear cell infiltration were observed on day 37(B, E) and became more severe as chronic rejection gradually progresses on POD 77 (C, F).

Introduction: Despite the fact that acute rejection largely can be managed, graft coronary artery disease (GCAD), or chronic rejection, remains the main limiting factor for the long-term survival after heart transplantation. The hallmark of chronic cardiac rejection is generalized concentric proliferative vasculopathy, whereas the dominant feature in acute rejection is lymphocytic and monocytic inflammation. Although the frequency and severity of acute rejection are known to be the most predictive factor for developing chronic rejection later in time, the mechanistic relation between acute and chronic rejection is poorly understood. In addition, it is not clear how and whether immune cell infiltration is contributing to the development of GCAD.

Shirwan et al. (1) have developed a rodent single-gene-mismatched transplantation model for chronic cardiac allograft rejection, transplanting between PVG.1U (RT1.AuBuDuCu) and PVG.R8 (RT1.AaBuDuCu) rats. The allografts develop chronic rejection in the absence of acute rejection and in no need of immunosuppressive manipulation. Chronic rejection is evident by post-operational day (POD) 20 and very extensive by POD 100. A distinct advantage of this rat model is the antigenic simplicity without immunomodulation, thus facilitating studies aimed at the elucidation of immunological mechanisms of chronic allograft rejection, including the effects of immunosuppressive drugs.

Purpose: The goal of this study is to investigate the possible involvement of macrophages in the GCAD by non-invasive in vivo MRI monitoring.

Methods:

1. Animal model: An abdominal heterotopic working heart and lung transplantation model is implanted, exhibiting physiological cardiac outputs.
2. MRI methods: T2* imaging was used to evaluate iron oxide particle accumulation. Tagging was achieved by a modified DANTE sequence. Gd (0.03 mmol/kg) contrast-enhanced-first-pass perfusion is used to monitor myocardial perfusion. All in vivo MRI scans were performed on a Bruker AVANCE 4.7 T system; whereas MR microscopy at 11.7 T.
3. Cell labeling: Immune cells, mostly macrophages, are labeled by direct i.v. injection of 1 to 3 mg micrometer-sized paramagnetic iron oxide (MPIO) particles, purchased from Bangs Laboratory.

Results: After single administration of MPIO particles, macrophage infiltration is monitored by repetitive in vivo MRI at 24 hours, then every 2 weeks for 4 months after transplantation surgery. Myocardial function is monitored by cardiac tagging, as an index for acute rejection; whereas quantitative myocardial perfusion is monitored by Gd contrast-enhanced-first-pass perfusion, as an index for chronic rejection.

There is no or little myocardial wall motion abnormality observed up to 12 weeks after transplantation, evaluated by tagging. Pathological analysis confirms that there is no acute rejection on POD 37. Interestingly, although no apparent acute rejection is observed both by tagging and histology, some immune cells, mainly macrophages, can be seen in the rejecting grafts. As early as POD 22, when there was no detectable acute rejection and no alteration with myocardial perfusion, few but very distinct punctate circular spots of hypointensity can be seen in allograft hearts (Fig. 1). This early infiltration of immune cells can be monitored non-invasively over time for a few months (Fig. 2).

As shown earlier in our acute rejection model (2), each spot of hypointensity is likely to be one single macrophage infiltrated in the graft. High-resolution MR microscopy (Fig. 3) and pathology (Fig. 4) confirms the few macrophage infiltrations in the very early stage. This is indicative that macrophages, although very few, are present at very early stage of chronic rejection without detectable acute rejection.

Conclusions: Our result indicates that macrophage infiltration might be an early marker for chronic rejection. Our approach may have great potential of impacting understanding cellular mechanism for chronic rejection.

REFERENCES

1. Shirwan H, et al. Transpl Immunol 2003;11:179–85.
2. Wu YL, et al. Proc Natl Acad Sci 2006;103:1852–1857.

135. MONITORING OF MATRIX METALLOPROTEINASE ACTIVITY IN ATHEROSCLEROTIC PLAQUES OF HYPERCHOLESTEROLEMIC RABBITS WITH A SPECIfiC CONTRAST AGENT AND MRI

Fabien Hyafil, MD,[1] Jean-Christophe Cornily, MD,[1] Esad Vucic, MD,[1] Vardan Amirbekian, MD,[1] Karen Briley-Saebo, PhD,[1] Eric Lancelot, PharmD,[2] Claire Corot, PharmD,[2] Laurent J. Feldman, MD, PhD,[3] Zahi A. Fayad, PhD.[1] *[1]Mount Sinai School of Medicine, New York, NY, USA, [2]Guerbet, Aulnay, France, [3]Bichat Hospital, Paris, France.*

Introduction: Matrix metalloproteinases (MMPs) are involved in atherosclerotic plaque growth and rupture. P947 (Guerbet) is a new MRI contrast agent formed of a peptide with a high affinity for MMPs, bound to a molecule of gadolinium chelate (molecular weight: 1210 daltons; R1 = 5.5 mM-1s-1 at 1.5 Tesla).

Purpose: We assessed the hypothesis that MMP activity can be monitored in atherosclerotic plaques of hypercholesterolemic rabbits with P947-enhanced MRI.

Methods: Atherosclerotic plaques were induced in the aorta of New-Zealand White rabbits (n = 8) by two consecutive balloon injuries (4 weeks apart) and 4 months hypercholesterolemic diet. At four months, a T1-weighted MRI of the aorta was acquired in the eight rabbits before and 90 minutes after intravenous injection of 50 μmol Gd/kg of P947. One week later, the same animals were imaged with the same imaging protocol after injection of 50 μmol Gd/kg of a conventional MRI contrast agent (Gd-DOTA). After this first imaging session,

4 rabbits were maintained on a high-cholesterol diet ("progression" group) and 4 rabbits were switched to a chow diet ("regression" group). A second imaging session was performed 4 months later in both groups using the same imaging protocol as for the first imaging time point. On each axial slice, signal intensities (SI) were measured on images acquired before and 90 minutes after the injection of each contrast agent in regions of interest placed in the aortic wall, in the muscle and outside of the rabbit (noise). Contrast to noise ratio (CNR) was calculated by dividing the signal to noise ratio of atherosclerotic plaques by the signal intensity of muscle. Enhancement of atherosclerotic plaques was measured as follows: Enhancement = [(CNR after contrast agent/CNR before contrast agent) $\times$ 100]$-$100. The MMP activity was quantified in the media culture of 5 mm long aortic segments incubated 24 hours using SDS-PAGE gelatin zymography.
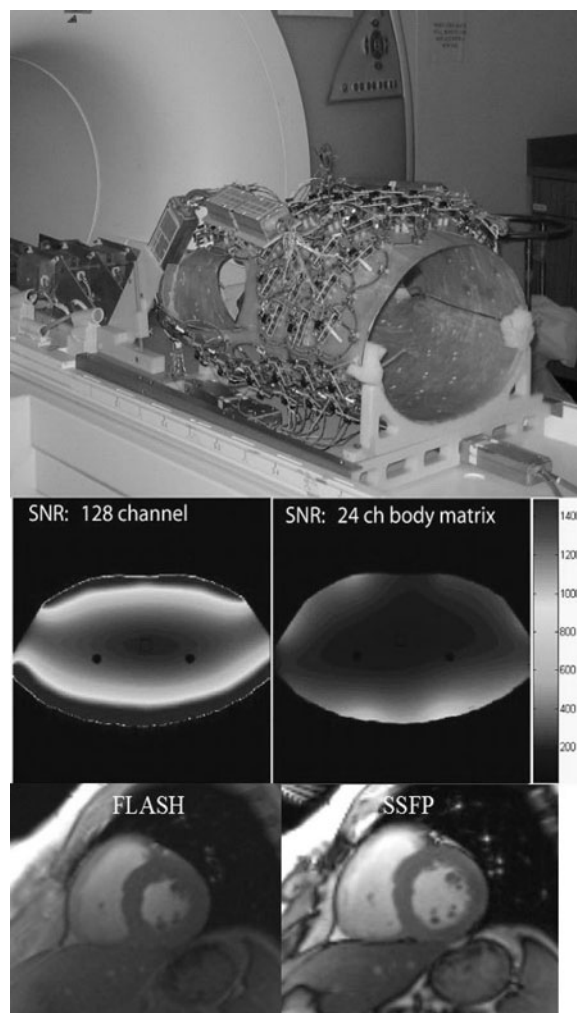
Results: On the first P947-enhanced MRI, signal intensities of atherosclerotic plaques increased similarly in rabbits from the "progression" group (42.4 $\pm$ 4.8%) and from the "regression group" (43.5 $\pm$ 9.1 %). On the second P947-enhanced MRI, signal enhancement in atherosclerotic plaques from the "progression" group was similar to the first MRI (40.4 $\pm$ 5.6%; p = NS vs. first MRI), whereas a significantly lower enhancement was found in the "regression group" (18.6 $\pm$ 5%; p = 0.05 vs. first MRI). No significant difference in signal intensity was found in atherosclerotic plaques on MRI after injection of Gd-DOTA. The mean gelatinolytic activity of MMP2 measured with SDS-PAGE gelatin zymography was significantly higher in the media culture of atherosclerotic plaques from the "progression group" compared to atherosclerotic plaques from the "regression group" (optical density: 42183 $\pm$ 19006 vs. 23514 $\pm$ 10109; p < 0.05).

Conclusions: P947-enhanced MRI allows for the monitoring of MMP activity in atherosclerotic plaques of hypercholesterolemic rabbits and represents a very promising non-invasive technique for the evaluation of therapies aimed at plaque stabilization.

136.   A 128 CHANNEL RECEIVER COIL FOR CARDIAC MR AT 3T

Melanie Schmitt,[1] Andreas Potthast,[2] David E. Sosnovik,[1] Graham C. Wiggins,[1] Lawrence L. Wald.[1] [1]*Massachusetts General Hospital, Charlestown, MA, USA,* [2]*Siemens Medical Solutions, Malvern, PA, USA.*

Introduction: MR coronary angiography is currently limited by both sensitivity and the ability to encode 3D high resolution images within a short scan time. Parallel imaging methods offer the potential to both significantly accelerate the encoding of 3D images and improve their sensitivity. Preliminary results from ourselves and others have demonstrated the increasing benefit of increased parallel detection for both sensitivity and accelerated

encoding (1, 2). In this work, we test the utility of expanding this approach to determine the added benefits of parallel imaging technology if the coil designer was unconstrained by the number of RF channels available on the instrument.

We have therefore developed a 128-channel receiver coil, specifically for cardiac MR imaging at 3T.

Methods: The coil (Fig. 1 top) consists of a fiberglass cradle molded to a model thorax ($\sim$85 kg male) with a "clamshell" geometry. The posterior portion houses 68 circular coil elements, while the anterior portion houses 60 elements, each with a diameter of 75 mm. The coils were arranged in a continuous overlapped array of hexagonal symmetry to minimize next neighbor coupling. The preamplifier of each coil element is positioned approximately 3 cm above the corresponding element to improve compactness. Initial testing of the coil was done on a Siemens Tim TRIO 3T whole body scanner extended to accommodate 128 independent receive channels. SNR values and G-factor maps were evaluated on a pixel by pixel basis from images acquired with a GRE sequence. The results of the 128 channel coil were then compared to those acquired with the Siemens Body Matrix and Spine Matrix coils using 24 elements. To also

show the properties of the coil for in vivo imaging, ECG-gated gradient echo and SSFP (tru-fisp) cines imaging was performed in a healthy volunteer.

Results: The images in the middle row of Fig. 1 show the SNR maps for both the 128 channel coil and the 24 element body matrix coil, calculated with an optimum reconstruction method, in which the noise correlation between the coils is accounted for in the reconstruction. The 128 channel array showed considerable gains in SNR in the periphery ($\sim$2 fold) and an increase of 25% in the middle of the phantom compared to the values from the conventional 24 channel array. The G-factor maps for an acceleration factor of 5 indicate a maximum G-factor of only 1.5 for the 128 channel coil, and a maximum G-factor of 6 for the matrix coil. Additionally, in-vivo images with the coil showed a high degree of image quality (bottom row of Fig. 1).

Conclusion: A prototype 128 channel cardiac coil has been successfully developed and tested for cardiac imaging. The SNR gain and the 4 times lower G-factor found for the 128 channel coil makes this coil highly promising for parallel imaging using high acceleration factors. This raises the possibility that whole heart coronary angiograms will be able to be performed robustly in a single breath hold using this coil.

REFERENCES

1. Wiggins GC, et al. MRM 2006;56:216–223.
2. Niendorf T, et al. MRM 2006;56:167–176.

137. MOLECULAR IMAGING OF MACROPHAGE ACTIVITY IN ATHEROSCLEROTIC PLAQUE USING QUANTUM DOT CONTAINING BIMODAL PEG-MICELLES

Esad Vucic, MD,[1] Willem Mulder, PhD,[1] Gustav Strijkers, PhD,[2] Karen C. Briley-Saboe, PhD,[1] Juan C. Frias,[1] Juan

G. S. Aguinaldo, MD,[1] Vardan Amirbekian, MD,[1] Cheuk Tang, PhD,[1] Patrick T. K. Chin, PhD,[2] Klaas Nicolay, PhD,[2] Zahi A. Fayad, PhD.[1] [1]*Mount Sinai School of Medicine, New York, NY, USA,* [2]*Eindhoven University of Technology, Eindhoven, The Netherlands.*

Introduction: A relatively new and emerging diagnostic imaging method for atherosclerosis is MR based molecular imaging. The aim of the technique is to visualize pathological processes related and associated to atherosclerosis at the cellular and molecular level for improved characterization of disease progression and characterization of plaque phenotype, in particular. Molecular imaging of macrophages may be of great use in predicting the severity of the disease, since macrophage rich plaques are believed to be unstable. We developed a molecular imaging method to improve the detection and characterization of atherosclerotic plaques with magnetic resonance imaging in vivo.

Methods: Pegylated, fluorescent and paramagnetic micelles were developed. The micelles were prepared from a Gd-DTPA based amphiphile and a pegylated lipid. For improved plaque detection and characterization the micelles were conjugated with macrophage scavenger receptor (MSR) specific antibodies. The abdominal aorta of atherogenic ApoE-KO mice were imaged with T1-weighted high resolution MRI before and 24 hours after intravenous administration of the contrast agent. Non-targeted micelles served as a control contrast agent. To allow fluorescence microscopy and optical imaging of the excised aorta, the micelles were made fluorescent by either incorporating a quantum dot (QD) in the micelle corona or by incorporating rhodamine lipids in the micelle both nanoparticles had a mean size of 15 nm.

Results: Pronounced signal enhancement (up to 200%) was observed for apoE-KO mice that were injected with MSR targeted micelles, while the aortic vessel wall of mice injected with
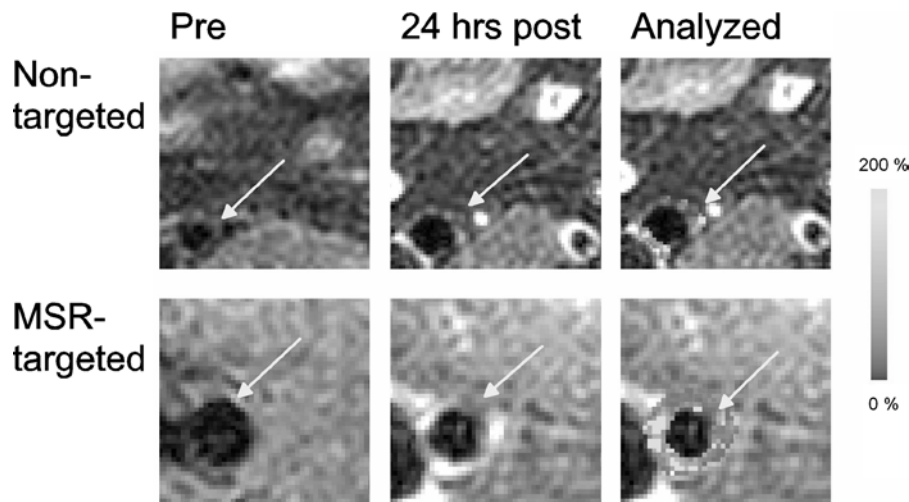

FIG. 1. High resolution T1-weighted MR images before and 24 hours after administration of non-targeted (upper row) and macrophage scavenger receptor (MSR) Ab-micelles (lower row). Analyzed pixels in the ROI of the aortic wall were color according to the observed signal enhancement (3rd row).
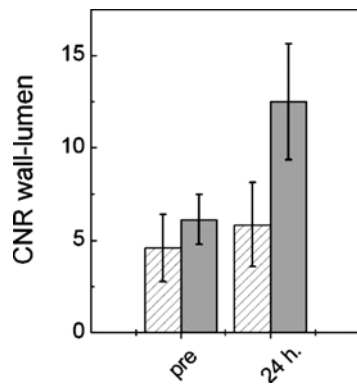
FIG. 2. Contrast to noise ratio (CNR) before and 24 h after injection of either micelles (white bars) or antibody conjugated micelles (grey bars).
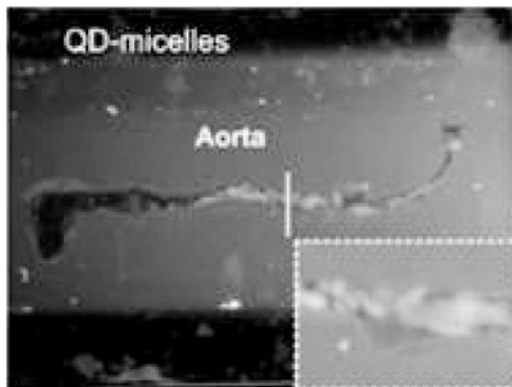

FIG. 3. UV illumination of an excised aorta showed green fluorescence emitting regions.
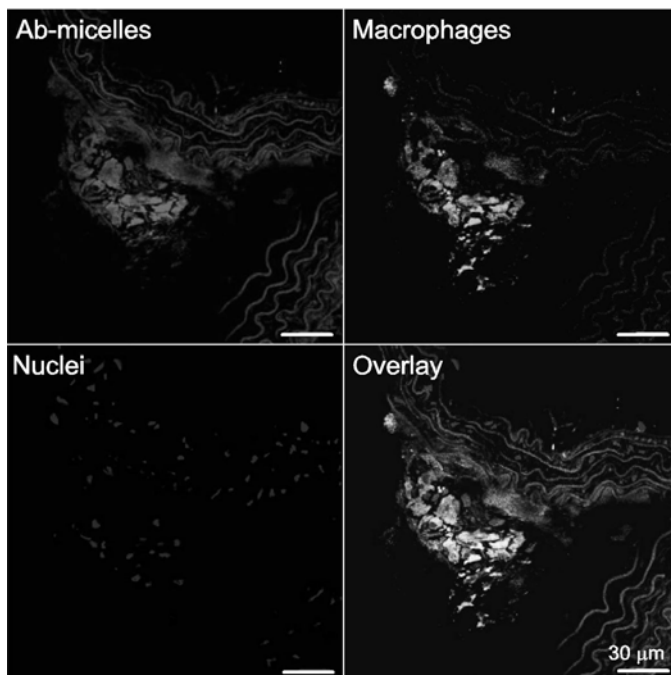

FIG. 4. Confocal microscopy of athersclerotic plaque after injection of rhodamine tagged macrophage targeted micelles (red) with costaining for macrophages (CD 68, green).

non-targeted micelles showed little signal enhancement (Figs. 1, 2). UV illumination of the aorta allowed the identification of regions with high macrophage content (Fig. 3), while MRS targeted rhodamine micelles could be detected with fluorescence microscopy and were found to be associated with macrophages (Fig. 4).

Conclusion: This study demonstrates that macrophage activity in apoE-KO mice can be effectively and specifically detected by molecular MRI and optical methods upon administration of the pegylated micellular contrast agent. The size, specificity, and the bimodal character of the micellular contrast agent allows MR and optical molecular imaging of extravascular targets and may be employed for detection of other markers of atherosclerosis.
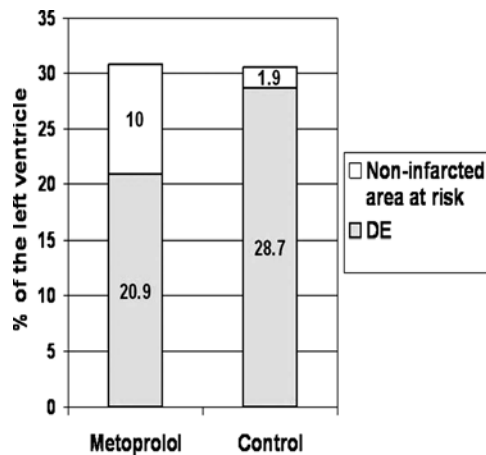
138. IMMEDIATE ADMINISTRATION OF INTRAVENOUS METOPROLOL DURING ONGOING MYOCARDIAL INFARCTION RESULTS IN REDUCED INFARCT SIZE. A CARDIAC MAGNETIC RESONANCE STUDY

Javier Sanz, MD, Borja Ibanez, MD, Susanna Prat-Gonzalez, MD, Gemma Vilahur, DVN, Antonio Pinero, MD, Walter Spiedl, MD, Giovanni Cimmino, MD, Valentin Fuster, MD, PhD, Juan Jose Badimon, PhD. *Mount Sinai School of Medicine, New York, NY, USA.*

Introduction: Clinical guidelines recommend administration of betablockers in acute myocardial infarction (MI). In this scenario, betablockers have been shown to improve survival and prevent left ventricular remodeling. However, the effect of "early" betablocker therapy on infarct size when administered during an ongoing MI remains controversial, particularly in reperfused MI. Cardiac magnetic resonance (CMR) constitutes an optimal imaging modality for non-invasive assessment of both necrotic area and non-infarcted area at risk (defined as edematous tissue without necrosis).

Purpose: To test the effect of "early" intravenous metoprolol administered during an ongoing MI on the extent of the necrotic area and the non-infarcted area at risk in a porcine model of experimental MI.

Methods: Acute MI was induced in Yorkshire albino pigs (n = 10; weight 35 ± 5 kg) by balloon occlusion of the left anterior descending (LAD) artery distal to the first diagonal for 90 minutes. Amiodarone and lidocaine were infused continuously during the procedure. Oral clopidogrel was started 24 hours before the intervention and maintained for 5 days after. The pigs were randomized to receiving 7.5 mg of intravenous metoprolol immediately after the LAD occlusion or to a control group. CMR was performed 4 and 21 days post-MI using a 1.5 Tesla magnet, electrocardiographic gating and a dedicated phased-array surface coil. Contiguous short-axis cine images of the entire left ventricle were acquired with a standard

steady-state free precession (TrueFISP) sequence. For the evaluation of edema, a multislice, T2-weighted, triple inversion-recovery fast spin-echo sequence was employed (TR 2–3 heart-beats, TE 65 ms, field-of-view 300 × 225 mm, matrix 256 × 125, slice thickness 6 mm, bandwidth 349 Hz/px). Delayed enhancement (DE) images were acquired 10–15 minutes after the administration of 0.2 mmol/kg of Gd-DTPA using a 2D multi-slice, inversion-recovery TurboFLASH (TR 8 ms, TE 4 ms, TI optimized to null normal myocardium, gating factor 2–3, field-of-view 300 × 225 mm, matrix 256 × 144, slice thickness 6 mm, bandwidth 160 Hz/px). DE and edema were quantified as percentage of the left ventricle using prototype software. They were defined as those regions with signal intensity >3 standard deviations of the mean signal of remote normal myocardium. Necrotic area was defined as that showing DE. Area at risk was defined as edematous area on T2-weighted images. Non-infarcted area at risk was defined as area of edema—area of DE.

Results: No differences in heart rate were observed among groups. The heart rate during the catheterization was 65 ± 6 bpm in the control group vs. 66 ± 3 bpm in the metoprolol group (p = NS). On the first CMR (4 days post-MI), the area at risk was similar in the metoprolol group ($30.9 \pm 1.9\%$ of the left ventricle) and the control group ($29.4 \pm 1\%$, p = NS; Fig.). In the control group, $97.4 \pm 7\%$ of the area at risk was infarcted in comparison with $68.8 \pm 6\%$ in the metoprolol group (p = 0.01). In the metoprolol group, the non-infarcted area at risk was 5-fold larger (p = 0.03) and the area of DE was smaller (p = 0.02, Figure). On the first CMR (21 days post MI) there was no significant improvement in left ventricular ejection fraction in the control group (35.1 ± 6 vs. $35 \pm 3\%$, p = NS). The left ventricular ejection fraction improved significantly in the metoprolol group ($37.1 \pm 3\%$ at day 4 vs. $42.9 \pm 3\%$ at day 21, p = 0.04).

Conclusions: Despite a comparable size of the area at risk, immediate administration of intravenous metoprolol during an ongoing MI resulted in smaller infarct size after reperfusion. This cardioprotective effect of metoprolol was independent of the decrease in heart rate. Our results suggest a potential beneficial effect of intravenous metoprolol administration during ongoing MI (while the coronary artery is still occluded).

139. CARDIAC MRI IN MICE AT 9.4 TESLA WITH A TRANSMIT-RECEIVE SURFACE COIL AND A CARDIAC-TAILORED INTENSITY CORRECTION ALGORITHM

David E. Sosnovik, MD,[1] Guangping Dai, PhD,[1] Matthias Nahrendorf, MD,[1] Bruce Rosen, MD, PhD,[1] Ravi Seethamraju, PhD.[2] [1]*Massachusetts General Hospital, Charlestown, MA, USA,* **[2]***Siemens Medical Solutions, Malvern, PA, USA.*

Introduction: Many important cardiovascular structures in mice lie close to the surface of the anterior chest wall. These structures including the aortic root, anterior myocardium and coronary arteries should thus theoretically be best imaged with small surface receive coils. We aimed in this study, however, to evaluate the use of a surface coil for cardiac MRI in mice not only in receive mode, but in a transmit-receive configuration. In addition, we aimed to develop a cardiac-tailored intensity correction algorithm to compensate for the sensitivity profile of the surface coil and allow important far-field structures, such as the descending aorta, to be well visualized as well in a single dataset.

Methods: FLASH cines, with and without DANTE tagging, were acquired in 13 mice at 9.4 T with the transmit-receive surface coil. The developed intensity correction algorithm was based on the concept of dividing the original image by the sensitivity profile of the coil, which was obtained from a lowpass filtered version of the image. An example of such a sensitivity profile, with the grayscale image of the mouse overlaid, is shown in Fig. 1. The coil profile demonstrates high sensitivity over the heart. Further transformation of the sensitivity profile was performed to account for the unique distribution of noise and flow artifacts in cardiac MR images. This prevented pixels in the lungs, which are highly noisy, and flow artifacts propagating across the image in the phase encoding direction from being excessively boosted.

Results: The quality of the FLASH cine images was extremely high and allowed fine structures such as myocardial trabeculations, valve cusps and coronary arteries (black arrows) to be clearly visualized (Fig. 2). The tag lines, created with the transmit-receive surface coil, were also sharp and clearly visible (Fig. 3). Application of the intensity correction algorithm improved signal intensity, tissue contrast and image quality even further. The average signal in the descending aorta, for instance, increased from 7376 ± 1205 to 10150 ± 1496 (p < 0.001) allowing for excellent visualization of the structure (Fig. 4, arrow). Importantly, the cardiac-tailored properties of the correction algorithm prevented noise and flow artifacts from being significantly amplified.

Conclusion: The feasibility and value of cardiac MRI in mice with a transmit-receive surface coil has been demonstrated, even when using complex sequences such as DANTE tagging. The clarity of anterior structures imaged with the coil, such as the coronary arteries, was particularly high. However, the intensity
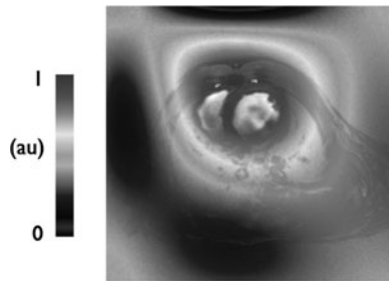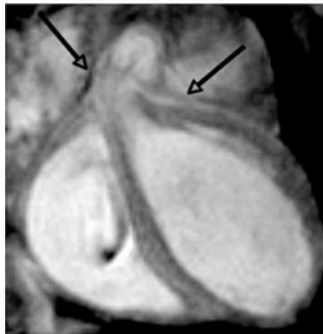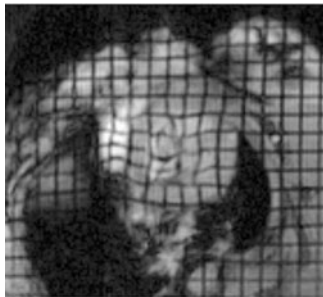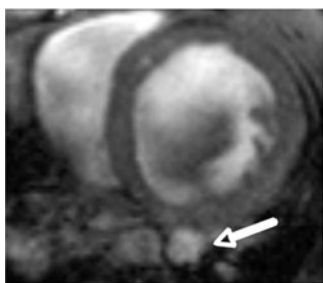
FIG. 1.

FIG. 2.

FIG. 3.

FIG. 4.

correction algorithm also allowed far field structures such as the descending aorta to be well visualized in the same dataset and without a significant increase in image noise or flow artifacts. The use of transmit-receive surface coils and the developed intensity correction algorithm could thus be of significant value for cardiac MRI in mice over a broad range of scanners, coil configurations and field strengths.

Friday, February 2, 2007
Oral Abstracts: Congenital-Session VII

140. IMPROVEMENT IN CARDIOVASCULAR FORM AND FUNCTION LESS THAN ONE YEAR POST TRANSCATHETER ENDOVASCULAR STENTING OF AORTIC COARCTATION IN ADULTS

Sonya V. Babu-Narayan, Raad H. Mohiaddin, MD, PhD, FRCR, FRCP, Timothy M. Cannell, BASc, Isabelle Vonder Muhll, MD, Michael J. Mullen, MD, MRCP. *Royal Brompton Hospital, London, United Kingdom.*

Introduction: Transcatheter endovascular stenting is a recent approach to treatment of adult aortic coarctation with good procedural outcomes, but little longer term data on efficacy and clinical endpoints. We hypothesized that stenting would have effects on blood pressure, presence and extent of collaterals, left ventricular (LV) mass and vascular function.

Purpose: We hypothesised that stenting would have effects on blood pressure, presence and extent of collaterals, left ventricular (LV) mass and vascular function.

Methods: Eighteen patients mean age 31.6 ± 12.8 years underwent endovascular stenting of coarctation of the aorta. All were studied prior to (2.0 ± 2.2 months) and after (10.2 ± 2.2 months) intervention with clinical assessment and cardiovascular magnetic resonance.

Results: Following endovascular stenting, Fredriksen coarctation index increased from 0.13 ± 0.14 to 0.65 ± 0.41 with no patient having significant coarctation (index <0.25) after stenting. Percentage coarctation decreased (67.7 ± 17.7 *versus* $22.3 \pm 21.7\%$; $p < 0.001$). A decrease in blood pressure was seen ($153 \pm 17/82 \pm 14$ *versus* $130 \pm 21/69 \pm 13$ mmHg; $p < 0.001$) unrelated to change in existing antihypertensive therapy. There was increase in LV ejection fraction (70 ± 10 *versus* $74 \pm 8\%$; $p = 0.01$) and decrease in LV mass index (91 ± 24 *versus* 82 ± 20 g/m^2; $p = 0.003$). Collaterals were diminished in size

FIG. 1. Appearance of collaterals and aorta pre- and post-endovascular stent repair. a) CE-MRA images pre-endovascular stent repair of coarctation showing native coarctation with extensive collateral vessels. b) CE-MRA images post-endovascular stent repair of coarctation showing mild appearance of collateral vessels. There is an area of signal loss caused by the metallic artefact from the stent (asterisk). c) Turbo Spin Echo CMR sequences are less susceptible to metallic artefact than other sequences and the stented area of the aorta can be imaged (asterisk).

FIG. 2. Changes following endovascular stent repair. Differences in variables between patients pre- and post-endovascular stent repair are illustrated.

and collateral flow decreased (40 ± 29 versus $-2 \pm 30\%$; p < 0.001) (Fig. 1).

Distensibility of the ascending aorta increased (4.0 ± 2.5 versus $5.6 \pm 3.5 \times 10^{-3}$ mmHg^{-1}; p = 0.02). Additionally, right ventricular mass index decreased (35 ± 7 versus 29 ± 10 g/m^2; p = 0.039). With greater extent of collateral appearance at baseline there was a greater reduction in LV mass index (Kruskal Wallis p = 0.007). Important results are summarized in Fig. 2.

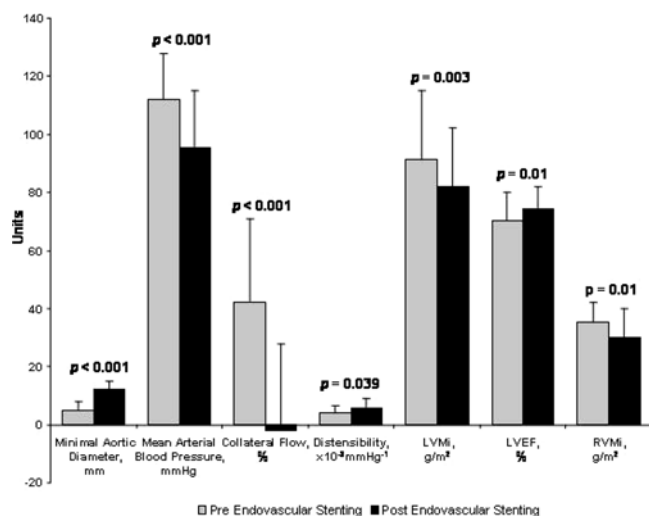*Conclusions:* All patients underwent successful relief of coarctation by endovascular stenting. Both cardiac and vascular beneficial outcomes of endovascular stenting were demonstrated. The reduction in LV mass as early as ten months after stenting suggests a reduction in risk of adverse events.

141. ASSESSMENT OF MYOCARDIAL BLOOD FLOW AND CORONARY FLOW RESERVE IN CHILDREN, USING 3 TESLA CARDIAC MAGNETIC RESONANCE IMAGING

Ronald Wells, MD, Michael Jerosch-Herold, PhD, David Sahn, MD, William Woodward, ARMRIT, Erwin Schwartz, Veronica Swanson, MD, Daniel J. Woodward, MD, Angela Zimmerman, MD, Michael Silberbach, MD. *Oregon Health and Science University, Portland, OR, USA.*

Introduction: The feasibility of measuring myocardial blood flow (MBF) and adenosine coronary flow reserve (CFR) at 3T in the pediatric age-group is unknown.

Methods: We have performed 11 adenosine-infusion CMRs (AI-cMR) in 10 infants and children with and without congenital heart disease since May 2005. Perfusion images were acquired during first pass of gadolinium-DTPA contrast (0.03 mmol/kg) before and during 3 minute adenosine infusion (140 mcg/kg/min) using single shot gradient echo sequences

(TR/TE = 2.4/1 ms) with saturation recovery magnetization preparation for T1 weighting. Temporal resolution equaled the cardiac cycle length. Deep sedation was provided by a pediatric cardiac anesthesiologist and pediatric sedation nurse in all children less than 12 years old. Heart rate and oxygen saturation were monitored continuously. Blood pressure was measured each minute during adenosine administration. Perfusion images were analyzed by segmenting along endo- and epicardial borders and determining the changes of the average signal intensity during contrast transit in 6–8 myocardial sectors per slice, using deconvolution of the tissue curves with an arterial input, measured in the LV, to determine absolute blood flow (in mL/min/g). CFR was calculated as hyperemic MBF (during adenosine infusion) divided by baseline MBF.

Results: Mean age was 9.2 years, range 2.9 months to 17.3 years. Diagnoses include d-transposition of the great arteries (d-TGA) after arterial switch operation (ASO; n = 2); anomalous coronary artery origin or branching (n = 3 patients, 4 studies); history of Kawasaki Disease (KD) with coronary artery involvement (n = 2); pulmonary atresia intact ventricular septum with right ventricular-dependent coronary circulation (PA-IVS-RVDCC; n = 1); tetralogy of Fallot (TOF) with chest pain (n = 1); and double outlet right ventricle (DORV) with exercise intolerance (n = 1). There were no complications. Heart rate increased an average of 13.8 bpm (range −2 to +35 bpm). Systolic cuff blood pressure fell by an average of 9.3 mmHg (range −25 to +11 mmHg). Clinically relevant information was obtained in all cases. In 2 patients MBF and CFR were considered normal and they were permitted to participate in sports (CFR 2.67 ± 0.45). Abnormalities were identified in the other 8 patients (CFR 2.36 ± 0.68). Regional perfusion abnormalities were seen in 5 patients. Two were abnormal at baseline (d-TGA after ASO; anomalous coronary artery). Three others were abnormal only after adenosine infusion (DORV; anomalous coronary artery; d-TGA after ASO). Both patients with KD demonstrated significantly impaired global CFR, confirming endothelial dysfunction. In the patient with PA-IVS-RVDCC CFR was globally decreased; regional variation could not be assessed due to small cardiac dimensions.

Conclusions: The lack of normative data makes CFR data difficult to interpret in infants and children. AI-CMR is a useful test in infants and children that can be performed safely and easily and will ultimately play a central role in the evaluation of coronary artery function in children with acquired or congenital heart disease.

142. EXCLUSION OF CORONARY ARTERY ANOMALIES IN PATIENTS WITH CONGENITAL CARDIOVASCULAR ABNORMALITIES USING WHOLE HEART APPROACH

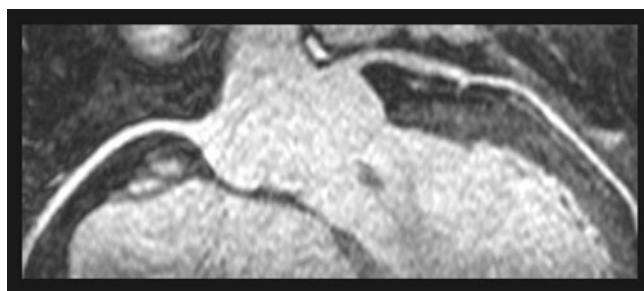**Randolph M. Setser, DSc,[1] Janine Arruda, MD,[1] Joanie A. Weaver, RT (MR),[1] Angel Lawrence, RT (MR),[1]**

Renate Jerecic, PhD,[2] Vibhas Deshpande, PhD,[3] Paul Schoenhagen, MD,[1] Mario J. Garcia, MD,[1] Milind Y. Desai, MD.,[1] *[1]Cleveland Clinic, Cleveland, OH, USA, [2]Siemens Medical Solutions, Malvern, PA, USA, [3]Siemens Medical Solutions, Los Angeles, CA, USA.*

Introduction: The feasibility and accuracy of magnetic resonance coronary angiography (MRCA) has been demonstrated previously, particularly for assessment of the proximal coronary arteries (1). However, most MRCA techniques are cumbersome and time-consuming, and require meticulous planning, thus diminishing their widespread usage. Recently, a free-breathing whole-heart MRCA technique has been developed to assess the epicardial coronary tree (2), without the use of iodinated contrast agents or radiation. MRCA combined with a routine cardiovascular MR examination would be an attractive proposition, especially in younger patients being evaluated for congenital abnormalities, in whom the exclusion of anomalous coronaries is clinically relevant.

Purpose: To evaluate the feasibility of performing free-breathing, whole-heart MRCA in patients with known congenital cardiovascular abnormalities.

Methods: Eleven patients (6M/5F, 24 ± 14 years) were referred clinically for cardiac MRI with the following known or suspected congenital cardiovascular abnormalities: arrhythmogenic right ventricular dysplasia (n = 4), tetralogy of Fallot (3), aortic coarctation (2), Marfan's syndrome (1) or congenital pulmonary valve stenosis (1). Coronary arteries were imaged at 1.5T (Avanto, Siemens) using an ECG-triggered, free breathing 3D whole heart coronary MRA sequence with T2 preparation (40 ms) and navigator gating with motion adaptive gating (2–4 mm acceptance window dependent on patient size): balanced steady state free precession (TrueFISP), TR 3.8 ms, TE 1.5 ms, α 90°, 19-23 lines per heartbeat, bandwidth 980 Hz/pixel, resolution 1.0 × 0.9 × 0.75 mm, 72–144 transverse slices acquired. In each patient, the data acquisition window location/duration was determined visually from cine 4-chamber images. MRCA was performed after gadolinium contrast administration in 6/11 patients (64%). Image quality was assessed subjectively using a 4-point scale (1: poor, 2: good, 3: very good, 4: excellent) (3) by 2 experienced observers. Coronary blood signal intensity, myocardial signal intensity and background noise were measured in raw images for calculation of signal to noise ratio and contrast to noise ratio (SNR and CNR) using the following formulae: $SNR = SI_{coronary}/Noise$, $CNR = (SI_{coronary}-SI_{myocardium})/Noise$. The visible length of each coronary vessel was measured using curved multi-planar reformatted (MPR) images.

Results: On average, imaging of all 3 epicardial coronary arteries, during a single acquisition, required 11 ± 4 minutes of scan time. Proximal coronary anatomy was adequately visualized in all patients (Fig.), with second-order branch vessels visible in 6/11 patients (55%). One patient (9%) was found to have an anomalous coronary origin: small left circumflex (LCX) off the right coronary artery (RCA) with a posterior course. Image quality averaged 2.7 ± 0.9 for Reader 1 and 2.5 ± 1.0 for Reader 2 (p = 0.17, weighted-κ = 0.77). On average, the visualized lengths of the coronary arteries were as follows: 76 ± 26 mm (left anterior descending or LAD), 51 ± 31 mm (left circumflex or LCX) and 72 ± 20 mm (right coronary artery or RCA). Mean SNR results were as follows: 61 ± 35 (LAD), 60 ± 40 (LCX) and 67 ± 34 (RCA). CNR results were as follows: 30 ± 21 (LAD), 30 ± 26 (LCX) and 37 ± 22 (RCA). Note that SNR and CNR values are larger than those typically reported in the literature; in the 4 patients imaged without gadolinium contrast, SNR was more typical (26 ± 7 LAD, 26 ± 8 LCX, 27 ± 7 RCA), as was CNR (12 ± 6 LAD, 12 ± 4 LCX, 13 ± 6 RCA).

Conclusions: Using a free-breathing whole-heart MRCA technique, it is feasible to noninvasively obtain high-quality images of the proximal portions of all 3 epicardial coronary arteries in a reasonable amount of time. This imaging sequence could potentially be incorporated with the standard cardiac MR examination, particularly in individuals being evaluated for congenital cardiovascular abnormalities, in whom the exclusion of coronary anomalies is clinically relevant.

REFERENCES

1. Kim WY, et al. NEJM 2001; 345: 1863–1869.
2. Weber OM, et al. MRM 2003; 50: 1223–1228.
3. McConnell MV, et al. AJR 1997; 168: 1369–1375.

143. FEASIBILITY OF USING FREE-BREATHING 3D WHOLE-HEART CORONARY MR ANGIOGRAPHY AT 3T TO ASSESS CORONARY ARTERY ANOMALIES AND VARIANTS

Ahmed M. Gharib,[1] Vincent B. Ho, MD,[2] Douglas R. Rosing, MD,[1] Daniel A. Herzka, PhD,[3] Matthias Stuber, PhD,[4] Andrew E. Arai, MD,[1] Roderic I. Pettigrew, PhD, MD.[1] *[1]NIH, Bethesda, MD, USA, [2]Department of Radiology, Uniformed Services University of the Health Sciences, Bethesda, MD, USA, [3]Philips Research North America, Clinical Sites Research Program, Bethesda, MD, USA, [4]Radiology, Medicine, Electrical and Computer Engineering, Johns Hopkins University, Baltimore, MD, USA.*

Introduction: Several case series have demonstrated the excellent correlation between coronary MRA and conventional angiography for the diagnosis of anomalous coronary anatomy. However, all were performed at 1.5T used focused coverage of the coronary arteries which requires serial volume-targeted acquisitions in axial and oblique orientations. Additionally, whole-heart techniques at 1.5T require the use of steady-state-free-precession and T2-Prep for optimal visualization or the coronary tree. Due to specific absorption rate restrictions and field inhomogeneities, such techniques cannot be easily used at 3T.

Purpose: To assess the potential of whole-heart coronary MR Angiography (MRA) performed at 3T using gradient echo and adiabatic T2-Prep, in patients with known or suspected coronary artery anomalies and variants.

Methods: Twelve subjects were included after obtaining written informed consent. Subjects were suspected of having anomalous coronary arteries by x-ray angiography ($n = 8$) three of whom also underwent coronary CT angiography, echocardiogram ($n = 1$), prior MRI ($n = 1$) or clinical history ($n = 2$). Coronary MRA was performed on a 3T MR scanner using a 6-element cardiac coil. A 3D free-breathing navigator and vectorcardiographic-gated gradient echo sequence was used to acquire both small (TR $= 8$ ms, TE $= 21$ ms, $\alpha = 20°$, acquired voxel dimension $= 0.7 \times 1 \times 3$ mm^3) and large imaging volumes (TR $= 4$ ms, TE $= 1.35$ ms, $\alpha = 20°$, acquired voxel size $= 1 \times 1 \times 2$ mm^3). Adiabatic T2-Prep and parallel imaging (SENSE factor $= 2$) were utilized. Curved multiplanar reformation was performed with the SoapBubble Tool and/or commercially available image analysis software (AZE, Tokyo, Japan). The latter was also used for generating 3D volume rendered images.

Results: Small and/or large volume coronary 3D MRA were successfully acquired in the 12 subjects. Whole heart acquisitions ($n = 10$) were acquired in 13.8 ± 3.6 minutes. Total exam time was 41 ± 14 minutes. Two whole-heart acquisitions were not completed because of arrhythmias and patient restlessness. Two blinded readers diagnosed the coronary anomalies, which included aneurysms, ectasia, arteriovenous fistula, and anomalous origin. Representative images are shown in Figs. 1 and 2.

Figure 1 demonstrates right coronary artery (RCA) and left anterior descending artery (LAD) originated from the right si-nus of Valsalva. The LAD then passes anterior to the pulmonary artery (PA). (a) Multiplanar reformatted image showing single origin of the LAD and RCA from the right sinus of Valsalva. The LAD passes anterior to the PA. (b) Anterior oblique view of volume-rendered image from the coronary MR angiogram revealing the common origin of the LAD and RCA (c) Right lateral oblique view of volume-rendered image from the coronary MR angiogram.

Figure 2 shows coronary images of congenital arteriovenous (A-V) fistula. (a) Volume rendered image of whole-heart coronary CMR angiogram showing a tortuous and dilated left circumflex artery (LCX in red) terminating in an aneurysm (arrow) at the tip of the right ventricle (RV). (b) Three dimensional maximum intensity display of the whole-heart coronary MR angiogram of a dilated tortuous LCX (arrow) ending in an A-V fistula with the RV apical aneurysm (arrowhead). (c) Multiplanar image of the LCX rendered from whole-heart coronary MR angiogram revealing a dilated tortuous LCX (arrow) ending in an A-V fistula with the RV apical aneurysm (arrowhead). (d) Multiplanar reformatted image of contrast enhanced coronary CT angiogram demonstrating close resemblance to the coronary MR angiogram multiplanar reformatted image (Fig. 5c) performed without contrast. (e) Volume rendered image of the contrast enhanced CT angiogram images showing the LCX A-V fistula leading to the RV (in red).

Conclusions: Large 3D whole-heart acquisitions at 3T allow for successful evaluation of anomalous coronary arteries and provide 'ease-of-use' by covering the entire coronary arterial tree. The high signal-to-noise ratio available at 3 T supports the use of gradient echo, adiabatic T2-Prep and scan acceleration using SENSE, resulting in high quality, fast acquisitions favoring patient compliance and successful study completion.

144. DELAYED ONSET OF TRICUSPID FLOW AT PHASE-CONTRAST MR: FURTHER EVIDENCE OF INTERVENTRICULAR DYSYNCHRONY AFTER REPAIR OF TOF

Ai-Min Sun, MD, Fahad Al-Habshan, MD, Michael Cheung, MD, Gabriele Bronzetti, MD, Andrew N. Redington, MD, Lee N. Benson, MD, Christopher Macgowan, MD, Shi-Joon Yoo, MD. *Hospital for Sick Children, Toronto, ON, Canada.*

Introduction: There is increasing evidence of systolic interventricular dysynchrony in patients after repair of tetralogy of Fallot. Delayed onset of tricuspid flow may represent diastolic dysnchromy.

Purpose: To assess the incidence of delayed onset of tirsupid flow and to explore uts underlying mechanisms.

Methods: The study population included 31 children with repaired TOF (mean age $\pm$ SD, 12.3 ± 4.1 years) who underwent postoperative magnetic resonance (MR) between January 2003 and March 2005. The MR protocol included simultaneous

phase-contrast (PC) imaging of the atrioventricular valves, which enabled direct comparison of the tricuspid (TV) and mitral (MV) valve flow. The TV and MV flow from 14 normal subjects was also studied for comparison. The MR results were correlated with the findings of echocardiography and electrocardiography.
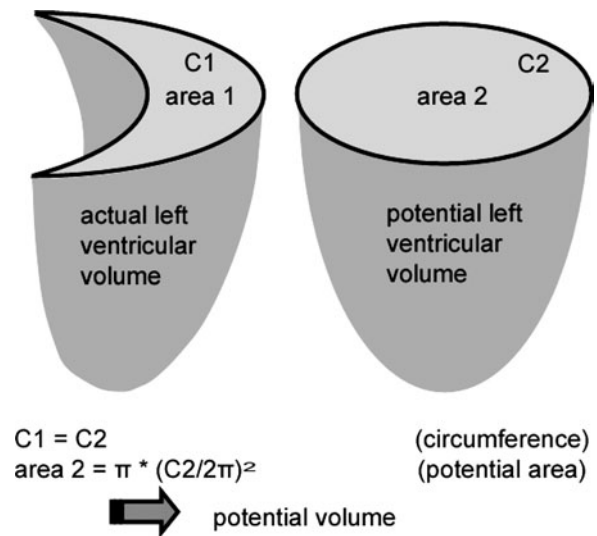
Results: Delayed onset of the TV flow (>20 ms) was observed in 16 of 31 patients (51.6%) and in none of the controls ($p < 0.001$). The mean delay time (time interval between the onsets of the TV and MV flow) was 64.8 ± 27.1 ms (28–105 ms), which was $8.5\% \pm 3.2\%$ (5.0%–15.2%) of the R-R interval in patients with delayed onset of the TV flow. This group also had significantly decreased E/A ratio of the TV ($p < 0.017$) and right ventricular ejection fraction ($p < 0.05$), and a tendency toward a prolonged QRS (150.27 ± 23.97 ms) compared to those without delay (134.40 ± 33.13 ms) ($p = 0.14$). Meanwhile, there was a significant correlation between the delayed onset of the TV flow and decreased ejection fraction of both right and left ventricles ($p = 0.02$ and $p = 0.05$, respectively). No linear relationship was found between the delay time and the E/A ratio. There was no significant difference in the pulmonary artery regurgitant fraction, right ventricular end-diastolic volume index (RVEDi) or duration of QRS between the patients with and those without delay ($p > 0.05$). Furthermore, there was also no relationship between delayed onset of the TV flow and diastolic forward flow in the pulmonary artery or right venricular systolic pressure ($p > 0.05$).

Conclusions: The present PC MR study shows that delayed onset of the TV flow is common in patients with repaired TOF and is associated with abnormal right ventricular diastolic and biventricular systolic function. These data further support the role of ventricular dysynchrony in the pathogenesis of late morbidity in TOF and may provide additional rationale for resynchronisation strategies in these patients.

145. MAGNETIC RESONANCE IMAGING IN THE PREOPERATIVE ASSESSMENT OF MARGINALLY HYPOPLASTIC LEFT VENTRICLES

Lars Grosse-Wortmann, Tae Jin Yun, Masaki Nii, Siho Kim, Andrew Redington, Shi-Joon Yoo, Glen an Arsdell. *The Hospital for Sick Children, Toronto, ON, Canada.*

Introduction: The decision between uni- and biventricular repair for a heart with a smaller than normal left ventricle, usually made early in the neonatal period, will forever change the life of this patient. Due to right ventricular overload, the left ventricle may be compressed, leading to a discrepancy between its actual and its potential volume after unloading the right ventricle (Fig.). Various strategies, most of them based on echocardiography, have been proposed to aid in the decision whether biventricular repair or a Norwood-type palliation should be pursued. While morphology and size of the left ventricle and the underlying

lesion are important, information on the amount of extra- and intracardiac shunts and on how much blood passes through the left ventricular outflow tract and the ascending aorta is crucial in determining the surgical approach. Magnetic resonance imaging (MRI) is the current gold standard for the assessment of ventricular volumes and blood flow.

Purpose: To compare left ventricular sizes by MRI with those obtained by echocardiography; to compare potential with true preoperative left ventricular volumes; to address whether preoperative ventricular volumes, flow in the ascending aorta and Qp/Qs determine early and late postoperative outcome; and to determine the potential for early and late left ventricular growth in patients with marginally hypoplastic left ventricles.

Methods: Sixteen patients with a mean age of 9 (2–37) days and a mean weight of 3.4 (2.3–4.4) kg at the time of MRI, ventriculo-arterial concordance and a left ventricular volume $<50\,\mathrm{mL/m^2}$ (mean 30, max 47, min 20 $\mathrm{mL/m^2}$) were entered into this retrospective analysis. The primary diagnosis was critical aortic stenosis in 6, mitral valve stenosis in 2, hypoplastic aortic arch in 5 and unbalanced atrioventricular septal defect in 3 patients. By MRI, actual and potential ventricular volumes (Fig.), annulus diameters and opening areas of mitral and aortic valves, flow in the ascending, as well as Qp/Qs were assessed. These were compared with echocardiographic measurements of valve annuli and left ventricular volumes and correlated with clinical parameters of early postoperative outcome, including duration of inotropic support, mechanical ventilation, ICU stay, as well as with survival with a biventricular circulation. Postoperative growth of left sided structures was followed with echocardiography in patients who underwent biventricular repair.

Results: The preoperative potential volume of the left ventricle by MRI exceeded the actual volume by 16.9%. Measurements by echocardiography were 26.7% lower than those by MRI. Preliminary results from 4 patients show that ventricular volumes by preoperative CMRI correspond better to early postoperative than to preoperative echo measurements (Table). In

TABLE 1
Left ventricular volume in 4 patients, measured by CMRI and
echocardiography

		left ventricular end-diastolic volume index (mL/m^2)		
Case	primarydiagnosis	Pre-operative MRI	Pre-operative echo	Early post-operative echo
1	Aortic stenosis	21.9	10.0	29.0
2	Aortic stenosis	20.3	7.8	17.7
3	Mitral stenosis	21.7	13.3	27.0
4	Mitral stenosis	34.0	18.0	33.0

these 4 patients, the mean mitral and aortic valve z-scores increased from -4.7 to -1.5 and from -5.5 to -0.6, respectively, over a mean follow-up period of 8 months after biventricular repair. In the 16 patients, flow in the ascending aorta average 1.59 L/min/m^2. Qp/Qs was 2.1. On average, 45.8 % of the total left-to-right shunt was via an atrial or ventricular septal defect and 54.2 % via a patent ductus arteriosus (PDA). The correlations with clinical parameters of outcome are pending.

Conclusions: Non-invasive assessment of ventricular volumes and blood flow as well as selective calculations of intracardiac and PDA shunts in neonates with marginally hypoplastic left ventricles are feasible with MRI. The potential left ventricular volume after decompression is substantially higher than the actual preoperative volume and should be considered in surgical decisions. Following biventricular repair, left sided structures including the mitral and aortic valves grow to normal size with the first year of life.

146. THE GEOMETRY OF THE PULMONARY ARTERY BIFURCATION IN CHILDREN—AN MRI IN VIVO STUDY

Emanuela R. Valsangiacomo Buechel, MD, Zita Knobel, MD, Manuela Albisetti, MD, Eva Bergsträsser, MD, Christian J. Kellenberger, MD. *University Children's Hospital Zurich, Zurich, Switzerland.*

Introduction: Children with congenital heart disease frequently present with associated anomalies of the pulmonary arteries (PAs), and in many cases the pulmonary artery bifurcation needs to be reconstructed during surgical repair. Residual abnormalities of the PAs may persist after surgery and are one of the major reasons for reinterventions. Information about the normal size and geometry of the mediastinal branches of the PAs and of their bifurcation is needed for the indication and planning of interventions. However, normal values of the pulmonary arteries geometry in children do not exist.

Purpose: To establish such normal values for the size and geometry of the central pulmonary arteries in children with normal cardiovascular anatomy.

TABLE 1
Diameters obtained in two dimensions, normalized to body surface
area (mm/m^2)

Vessel	Location of measurement	Dimensions	
MPA	Mid portion	18 ± 5 X	17 ± 4
RPA	At origin	11 ± 3 X	13 ± 3
	Before 1st branching	10 ± 3 X	13 ± 3
LPA	At origin	13 ± 3 X	14 ± 3
	Before 1st branching	11 ± 2 X	11 ± 2

Methods: Seventy-four children with previous history of a malignancy, but normal cardiovascular anatomy, underwent three-dimensional contrast-enhanced magnetic resonance angiography (CMRA) for investigation of porth-a-cath related complications. Mean age was 10 ± 5 years (range 2–22 years), weight 38.3 ± 19.3 kg and heart rate during examination 82 ± 12 bpm. Twenty-three MRA examinations were performed in deep sedation; images were acquired with breathhold in 48 patients and during free breathing in 26.

The source images of the MRA acquired during the arterial phase were used to reconstruct the vascular anatomy in a standardized way for all children. Subvolume maximum intensity projection (MIP) images were reconstructed in an axial plane at the level of the pulmonary artery bifurcation, in coronal oblique planes along the mediastinal segments of the right and left pulmonary arteries (RPA and LPA), and in a left sagittal oblique plane along the main pulmonary artery (MPA). The diameters of the PAs (MPA, RPA, LPA), their course in respect to the sagittal and horizontal planes of the body, and their angulation were measured on a workstation with commercially available software. Measurements are given as mean $\pm$ SD, diameters are normalized to body surface area.

Results: Image quality was excellent in 33 cases, good in 28, fair in 10 and poor in 3 (excluded from the study).

The MPA shows an oblique course from left anterior inferior to right posterior superior, with an angle of $17 \pm 6°$ in respect to the sagittal plane and an inclination of $57 \pm 8°$.

The MPA bifurcates with a total angle of $99 \pm 10°$; the RPA takes off with an angle $47 \pm 7°$ to the right and the LPA with an angle of $51 \pm 8°$ to the left in respect to the long axis of the MPA (Fig. 1). The RPA is caudally angulated by $8 \pm 6°$ and the LPA by $2 \pm 8°$. The bifurcation is rotated with the origin of the LPA located 7 ± 2 mm higher than the origin of the RPA. The distance from the bifurcation to the take off of the first segmental pulmonary artery is 17 ± 6 mm/m^2 for the RPA and 15 ± 5 mm/m^2 for the LPA.

The size of the pulmonary arteries is listed in Table 1.

Conclusions: The normal geometry and dimensions of the central pulmonary arteries and their bifurcation in children are described with the diameters indexed to body size. These data may be helpful to cardiac surgeons and interventional cardiologists for planning interventions of the pulmonary arteries and their bifurcation.

Abstract Sessions X, XI, XIII, XIV and XV

Saturday, February 3, 2007
Oral Abstracts: Clinical-Session X

147. MRI DELAYED ENHANCEMENT PATTERNS IN PATIENTS WITH DILATED CARDIOMYOPATHY

Peter J. Larsen, MBBS (Hons), Andrew McCann, Richard Slaughter, Wendy Strugnell. *The Prince Charles Hospital, Chermside, Australia.*

Background: Multiple studies have shown that Cardiovascular Magnetic Resonance (CMR) with Delayed Enhancement (DE) can distinguish ischaemic from non-ischaemic Dilated Cardiomyopathy (DCM). Recently, it has been reported that up to two-thirds of patients with DCM have DE on CMR. However, the patterns and significance of DE in patients with DCM are not well characterised.

Objectives: To describe the patterns of DE in patients with DCM and to determine if there is an association between the presence and/or pattern of DE and left ventricular systolic function as measured by ejection fraction (EF).

Methods: Retrospective case-review of 125 consecutive patients with a clinical diagnosis of idiopathic DCM prospectively enrolled in a database. Sixty-two patients underwent coronary angiography and had no evidence of obstructive coronary artery disease. The remaining 63 patients had no ischaemic type DE on CMR and were being treated with a clinical diagnosis of
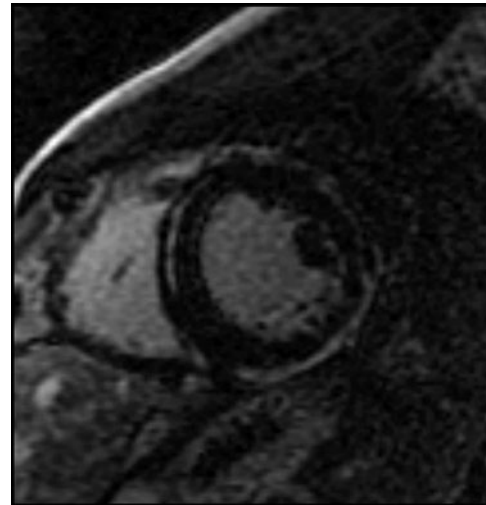

FIG. 1. Example of Septal mid-wall DE (short axis view)

idiopathic DCM. 2 patients were excluded because of image artifact. CMR imaging was performed using a GE Twin Speed 1.5 Tesla system. Steady state free precession (SSFP) cine MR images were acquired in vertical long axis, horizontal long axis and short axis orientations. Delayed enhancement imaging was performed in the same slice locations using a segmented inversion recovery fast gradient echo sequence. Images were acquired between 8–15 minutes after administration of 0.2 mmol/kg of GD-DTPA, using an inversion time of 200–250 ms. Measurements obtained included LVEF, EDV, ESV and SV indexed to BSA. The location of DE in the LV was scored using a 5 segment model (Septum, Anterior, Lateral, Inferior, and Apex) and the location of DE within the myocardium was categorized as subendocardial or mid-wall. DE was graded as absent or present. This was assessed in three views (short axis, two-chamber long axis, and four-chamber) by two independent observers (Fig. 1).

Results: Of the 123 patients studied, the mean age was 50 years (range 13–82) and 25% were female. The mean EF was 25% (8–54) and the mean EDV 171 mL/m^2 (61–313). The group
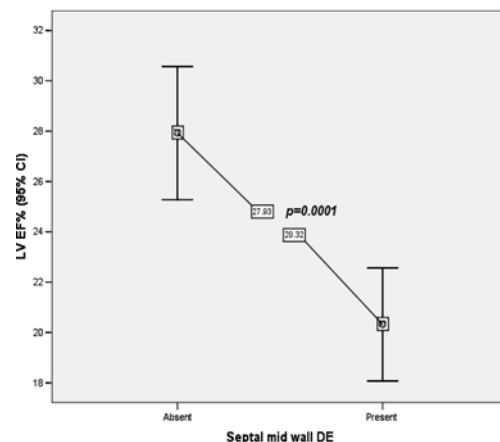

FIG. 2. Relationship between septal mid-wall DE and LVEF%.

who did not undergo angiography were younger (mean age 48 v 54, p = 0.001) and had more female patients (35% v 17%, p = 0.001). There was no difference in baseline EF or EDV between the two groups. Overall, DE was seen in 48% of patients. There was no difference in the presence or pattern of DE between the two groups. Overall, septal mid-wall DE was seen most commonly (43.2%) and was associated with more severe LV systolic dysfunction (mean EF 27.93% v 20.32%, p = 0.0001, Fig. 2). Subendocardial DE (1.6%) and patchy/mid-wall lateral DE (3.2%) were also seen.

Conclusion: DE occurs in stereotypical patterns in patients with DCM. Septal mid-wall DE is seen most commonly and is associated with more severe LV systolic function. These findings validate other recent studies and suggest that the presence of delayed enhancement may be useful in risk stratifying patients with DCM.

148. DETECTION OF CMR-DERIVED NON-INVASIVE ASSESSMENT OF FIBROSIS IN DIFFERENT FORMS OF LEFT VENTRICULAR HYPERTROPHY—RELATION TO SEVERITY OF DISEASE AND PRESSURE OVERLOAD

Andre Rudolph, Hassan Abdel-Aty, Steffen Bohl, Philipp Boyé, Mirko Fröhlich, Rainer Dietz, Jeanette Schulz-Menger. *Franz-Volhard-Klinik, Charite Campus Buch, Helios-Kliniken Berlin, Berlin, Germany.*

Background: Left ventricular hypertrophy (LVH) is an independent predictor of cardiac mortality. The relation between primary (hypertrophic cardiomyopathy [HCM]) or secondary LVH (pressure overload: arterial hypertension [AH], aortic stenosis [AS]) and myocardial fibrosis as defined by contrast-enhanced cardiovascular magnetic resonance (ce-CMR) is not well understood. We aimed at assessing the volume of focal fibrosis and to explore its relation to LVH in these three clinical settings by CMR.

Methods: We analyzed image data sets of 77 patients (50 males, age: 56 ± 15 years) with LVH (defined as left ventricular (LV) mass index (LVMI, g/cm) > 1.06 in males and > 0.8 in females): HCM (n = 36), AS (n = 21) and AH (n = 20) and exclusion of coronary artery disease. In HCM we defined obstruction (HOCM, n = 19) as a left ventricular outflow tract area $<2.7 cm^2$ as recently published. In AS an aortic valve area $<1.0 cm^2$ was defined as severe AS (n = 11). On a 1.5 T scanner, the LV myocardium was covered with short axis SSFP cine images followed by gradient recovery inversion recovery after 0.2 mmol/kg Gd-DTPA i.v. injection to assess late hyperenhancement (LHE). Using a dedicated software (MASS 6, Medis, The Netherlands), the endo-and epicardial contours were defined and areas of LHE were manually traced and expressed as percentage of the total LV mass. LV ejection fraction (EF), end diastolic volume index (LVEDVI) and LVMI were quantified.

Results: There was no difference in LVMI between groups (HCM: 1.4 ± 0.4 g/cm, AS: 1.3 ± 0.3 g/cm, AH: 1.4 ± 0.3 g/cm, p = n.s.). EF was in normal range, but significant differences (p < 0.05) between AH and the other groups were noted (HCM: $75 \pm 9\%$, AS: $70 \pm 9\%$, AH: $56 \pm 14\%$). Presence of myocardial fibrosis was 72% (HCM), 62% (AS) and 45% (AH). Difference in frequency of fibrosis between HCM and AH was significant (p = 0.043). If LHE was observed, the percentage of fibrosis related to left ventricular mass was significantly higher (p < 0.05) in HCM ($12 \pm 8\%$) and not different between AS ($3 \pm 3\%$) and AH ($5 \pm 4\%$). Patients with LHE had a higher LVMI (1.4 ± 0.4 vs. 1.2 ± 0.3, p = 0.002). LHE in HCM was predominantly located in the anteroseptal and inferoseptal segments (82%) in contrast to AS and AH, where no specific pattern of fibrosis could be identified. In all groups the lesions were predominantly non-subendocardial (Fig. 1).

Obstruction in HCM was not related to presence of LHE (LHE in HOCM: 79%, LHE in HNCM: 65%, p = 0.46). In HCM, the presence of fibrosis depends of LVMI (1.5 ± 0.5 g/cm in HCM with LHE vs. 1.2 ± 0.2 g/cm, p = 0.018). There is no relation to LVEDVI (p = 0.8).
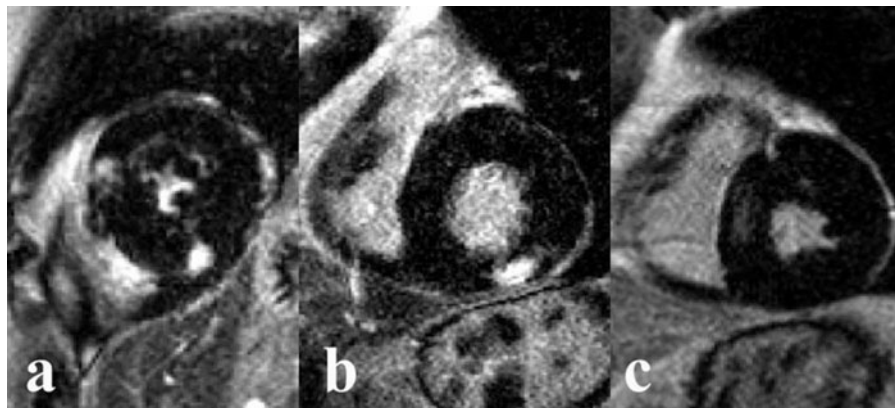

FIG. 1. Contrast-enhanced images obtained by cardiac magnetic resonance in short-axis views in different forms of left ventricular hypertrophy (a: Hypertrophic Cardiomyopathy, b: Aortic stenosis, c: Arterial Hypertension). Bright signal (LHE) shows myocardial fibrosis.

In AS the severity was not related to the presence of fibrosis (p = 0.7). AS with LHE had a higher LVMI (1.4 ± 0.2 vs. 1.1 ± 0.3 g/cm, p < 0.028) and a higher LVEDVI (1.0 ± 0.2 vs. 0.8 ± 0.2 mL/cm, p < 0.015) compared to AS without LHE.

In AH there was a relation between LVMMI and presence of fibrosis (no LHE: 1.2 ± 0.3 g/cm, LHE: 1.4 ± 0.3 g/cm), but the difference was not significant (p = 0.1). LVEDVI was not increased in AH with LHE (1.0 ± 0.3 vs. 1.0 ± 0.4 mL/cm, p = 0.5).

Conclusion: ceCMR allows the detection of fibrosis in LVH due to HCM, AS and AH. The pattern and distribution of focal fibrosis has the potential to differentiate different forms of LVH. Likelihood of fibrosis is higher in increased LVMI. Focal fibrosis is more frequent in primary than in secondary LVH. Fibrosis in AS and AH seems to be independent of pressure overload.

149. CHARACTERIZATION OF CARDIAC AMYLOIDOSIS BY ATRIAL LATE GADOLINIUM ENHANCEMENT USING CONTRAST ENHANCED CMR: CORRELATION WITH LEFT ATRIAL CONDUIT AND CONTRACTILE FUNCTION
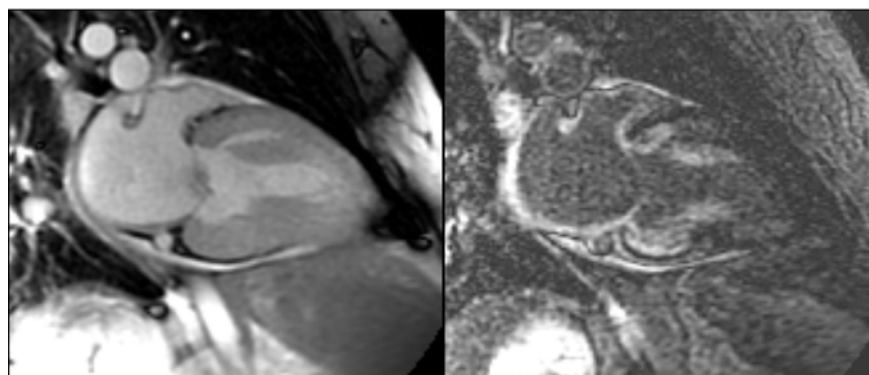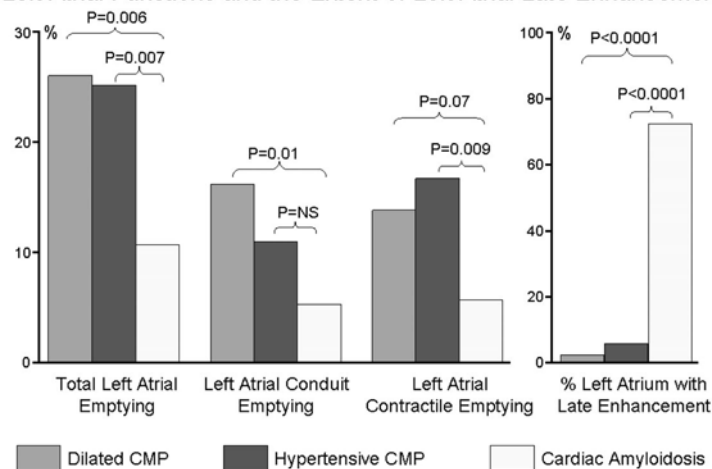
Raymond Kwong, MD MPH, Kevin E. Steel, DO, Mouaz Al-Mallah, MD, Rodney H. Falk, MD. *Brigham and Women's Hospital, Boston, MA, USA.*

Introduction: Noninvasive differentiation of cardiac amyloidosis from other forms of cardiomyopathy remains a challenge. Amyloid infiltrates all cardiac chambers and can result in atrial dysfunction. However, atrial infiltration and its effect on atrial emptying have not been previously characterized by CMR.

Purpose: We tested the hypothesis that contrast-enhanced CMR can characterize left atrial (LA) myocardial infiltration in amyloidosis, and we quantified the effect of such infiltration on atrial emptying function compared to clinical control groups.

Methods: CMR was performed in 8 patients with endomyocardial biopsy-proven cardiac amyloidosis (AMY) and in 2 other control groups: hypertensive cardiomyopathy (HTN) (n = 30) and non-ischemic dilated cardiomyopathy (DCM) (n = 19). All CMR was performed in a 1.5 T (GE Signa CV/i) scanner. Cine SSFP imaging (temporal resolution < 50 ms) and late gadolinium enhancement (LGE) were performed in matching 3-radial planes to assess LA function and any segmental infiltration of LA myocardium. LGE imaging of the LA was assessed in a 9-segment model and quantified as a % extent of infiltration ($LGE\%_{LA}$). LA volumes were measured by an average of the 3 radial views and at 3 diastolic time points (end-ventricular systole, pre-atrial contraction, and post-atrial contraction), respectively. LA emptying function (total, conduit, and contractile) were derived from the percent reduction in LA volume between the time points. One-way ANOVA with Bonferroni Corrections was used to compare all variable means between groups and

Cardiac Amyloidosis Compared to the Control Groups
Left Atrial Functions and the Extent of Left Atrial Late Enhancement

imaging data were evaluated blinded to the underlying clinical diagnosis.

Results: All 8 AMY patients (100%) had extensive LGE of the LA, which was significantly higher than either the HTN or DCM control groups (17 and 11% of patients, respectively, $p < 0.001$). The extent of LA infiltration was markedly higher in AMY patients compared to HTN and DCM controls (mean LGE%$_{LA}$ = 71% versus 7%, $p < 0.001$, and 3%, $p < 0.001$, respectively). In all patients, LGE%$_{LA}$ demonstrated strong inverse correlations with total LA emptying function ($r = -0.45$, $p = 0.0007$), LA conduit emptying function ($r = -0.39$, $p = 0.006$), and LA contractile emptying function ($r = -0.33$, $p = 0.02$). While LA conduit emptying function of AMY patients was not significantly different from the HTN group, (probably reflecting similar early diastolic filling impairment), LA contractile emptying function of AMY patients was markedly reduced compared to the control groups (Fig. 1).

Conclusions: In cardiac amyloidosis, LGE by CMR can characterize the presence and the extent of LA myocardial infiltration. LA myocardial infiltration is strongly associated with LA emptying impairment. These CMR quantitative atrial markers may provide noninvasive differentiation of cardiac amyloidosis from other causes.

150. UNCOMPLICATED OBESITY IS CHARACTERIZED BY ALTERED SYSTOLIC AND DIASTOLIC MYOCARDIAL VELOCITIES AS ASSESSED BY PHASE CONTRAST MAGNETIC RESONANCE IMAGING

**Mohammed K. Ali, MBChB,[1] Oliver J. Rider, MA, MRCP,[1] Steffen E. Petersen, MD, Dphil,[1] Jane M. Francis, DCCR, DNM,[1] Matthew D. Robson, PhD,[1] Clare E. Jackson, PhD,[1] Bernd A. Jung, PhD,[2] Monique R. Robinson, MBBS, Dphil,[1] Stefan Neubauer, MD, FRCP.[1] [1]*Oxford Centre for Clinical Magnetic Resonance Research, University of Oxford, Oxford, United Kingdom,* [2]*Department of Diagnostic Radiology, Medical Physics, University of Freiburg, Freiburg, Germany.*

Introduction: The increasing prevalence of obesity poses a wide range of problems for society, both health-related and socioeconomic. The effects of uncomplicated obesity, a subgroup with no other cardiovascular risk factors, on the cardiovascular system have not been fully elucidated. Tissue velocities are highly sensitive indices of ventricular function and have also been found to have prognostic value in terms of cardiac health.

Purpose: To investigate whether subtle pre-clinical changes in cardiac function occur in uncomplicated obesity, this study aimed to characterise three-dimensional velocities of the left ventricle derived from CMR scanning and compare these to data from a sample population of normal-weight controls. We hypothesized that obesity alone leads to alterations in global left ventricular (LV) myocardial tissue velocities.

Methods: Thiry-six obese individuals (19 men, 17 women, BMI 35.6 ± 5.2 SD) selected on the basis of having no identifiable cardiac risk factors (non-smoking, normotensive, normo-cholesterolemic with non-diabetic range fasting glucose measurements) were compared to 34 healthy controls (19 men, 15 women, BMI 22.4 ± 1.6 SD). All subjects underwent "tissue phase mapping" using a black-blood segmented k-space gradient-echo sequence at 1.5 Tesla with a temporal resolution between 52 and 58.5 ms, a method of quantifying 3D tissue motion in systole and diastole (1). Images were acquired at 3 slice positions corresponding to basal, mid-ventricular and apical regions of the heart. Offline analysis and post-processing with Matlab software yielded 3D velocity data.

Results: There were no significant differences in age (44.6 ± 10.3 SD vs 43.3 ± 11.8 SD, $p = 0.414$), gender distribution, blood pressure (mean BP 92.4 ± 8.4 vs 95.0 ± 10.2, $p = 0.283$) and heart rate (65.9 ± 7.7 vs 65.2 ± 8.8, $p = 0.578$) between obese subjects and lean controls. LV volumes and ejection fraction (68.8 ± 5.0 % in obese vs 69.1 ± 6.2 % in controls, $p = 0.713$) were similar and within normal limits in both groups.
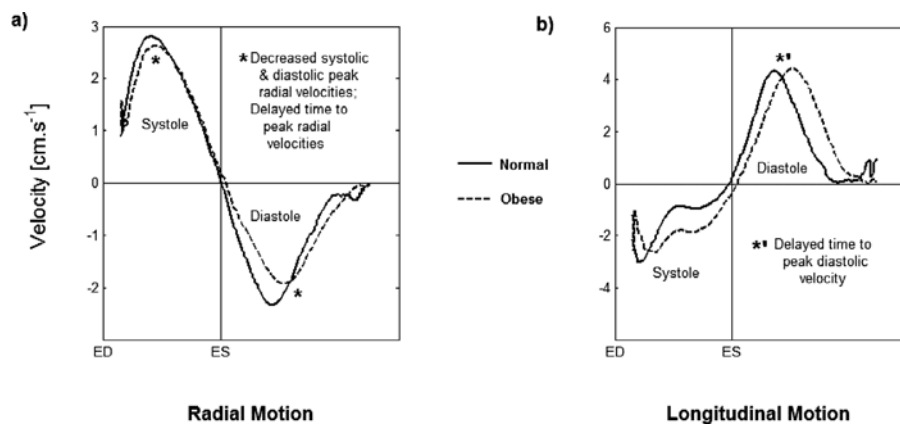

FIG. 1.   Global Myocardial Velocities: A comparison between Obese and Normal Weight Subjects. a) Shows the reduced peak systolic and diastolic RADIAL velocities found in the obese group. The maximal diastolic LONGITUDINAL velocities are similar in both groups in Figure 1b, however, the peak velocity was reached at a significantly later time-point in the obese cohort.

All results were adjusted for the higher LV mass in the obese group (131.9 ± 29.6 g vs 107.4 ± 26.5g, p < 0.001) using univariate regression analysis, even though LV mass in this group remained within the normal range.

Significant systolic changes were seen in the obese group with reduced peak radial velocities (2.63 vs 2.95 cm/s, p = 0.005) and later time to peak longitudinal contraction rate (155.5 vs 119.7 ms after the end-systolic time, p = 0.004). Significant alteration in diastolic parameters was also seen. Peak diastolic radial velocities were significantly lower in the obese cohort (−3.10 vs −3.69 cm/s, p = 0.001). Diastolic maximal longitudinal relaxation rates were similar in both groups (6.23 vs 6.36 cm/s, p = 0.78) but were reached at a significantly later time-point in the obese cohort (504.6 vs 449.3 ms, p < 0.001). This was in keeping with longer time to peak diastolic longitudinal strain rate in obesity (156.4 vs 134.8 ms, p = 0.002). No significant differences were shown in systolic (18.2 ± 6.5 vs 17.3 ± 6.1 cm/s, p = 0.849) and diastolic torsion rates (−15.0 ± 4.1 vs −14.0 ± 5.9 cm/s, p = 0.089) between obese and lean subjects.

Conclusions: Measuring tissue velocities of the heart in an obese group without co-morbid risk factors demonstrates the effects that obesity alone induces on cardiac motion. Our results demonstrate altered myocardial contraction and relaxation patterns in otherwise healthy obese people, independent of their higher LV mass. Obesity may thus be a cardiac risk factor independent of frequently associated co-morbidities such as hypertension, diabetes or hypercholesterolemia.

REFERENCE

1. Hennig J, Schneider B, Peschl S, et al. Analysis of myocardial motion based on velocity measurements with a black blood prepared segmented gradient-echo sequence: methodology and applications to normal volunteers and patients. J Magn Reson Imaging 1998; 8: 868–877.

151. MR IMAGING IN ARRHYTHMOGENIC RIGHT VENTRICULAR DYSPLASIA: INSIGHTS FROM THE MULTIDISCIPLINARY STUDY OF RIGHT VENTRICULAR DYSPLASIA

Harikrishna Tandri, MD,[1] Robson Macedo, MD,[1] Tichnell Crystal, MS,[1] Wojciech Zareba, MD, Phd,[2] Frank Marcus, MD,[3] Hugh Calkins, MD,[1] David Bluemke, MD, PhD.[1]
[1] *Johns Hopkins Hospital, Baltimore, MD, USA,* [2] *University of Rochester, Rochester, NY, USA,* [3] *University of Arizona, Tucson, AZ, USA.*
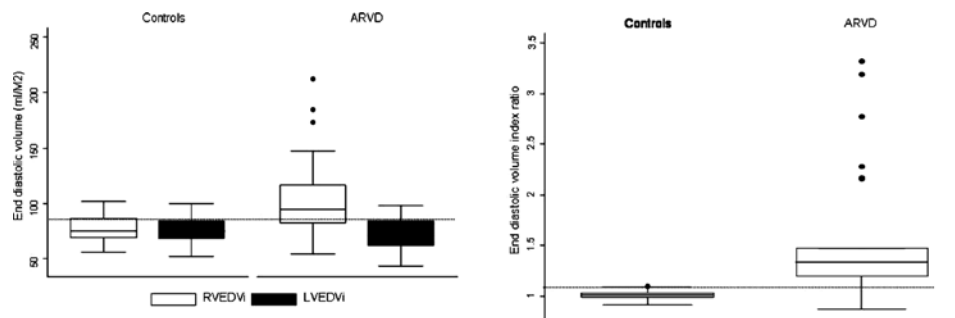
Introduction: Prior studies that have reported on MR imaging findings in arrhythmogenic right ventricular dysplasia (ARVD) were limited by small number of patients and non-uniform patient selection criteria. The purpose of our study was to define the prevalence of MR imaging abnormalities in probands enrolled in the Multidisciplinary Study of Right Ventricular Dysplasia and to define the sensitivity and specificity of quantitative MR findings in diagnosis of ARVD in this large cohort of patients.

Methods: MR images from 42 patients who met the TASK force criteria and were enrolled in the US ARVD study as probands were analyzed and compared with 25 controls. All the datasets were obtained on 1.5T MR scanners and included both fast spin echo and gradient echo sequences. Fat suppressed and non-fat suppressed fast spin echo sequences were acquired in the axial and short axis planes with breath hold double-inversion recovery blood suppression pulses. The TR was 1 or 2 R-R intervals and TE was 10 ms. The slice thickness was 5 mm, and slice gap was 5mm. The matrix and field of view were 256 × 256 and 24 cm, respectively. Gradient Echo sequences were acquired in the axial and short axis planes using breath hold steady state free precession imaging. MR images were analyzed by a blinded reader qualitatively for fat infiltration, wall thinning, and for global and regional dysfunction. RV (RVEDV) and LV end diastolic volumes (LVEDV) were quantified and indexed to body surface area. Data are presented as the mean ± one standard deviation and comparisons between the ARVD probands and controls were performed with paired t tests.

Results: The mean age of the probands was 38 ± 13 (range 15–60 yrs), and 65% (26) were men. Intramyocardial fat infiltration in the RV was observed in 24 (60%) of the probands. Wall thinning was observed in 9 patients (22%) and was most commonly seen in the basal and mid RV free wall (5/9, 55%) followed by the RVOT (3/9, 33%). Global RV dysfunction was observed in 24 (60%) patients with severe RV dysfunction in 10 patients (25%). In contrast LV dysfunction was observed in only 5 probands (13%) and was limited to mild global dysfunction. Majority of probands (80%) had regional RV dysfunction. Global RV volumes were higher and RVEF was significantly lower in ARVD probands compared to control subjects. Only six probands had a RVEF of >50% by quantitative analyses. The ratio of RVEDV to LVEDV (end diastolic volume ratio, EDV ratio) shows a clear separation of ARVD probands and control subjects and was a better discriminator compared with RVEDV index. None of the controls had a EDV ratio of >1.1 whereas 80% of the probands had a EDV ratio of >1.1. An EDV ratio of >1.07 had the optimal sensitivity and specificity (84% and 91%, respectively) in correctly classifying ARVD patients and controls.

Discussion: This study reports MR imaging findings from a large cohort of patients prospectively diagnosed with ARVD using uniform criteria (TASK force criteria), who underwent MR imaging using state of the art techniques and a standard imaging protocol. This study has several interesting findings. Firstly, contrary to several prior reports, fat infiltration was seldom the only MR imaging abnormality in ARVD. It was less sensitive for ARVD diagnosis compared with RV regional function, which appears to be abnormal in majority of patients with ARVD. Quantitative analysis revealed enlarged RVEDV in

majority of ARVD probands compared to controls and a EDV ratio of >1.07 has a high sensitivity and specificity for ARVD diagnosis.

152. DECREASE RIGHT VENTRICULAR FUNCTION AND TROPONIN ELEVATION IN MARATHON RUNNERS: A CMR STUDY

Gurpreet Baweja, Frank Molls, Vijaya kudithipudi, Mohammed Gaballa, Vincent Sorrell. *University of Arizona Sarver Heart Center, Tucson, AZ, USA.*

Introduction: Previous data on ultra-endurance athletes have shown mixed results in cardiac damage using biomarkers and echocardiography. Right ventricular, left ventricular or both have been incriminated. Because of superior spatial resolution and the ability for tissue characterization, we used cardiac magnetic resonance imaging (CMR) to assess cardiac dimensions and function, as well as tissue edema and fibrosis in runners immediately before and after running the Tucson city marathon.

Methods: Comprehensive CMR with first-pass and delayed contrast enhancement was performed 24–48 hours before and 4.6 ± 0.9 hours after successfully completing a marathon.

Blood work included cardiac enzymes for myocardial injury, troponin,CK,CKMB, myogloibin cortisol, atrial natriuretic peptide(ANP), high-sensitive CRP(hs CRP), B type natriuretic peptide(BNP) and N- terminal pro BNP .

Results: (Table) There was a significantly increased ANP and hs CRP in Group I after the race compared to baseline. One half (50%) had elevated cTn I ≥ 0.04 after the race (Group I) versus 5/10 (50%) with normal cTn I levels < 0.04 (Group II). There were no historical, clinical, or exercise predictors of an elevated Troponin.

There were no CMR findings of LV ischemia, edema, or fibrosis. There was no significant difference between pre and post race LV ejection fraction, LV and RV end diastolic volumes, and LV and RV stroke volumes in either group.

There was a decrese in RVEF, and a 2% absolute decrease in RVFS in Group I. Where as Group II had no significant changes in RVEF but with a 12% increase in RVFS.

Group I had shown increase in LV &RV end systolic volumes, and failed to show a significant decrease in LV end diastolic diameter compared to Group II.

Conclusions: In marathon runners, elevated troponin levels were found in 50% of volunteers and were associated with decreased RV function.

TABLE 1
Pre and post race bioassay and CMR results (all values mean $\pm$ SE)

	Group I (trop $\geq$ 0.04)			Group II (trop < 0.04)		
	Pre	Post	p-vlaue	Pre	Post	p-value
CKMB (ng/ml)	5.1 ± 1.7	80 ± 32	0.07	0.5 ± 1	29 ± 8	0.02
hsCRP (mg/l)	0.8 ± 0.4	6.5 ± 1.6	0.01	0.1 ± 0.07	1.6 ± 0.9	NS
Pro ANP (pmol/ml)	2.6 ± 1.7	3.4 ± 1.8	0.03	6.5 ± 2.3	7.5 ± 2.6	NS
BNP (ng/ml)	0.23 ± 0.06	0.17 ±0.05	NS	1.8 ± 1	1.5 ± 0.7	NS
LVEF (%)	63 ± 1.5	58.5 ± 2.6	NS	57 ± 2.3	53.8 ± 2.5	NS
LVESV (ml)	64 ± 4	75 ± 5	0.01	90 ± 8	85 ± 5	NS
RVEF (%)	55 ± 1.2	47 ± 1.2	0.02	51.8 ± 2	49 ± 3	NS
RVESV (ml)	70 ± 6	83 ± 6	0.007	85 ± 4	88 ± 6	NS

Saturday, February 3, 2007
Oral Abstracts: Basic-Session XI

153. MR CORONARY VEIN IMAGING IN CARDIAC RESYNCHROZATION THERAPY: INITIAL EXPERIENCE

Reza Nezafat, PhD, Yuchi Han, MD, Susan B. Yeon, MD, Dana C. Peters, PhD, John Wylie, MD, Peter Zimetbaum, MD, Beth Goddu, RT, Kraig V. Kissinger, RT, Warren J. Manning, MD. *Beth Israel Deaconess Medical Center, Harvard Medical School, Boston, MA, USA.*

A growing population of congestive heart failure (CHF) patients is being referred for cardiac resynchronization therapy (CRT). CRT is a novel therapy in which a pacing lead is placed in a lateral branch of the coronary sinus to synchronize left ventricular contraction. Proper placement of the coronary sinus lead is facilitated by knowledge of the coronary vein anatomy, particularly determination of the presence, location, and orientation of a suitable venous branch over the lateral wall of the heart is essential. We sought to develop CMR technology for imaging the coronary vein so as to benefit this population.

Methods: Sequence Design: A high resolution coronary vein imaging sequence, analogous to that used for coronary artery imaging was developed, based on a 3D gradient-echo free-breathing navigator-echo gated with fat-saturation, vector ECG-triggered Cartesian acquisition. Although a T2 preparation sequence is commonly used to improve blood-myocardium contrast in coronary artery imaging, the prep pulse suppresses coronary vein signal due to the short T2 (=35 ms) of deoxygenated venous blood. Therefore, we proposed to use magnetization transfer (MT) for contrast-enhancement. This preparation provides suppression of the myocardial signal with minimum saturation of the venous blood so as to maintain venous blood SNR.

Contrast Enhancement: An off-resonance MT scheme was used for improved blood-myocardium enhancement. Numerical simulations were performed comparing Gaussian, Fermi, Sinc, and Gaussian-weighted- Sinc pulses as the choices for the off-resonance pulse in a train of off-resonance RF pulses. SAR and flip angle outside the desired saturation-bandwidth of the preparation sequences were compared. The flip angle, off-set frequency and number of RF pulses were determined empirically by measuring the CNR between myocardium and ventricular blood as a metric.

Image Acquisition: Four phantoms, including water, 2%, 4% and 8% agar tubes were imaged to test the MT efficiency. In-vivo images were acquired in 11 healthy subjects and 3 CHF patients scheduled for CRT. Conventional x-ray coronary venography was performed on all the patients as a reference for coronary vein anatomy. Coronary vein image acquisition parameters were: $\alpha = 300$, TR = 7.6 ms, TE = 2.2 ms, 20–40 slices of 1.5 mm thickness (after zero-filling), FOV = 270 mm^2, in-plane resolution of 1.1 mm $\times$ 0.7 mm reconstructed to 0.53×0.53

FIG. 1. Reformatted coronary vein of a healthy subject (CS = Coronary-Sinus, LV = Lateral-Vein, PV = Posterior-Vein, GC = Great-Cardiac-Vein).

$\times$ 1.5 mm^3. A train of 8–10 RF pulses, with duration of 15–20 ms and flip angle of 800°–1000° with off-set frequency of 300–400 Hz was used for MT.

Results: Relative SAR of Fermi, Gaussian, Sinc, and Gaussian-weighted-Sinc pulses were 100%, 137%, 85%, and 90% respectively. This shows that the Gaussian-weighted-Sinc and Sinc pulses are the most energy efficient pulses. Numerical simulations of the flip angle outside the desired bandwidth demonstrated that the Gaussian-weighted-Sinc and Gaussian pulses have negligible flip angle outside the saturation-band.

FIG. 2. Example coronary vein images of CHF patient (male, 56-years-old).

FIG. 3.   Example coronary vein images of CHF patient (female, 66-years-old)

Therefore, we used a Gaussian-weighted-Sinc pulse. The phantom measurements showed a signal reduction in tubes with higher agar concentration with minimal suppression of water signal, which is the direct consequence of MT.

Figure 1, 2 and 3 shows example images in a healthy subject and CHF patients. In one CHF patient (Fig. 2), the coronary vein MRI demonstrated an acute takeoff for the target lateral vein. This finding was confirmed by x-ray coronary venography. Attempts to position a pacemaker lead in this vein were unsuccessful because the take off angle could not be negotiated, so the patient required surgical epicardial lead placement.
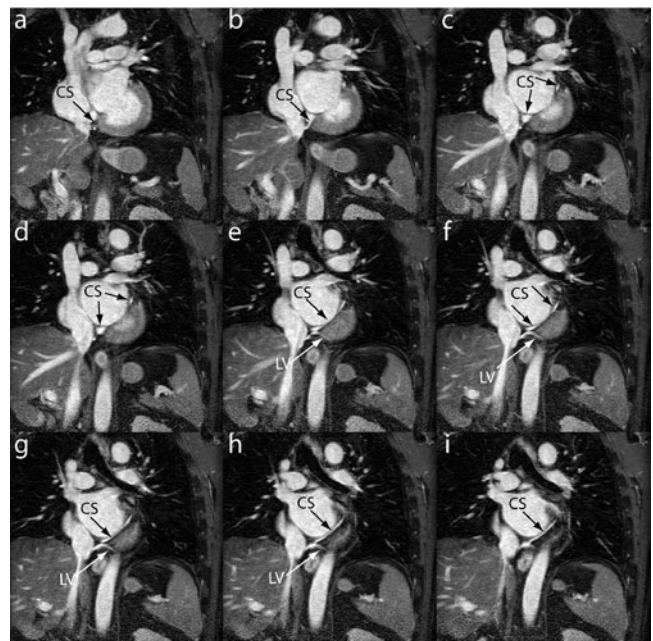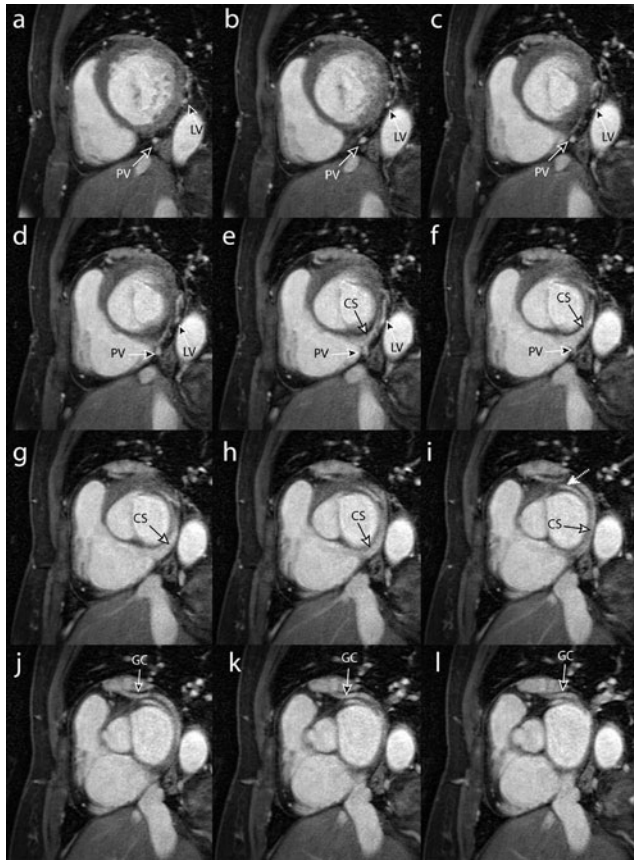
The SNR and CNR measurements in healthy-subjects were as follows: $SNR_{myocardium} = 28 \pm 8$, $SNR_{venous-blood} = 48 \pm 19$, $CNR_{myocardium-blood} = 22 \pm 12$.

Conclusion: A coronary vein CMR imaging sequence is provided which shows the potential of CMR to image coronary vein anatomy. This could be combined with CMR delayed-enhancement and functional-imaging to enable comprehensive planning for CRT candidates.

154.   SUB-MILLIMETER ISOTROPIC RESOLUTION CAROTID WALL MRI WITH A SWALLOWING COMPENSATED DARK BLOOD SSFP SEQUENCE: TOWARDS VESSEL MORPHOMETRY

Ioannis Koktzoglou, MS, Debiao Li, PhD. *Northwestern University, Chicago, IL, USA.*

Introduction: Carotid plaque morphology and composition may indicate the risk of plaque rupture and thrombosis, events preceding acute cerebral ischemia and infarction. Current MRI methods to assess vascular plaques are predominantly 2D methods that offer poor spatial resolution. Recently introduced 3D methods for carotid vessel wall imaging require long imaging times (>5 minutes) and may be corrupted by swallowing-induced motion artifacts. Ideally, acquisition of isotropic, sub-millimeter resolution MR image sets of the carotid arteries should be possible without the worry of swallowing induced motion artifacts.

Purpose: To assess whether very high, isotropic spatial resolution MR imaging ($0.6 \times 0.6 \times 0.6$ mm^3) of the carotid arterial wall is feasible at 1.5 T with a swallowing compensated, black-blood SSFP-based sequence, and determine whether image quality would be sufficient for semi-automated (i.e., computer-assisted) carotid wall segmentation.

Materials and Methods: MRI: Imaging was performed on a 1.5 T scanner (Siemens, Erlangen, Germany) with carotid array coils (Machnet BV, The Netherlands). The carotid arteries of seven healthy volunteers (n = 14) were imaged with a 3D navigator-gated diffusion-prepared steady-state free precession sequence (3D nDP-SSFP) (1). The navigator was placed through the epiglottis to track its motion and discard image data collected during incidents of swallowing (2). Imaging parameters for the 3D nDP-SSFP sequence were: 4.8 cm thick axial slab placed at the level of the carotid bifurcation, sequence TR = 1 s, SSFP TR/TE = 5.2/2.6 ms, flip = 45°, FOV = 11.5×11.5 cm^2, matrix = 192×192, 80 slices, slice oversampling = 20%, BW = 565 Hz/pixel, averages = 2, acquisition time = 596 s (with 100% navigator efficiency). Carotid wall-lumen contrast-to-noise ratio (CNR) was measured. *Semi-Automated Wall Segmentation:* A new wall semi-automated algorithm, inspired from previous algorithms used to segment 3D ultrasound data (3), was applied to segment the carotid artery wall from the 3D nDP-SSFP
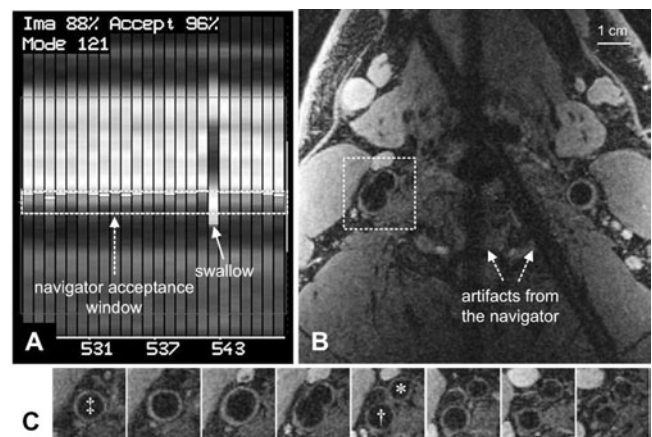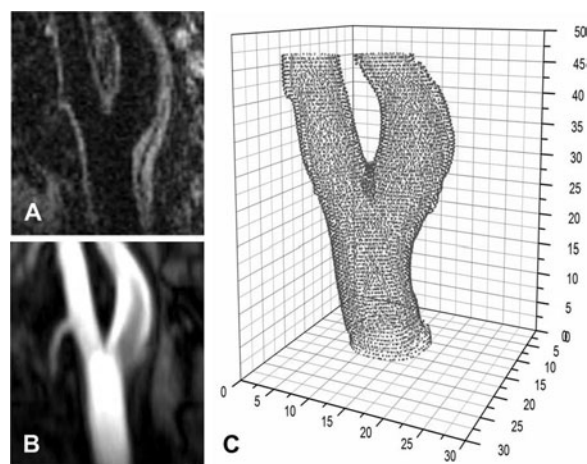

FIG. 1.

FIG. 2.

image sets. Semi-automated carotid lumen and wall measurements were compared to those made by an experienced user.

Results: Mean navigator efficiency with the 3D nDP-SSFP imaging sequence was 96.9%, corresponding to an imaging time of 620 s. In no volunteers did swallowing induce image degrading artifacts.

Figure 1 shows images acquired with the 3D nDP-SSFP sequence: (a) navigator image of the epiglottis depicting a swallow; (b) full field of view axial image displaying the two carotid arteries; (c) several axial slices of the right carotid artery at the location of the dashed boxed region of in (b).

Carotid wall-lumen CNR obtained with 3D nDP-SSFP was 5.2 ± 1.1. Morphometric measurements of carotid wall and lumen areas as made by the semi-automated algorithm were highly correlated to manual measurements (wall area: intraclass correlation coefficient (ICC) $= 0.961$, linear regression r $= 0.967$, p < 0.001 for both; lumen area: ICC $= 0.996$, r $= 0.997$, p < 0.001 for both). Computer extracted boundaries defining the carotid artery wall are shown in Fig. 2. Fig. 2 shows: (a) a multiplanar reformation (MPR) through the 3D nDP-SSFP image set depicting the right carotid artery of a volunteer; (b) a MPR through a corresponding time-of-flight MR angiogram; (c) inner (green) and outer (red) wall boundaries of the vessel in (a) as determined by the computer-aided segmentation algorithm.

Conclusion: Acquisition of isotropic, sub-millimeter resolution MR images of the carotid arterial wall with black-blood image contrast is feasible with 3D nDP-SSFP without swallowing-induced motion artifacts. Computer-assisted segmentation of the 3D nDP-SSFP data set provides carotid wall and lumen areas that are in excellent agreement with manual measurements.

REFERENCES

1. Koktzoglou, et al. Proceedings, 14th ISMRM 2006;652.
2. Crowe, et al. J Magn Reson Imaging 2005;22:583–588.
3. Zahalka, et al. Phys Med Biol 2001;46:1321–1342.

155. COMPARISON OF 3D BLACK BLOOD IMAGING TECHNIQUES FOR CAROTID VESSEL WALL IMAGING

Venkatesh Mani, PhD,[1] Ioannis Koktzoglou, PhD,[2] YiuCho Chung, PhD,[3] Claudia Calcagno, MD,[1] Karen B. Weinshelbaum, MD,[1] Renate Jerecic, PhD,[3] Debiao Li, PhD,[2] Zahi A. Fayad, PhD.[1] *[1]Mount Sinai School of Medicine, New York, NY, USA, [2]Northwestern University, Chicago, IL, USA, [3]Siemens Medical Solutions, Chicago, IL, USA.*

Introduction: MR imaging of atherosclerotic plaque in carotids is typically performed using 2D black blood turbo spin echo (TSE) sequences. Partial voluming artifacts limit the use of 2D imaging for assessment of plaque burden in vivo. Recently, several fast 3D black blood sequences have been developed to overcome this limitation. The purpose of the current study was to qualitatively and quantitatively compare three different 3D black blood imaging techniques; a) Double inversion recovery (DIR) steady state free precession (SSFP) (1), b) Diffusion SSFP (2) and c) variable flip angle TSE (SPACE) (3) for carotid vessel wall imaging.

Methods: Ten atherosclerotic patients were subjected to the three different 3D black blood imaging techniques on a 1.5T Siemens scanner. Sample images using the three techniques from an atherosclerotic patient are shown in the Fig. The imaging parameters were as follows: for DIR SSFP and Diffusion SSFP, all parameters were identical with 20 axial slices, each 1 mm thick acquired with a field of view of 14×14 cm^2 and a matrix size of 256^2. A TR of 1000 ms and TE of 2.5 ms and bandwidth of 980 Hz/px were used. For the diffusion module, the B-Value used was 11.96 s/mm^2. For SPACE, 60 coronal slices with an isotropic voxel size of approximately 0.9 mm were acquired with field of view of 20×12 cm^2. The TR/TE/ echo train length was 500 ms/115 ms/57. Imaging time for each scan was 3 minute 45 seconds. No cardiac triggering was used for any of the acquisitions.

Images were qualitatively analyzed for overall image quality, flow suppression, artifacts (ghosting, motion, etc) and vessel wall delineation by an expert observer. A 5-point scale with 1 being the poorest and 5 being the best was used. Quantitative analysis (signal to noise ratios (SNR) of the vessel wall, lumen and muscle and contrast to noise ratio (CNR) of the wall and lumen) were also performed. A Mann-Whitney rank sum test was used to compare the scores obtained using the qualitative analysis and a one-way ANOVA was used to compare the SNR and CNR values.

Results: Qualitative analysis showed that the DIR SSFP technique had better overall image quality, vessel wall delineation and fewer artifacts compared to the other two techniques. The flow suppression was best using the Diffusion SSFP sequence (Table 1).

Quantitatively, the DIR SSFP technique had the highest SNR from the vessel wall but also had the poorest flow suppression (highest SNR lumen). The Diffusion SSFP sequence had the
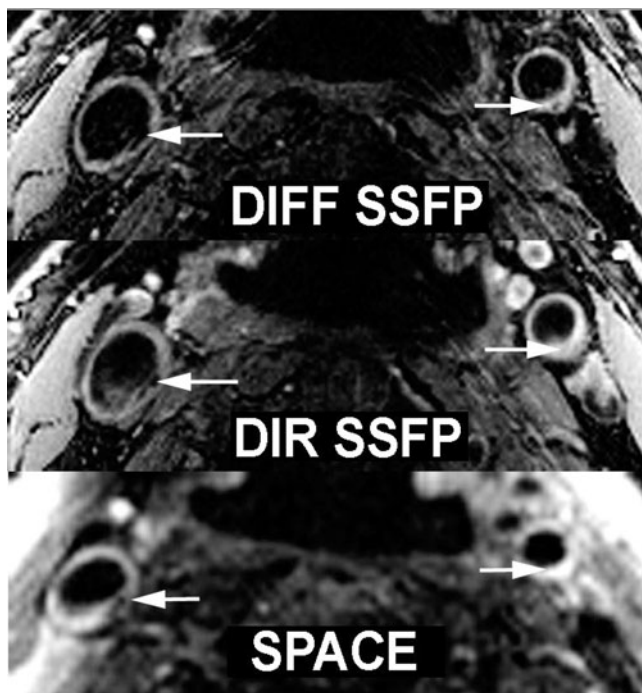
TABLE 1
Qualitative Analysis

Imaging Method	Overall Image Quality	Flow Suppression	Artifacts	Vessel Wall Delination
Diffusion SSFP	3.56 ± 0.70	**4.74 ± 0.43**	3.45 ± 0.78	3.51 ± 0.97
Double Inversion Recovery SSFP	**4.22 ± 0.49**	3.97 ± 0.77	**4.07 ± 0.65**	**4.11 ± 0.78**
Variable Flip Angle TSE	2.48 ± 0.73	4.28 ± 0.74	3.52 ± 0.86	3.30 ± 1.16

TABLE 2
Quantitative Analysis

Sequence	SNR Wall	SNR Lumen	SNR Muscle	CNR Wall Lumen
Diffusion SSFP	14.3 ± 3.99	**3.4 ± 0.65**	11.4 ± 3.66	10.5 ± 3.75
DIR SSFP	**24.3 ± 8.77**	6.8 ± 2.86	15.9 ± 4.54	17.5 ± 7.88
Variable Flip Angle TSE	22.2 ± 9.08	3.5 ± 1.68	**17.3 ± 7.95**	**18.6 ± 9.39**
ANOVA p value	**0.027**	**0.003**	0.094	0.062

best flow suppression (lowest SNR Lumen) but also the least SNR from the vessel wall. The SPACE sequence had the highest SNR from the sternocledomastoid muscle and the highest CNR between the wall and lumen (Table 2).

Conclusions: In 3D black blood imaging of the carotid arteries, the DIR SSFP sequence provided better image quality both qualitatively and quantitatively. The Diffusion SSFP sequence was best in terms of flow suppression. The SPACE sequence provided excellent CNR between wall and lumen, adequate SNR and flow suppression quantitatively but fared poorly in the qualitative evaluation. It, however, had the greatest anatomical coverage with isotropic voxel size albeit with a slightly poorer in plane resolution.

REFERENCES

1. Koktzoglou, et al. Proc. 13th ISMRM 2005;1743.
2. Koktzoglou, et al.; Proc 14th ISMRM 2006;652.
3. Chung, et al. Proc 14th ISMRM 2006;653.

156.   INCREASED CORONARY ATHEROSCLEROSIS DETECTED BY MAGNETIC RESONANCE IN ASYMPTOMATIC TYPE 1 DIABETES WITH DIABETIC NEPHROPATHY

Won Yong Kim, MD,[1] Anne Sofie Astrup, MD,[2] Matthias Stuber, PhD,[3] Lise Tarnow, MD,[2] Erling Falk, MD,[1] René M. Botnar, PhD,[4] Cheryl Simonsen, RT,[5] Lotte Pietraszek, Lab Tech,[2] Peter R Hansen, MD,[6] Warren J. Manning, MD,[7] Niels T Andersen, PhD,[8] Hans-Henrik Parving, MD.[2] [1] *Department of Cardiology, Skejby Hospital, Aarhus, Denmark,* [2] *Steno Diabetes Center, Gentofte, Denmark,* [3] *Department of Electrical and Computer Engineering, and Russell H. Morgan Department of Radiology and Radiological Science, Johns Hopkins University, Baltimore, MD, USA,* [4] *Department of Nuclear Medicine, Technical University Munich, Munich, Germany,* [5] *MR-center, Skejby Hospital, Aarhus, Denmark,* [6] *Department of Cardiology, Gentofte University Hospital, Gentofte, Denmark,* [7] *Department of Medicine, Cardiovascular Division and Department of Radiology, Beth Israel Deaconess Medical Center and Harvard Medical School, Boston, MA, USA,* [8] *Department of Biostatistics, Institute of Public Health, Aarhus University, Aarhus, Denmark.*

Introduction: Patients with type 1 diabetes and diabetic nephropathy maintain an excess cardiovascular mortality compared to patients with normoalbuminuria. Conventional cardiovascular risk assessment may not accurately predict cardiovascular events in type 1 diabetes since intensive multifactorial intervention has been implemented in recent years.
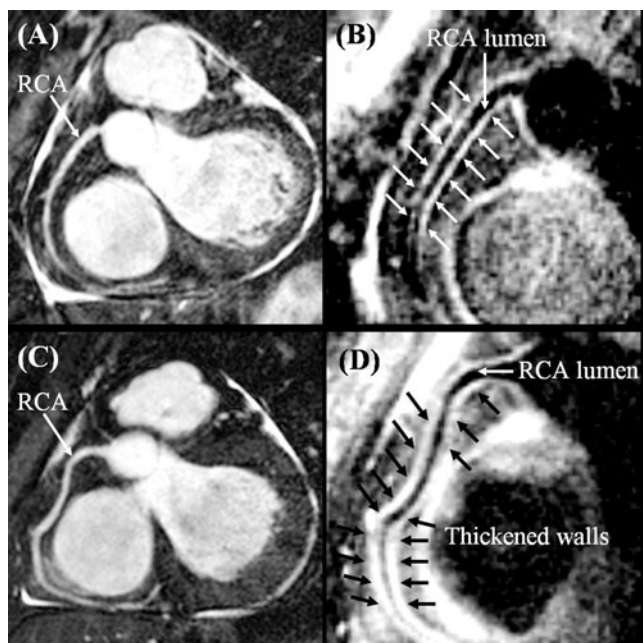
FIG. 1. Three-dimensional reformatted coronary MRI of the proximal RCA in two subjects without coronary luminal stenosis (A) 58-year-old male with longstanding type 1 diabetes and normoalbuminuria and (C) 44-year-old male with longstanding type 1 diabetes and diabetic nephropathy. The corresponding 3D black-blood vessel wall scans (B) showing no CMR evidence of atherosclerotic plaque (average and maximum vessel wall thickness 1.1 mm and 1.3 mm, respectively) (D) showing an increased atherosclerotic plaque burden (average and maximum vessel wall thickness 2.3 mm and 3.0 mm, respectively). The anterior and posterior RCA walls are indicated by arrows.

Purpose: We sought to evaluate the effect of diabetic nephropathy on atherosclerosis in type 1 diabetes using CMR to evaluate subclinical coronary and aortic atherosclerosis in asymptomatic type 1 diabetic patients with and without nephropathy.

Methods: From July 2003 to February 2005, 136 subjects from the Steno Diabetes Center with long-standing type 1 diabetes including 63 (46%) subjects with nephropathy without symptoms or clinical history of cardiovascular disease were randomly included from among those with and without nephropathy. Diabetic nephropathy was defined as previously persistent albuminuria (urinary albumin excretion rate >300 mg/24 h in two of three consecutive 24 h urine collections), presence of retinopathy, and no evidence of other renal or urinary tract disease.

All subjects underwent CMR examination using a Philips Intera 1.5 T MR whole body scanner (Philips, Best, The Netherlands), equipped with a 5-element cardiac phased array coil and a cardiac software package (R9.1.1). All coronary CMR angiograms were acquired during free-breathing using a diagphramatic navigator for respiratory motion compensation according to a previously validated protocol. Right coronary artery (RCA) vessel wall scanning was done in a subset of subjects when total scan time did not exceed one and a half hour (24 with and 37 patients without nephropathy, respectively) using 3D black-blood imaging. To evaluate aortic atherosclerosis, subjects underwent thoracoabdominal aortic CMR with acquisition of 24 transverse slices spanning the aortic arch to the aortoiliac bifurcation using a ECG-gated, T2-weighted, and fat-suppressed black-blood turbo spin-echo sequence. Coronary plaque burden (CPB) was quantitated as the mean and maximum RCA vessel wall thickness along the entire proximal course of the vessel by semi-automated segmentation of the 3D reformatted black-blood vessel wall scans. Atherosclerotic plaque was defined as characteristic luminal protrusions of >1 mm in radial thickness.

Results: Coronary artery stenoses were identified in 10% of subjects with nephropathy (vs. 0% with normoalbuminuria, $p = 0.007$). Coronary plaque burden (CPB) expressed as right coronary artery (RCA) mean wall thickness (1.7 ± 0.3 mm vs. 1.3 ± 0.2 mm, $p < 0.001$) and maximum RCA wall thickness (2.2 ± 0.5 mm vs. 1.6 ± 0.3 mm, $p < 0.001$) was greater in subjects with nephropathy (Fig. 1).

The prevalence of thoracic (3% vs. 0%, $p = 0.28$) and abdominal aortic plaque (22% vs. 16%, $p = 0.7$) was similar in both groups. Subjects with and without abdominal aortic plaques had similar CPB.

Conclusions: In asymptomatic type 1 diabetes, CMR reveals greater CPB in subjects with nephropathy compared to those with normoalbuminuria.

157. IN VIVO MAGNETIC RESONANCE IMAGING OF IRON OXIDE LABELED STEM CELLS IN A MOUSE MODEL OF MYOCARDIAL INFARCTION WITH POSITIVE CONTRAST

Venkatesh Mani, Karen C. Briley-Saebo, PhD, Eric Adler, MD, Juan Gilberto S. Aguinaldo, MD, Anne Bystrup, Gordon Keller, PhD, Zahi A. Fayad, PhD. *Mount Sinai School of Medicine, New York, NY, USA.*

Introduction: Animal studies suggest that stem cells may be able to home to sites of myocardial infarction (MI) and assist in tissue regeneration. Recently, iron-oxide labeled stem cells have been used for in-vivo tracking of stem cells using MRI. However, due to the negative contrast generated by iron oxides differentiation between the signal loss induced by iron-laden cells and the native low signal in tissue (or generated by artifacts) is problematic. As a reuslt, it may be preferable to have a technique that produces positive contrast in the presence of iron.

Objective: The aim of the current study was to test the feasibility of using a positive contrast white marker MR imaging technique employing reduced z-gradient rephasing (GRASP) for dynamically tracking stem cells in an in-vivo mouse model of myocardial infraction.

Methods: Ferumoxides and protamine sulfate, were complexed and used to magnetically label mouse embryonic stem (ES) cells, as shown in Fig. 1. Experiments to test the feasibility of MR tracking of iron labeled ES cells within the mouse

Figure 1: Method for labeling embryonic stem cells

Figure: In vivo images of a SCID mouse with myocardial infarction induced by coronary ligation and then transplanted with stem cells labeled with ferumoxides. (A) Pre stem cell transplantation image (conventional T2* GRE image). (B) Post stem cell injection-Conventional T2*GRE image. Dark spot on image indicates location of stem cells (arrow) (C) Pre stem cell injection GRASP image of mouse heart. (D) Post stem cell injection GRASP image. Bright spot indicates location of stem cells (arrow). (E) Color coded GRASP image superimposed on conventional T2*GRE image. (F) Histology of imaging slice (H & E staining). (G) Blue spots seen on Perls staining indicating presence of iron at the location (zoomed view of box in F). Good correlation between MRI and histology is seen.

heart were performed on mice with Myocardial Infarction (MI) induced using a direct coronary ligation model and on control animals. Viability of the iron laden stem cells was confirmed by observing beating ES cells in culture. The uptake of iron by thease cells was verified by imaging plates containing beating ES cells using both T2* (negative contrast) and positive contrast GRASP. After infarction, 500,000 ES cells or saline (as a control) were injected in the border zone of the infarct. MR imaging was performed on a 9.4T scanner using conventional T2* GRE sequences and the GRASP technique before MI, and two weeks after MI. Imaging parameters for GRASP were as follows: TR $=300$ ms, TE $= 5$, 10 and 15 ms, FOV of 2.8 x 2.8 cm^2, and a matrix size of 192×192 pixels (resolution of 145×145 um^2). The z-gradient rephasing used was 100% for conventional T2*-weighted sqeunces and 25% for GRASP. Following imaging, mice were sacrificed, and histology performed. Perl's staining was used to confirm iron within the myocardium.

Results: Fig. 2 shows representative images obtained for MI mice within 24 hours after the adminsitration of the iron-laden stem cells. A correlation was observed between signal loss seen on conventional T2* images and the bright areas observed using GRASP. The imaging data correlated well with histology that showed the presence of iron-laden cells within regions that enhanced by MRI.

Conclusion: The results of this study demonstrate the feasibility of in-vivo stem cell imaging with positive contrast MRI.

158. A FIBRIN-TARGETED MULTI-MODALITY NANOPARTICLE CONTRAST AGENT FOR MRI AND SPECT

Shelton D. Caruthers, PhD,[1] Michal Lijowski, PhD,[2] Grace Hu, MS,[2] Anne M. Neubauer, MS,[2] Michael J. Scott,[2] Ralph W. Fuhrhop,[2] Patrick J. Gaffney, MD, PhD,[3] Samuel A. Wickline, MD,[2] Gregory M. Lanza, MD, PhD.[2] [1]*Washington Univeristy and Philips Medical, St. Louis, MO, USA,* [2]*Washington Univeristy, St. Louis, MO, USA,* [3]*St. Thomas' Hospital, London, United Kingdom.*

Figure: Fibrin-targeted multi-modality perfluorocarbon nanoparticle contrast agent. The first panel shows a maximum intensity projection through a T1-weighed MRI dataset from fibrin clots in a 12-well plate. The corresponding nuclear image is in the middle panel. Tc- & Gd-bearing fibrin-bound CA concentration decreases from left to right in these images. (Note the one "cold" control in the first column. The agent used here had Gd, but no Tc, as a separate control from column #4, which had agent without Tc or Gd.) The bar graph shows signal intensity from 19F MRI (open) and SPECT (solid) decreasing as the concentration of bound CA decreases.

Introduction: Exposed fibrin is a hallmark of ruptured atherosclerotic plaques - the proximate cause of myocardial infarction and stroke. Many molecular imaging (MI) contrast agents have been developed to help overcome the innate insensitivity of MRI to imaging such biomarkers because MRI offers great potential for clinical MI through high spatial resolution, tissue characterization and spectroscopic analysis. Yet, the sensitivity of MRI to most MI contrast agents (CA) remains significantly less than that for other modalities, e.g., nuclear. A single MI CA exploiting the strengths of both modalities could therefore be detected with great sensitivity and characterized in high resolution.

Purpose: This study demonstrates a fibrin-targeted agent that can be imaged and quantified with SPECT and CMR (^{1}H and ^{19}F).

Methods: Nanoparticle emulsions (previously reported) were prepared, composed of perfluoro-15-crown-5-ether (CE) or perfluorooctyl-bromide (PFOB), and incorporated in the outer lipid surface of each particle approximately 100000 gadolinium (Gd-DTPA-BOA) and one ^{99m}Tc (^{99m}Tc-BisPyLys-PEG-PE) chelates. Biotinylated multi-modality CE nanoparticles were targeted, via avidin, to *in vitro* fibrin clots pre-treated with biotinylated anti-fibrin antibody. Varying concentrations were achieved by mixing with "cold" particles (PFOB-based, lacking Tc and Gd).

Results: Multi-modality CAs were successfully created and targeted to fibrin. Images from MRI and SPECT are shown (Fig.). On nuclear images of the fibrin-bound Tc-carrying nanoparticles, signal intensity varied, as expected, with CA concentration (solid bars in graph). T1-Weighted MRI demonstrated similar enhancement. Bound nanoparticles were detected via ^{19}F MR, regardless of the presence of Gd, but could also be selectively imaged through unique perfluorocarbon signatures. The CE-specific ^{19}F MR signal intensity (SNR) also behaved linearly with CA concentration (open bars).

Conclusions: This work presents a novel, quantifiable, multi-modality fibrin-targeted perfluorocarbon CA that exploits the sensitivity of SPECT while offering high resolution information of MRI augmented with the uniqueness of ^{19}F information.

Saturday, February 3, 2007
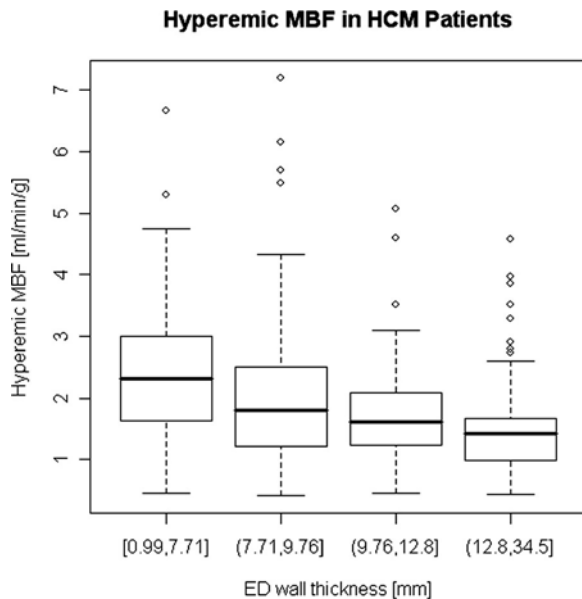## Oral Abstracts: Clinical-Session XIII

159. TRANSMURAL DISTRIBUTION OF MICROVASCULAR DYSFUNCTION IN HYPERTROPHIC CARDIOMYOPATHY ASSESSED BY MULTI-PARAMETRIC MAGNETIC RESONANCE IMAGING

Steffen E. Petersen, MD, D Phil,[1] Michael Jerosch-Herold, PhD,[2] Lucy E. Hudsmith, MA, MRCP,[1] Matthew D. Robson, PhD,[1] Jane M. Francis, DCRR, DNM,[1] Helen A. Doll, MSc, Dphil,[3] Joseph B. Selvanayagam, MBBS, FRACP, D Phil,[1] Stefan Neubauer, MD, FRCP,[1] Hugh Watkins, MD, PhD, FRCP.[1] [1] *John Radcliffe Hospital, Oxford, United Kingdom,* [2] *Advanced Imaging Research Center, Oregon Health & Science University, Portland, OR, USA,* [3] *Dept. Public Health, University of Oxford, Oxford, United Kingdom.*

Introduction: Sudden cardiac death is a well-recognized feature of hypertrophic cardiomyopathy (HCM) which is the most common cause of sudden death in the younger population, particularly in young athletes. Adverse microvascular remodelling and coronary microvascular dysfunction, reflected by an inadequate increase in myocardial blood flow in response to a coronary vasodilator, has been noted in HCM; it remains unknown whether the impairment of the hyperemic response is related to the degree of left ventricular hypertrophy. Microvascular dysfunction in HCM may create an ischemic substrate conducive to sudden death.

Purpose: We assessed the association of blood flow in relation to wall thickness and extent of fibrosis using high-resolution quantitative magnetic resonance imaging (MRI). Such pathophysiological interrelations may form an important initial step towards improved clinical risk assessment for sudden cardiac death in hypertrophic cardiomyopathy.

Methods: Degree of hypertrophy, myocardial blood flow at rest and during hyperemia (hMBF), and myocardial fibrosis were

Hyperemic MBF in HCM Patients

assessed with MRI in 35 HCM patients (26% men), and 14 healthy controls (29% men), of ages 18–78 years (mean ± SD: 42 ± 14 years) using the AHA LV 16 segment model. All cardiovascular MRI examinations were performed on a 1.5 Tesla MRI system (Sonata; Siemens Medical Solutions, Erlangen, Germany). After scout imaging, steady-state free precession cine images were acquired in horizontal and vertical long-axis views, and short-axis views were obtained parallel to the atrioventricular groove. A gadolinium-based contrast agent (Gadodiamide, Omniscan, Nycomed Amersham) was then administered intravenously as a bolus at a dose of 0.025 mmol/kg body weight (injection rate, 5 mL/s, concentration 0.5 mmol/mL). Perfusion imaging was performed every heartbeat during the first pass of the contrast bolus, using a T1-weighted fast (spoiled) gradient echo sequence with saturation-recovery magnetization preparation. To allow sufficient contrast wash-out, we performed stress (adenosine, 140 mcg/kg/min) perfusion imaging 10 minutes after the study at rest. After stress perfusion imaging, we gave an additional dose of 0.1 mmol/kg Gadodiamide to reach a total administered dose of 0.15 mmol/kg. The delayed enhancement images were acquired after a further 10 minute delay with the use of an inversion-recovery prepared, segmented gradient echo sequence. All MRI data were analyzed in a blinded manner.

Results: Resting MBF was similar between HCM patients and controls. hMBF was lower in HCM patients (1.84 ± 0.89 mL/min/g) compared with healthy controls (3.42 ± 1.76 mL/min/g), with a difference of −0.95 ± 0.30 (SE) mL/min/g; $p < 0.001$) after multivariable adjustment, including for end-diastolic segmental wall thickness ($p < 0.001$), and extent of delayed contrast enhancement (n.s.). In HCM patients, hMBF decreased with increasing end-diastolic wall thickness ($p < 0.005$, Fig. 1), and preferentially in the endocardial layer, and was significantly lower in patients with an LV outflow gradient >30 mm Hg ($p < 0.02$) by −0.9 mL/min/g. The frequency of endo-

cardial hMBF falling below epicardial hMBF in a myocardial sector rose with wall thickness ($p = 0.045$), as did the incidence of fibrosis ($p < 0.001$).

Conclusions: In HCM the vasodilator response is reduced, particularly in the endocardium, and in proportion to the magnitude of hypertrophy. Microvascular dysfunction and subsequent ischemia may be an important component of the risk attributable to HCM with substantial hypertrophy.
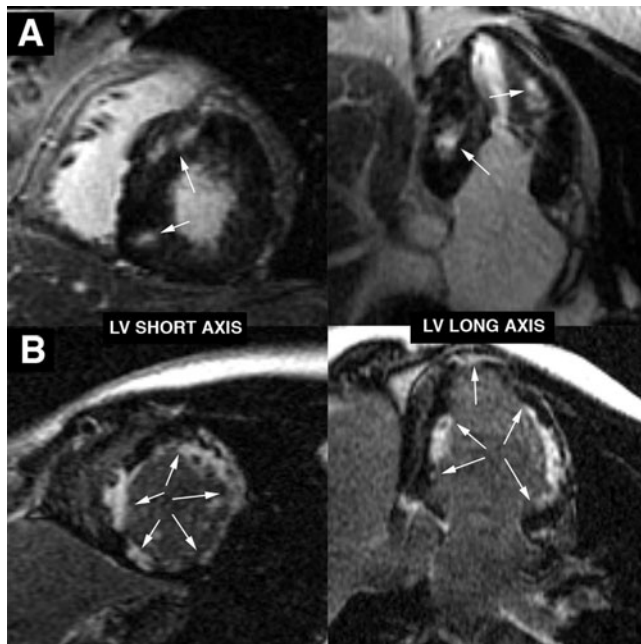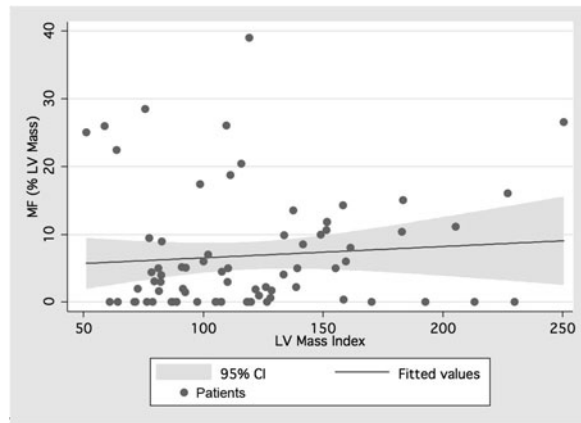
160. LACK OF CORRELATION BETWEEN HYPERTROPHY AND FIBROSIS IN PATIENTS WITH HYPERTROPHIC CARDIOMYOPATHY BY CARDIOVASCULAR MAGNETIC RESONANCE

Afonso A. Shiozaki, MD, Tiago S. Santos, MD, Edmundo Arteaga, MD, PhD, Jose Parga, MD, PhD, Luiz F. Avila, MD, PhD, Carlos E. Rochitte, MD, PhD. *Heart Institute (InCor), University of Sao Paulo Medical School, Sao Paulo, Brazil.*

Introduction: Cardiovascular Magnetic Resonance (CMR) has emerged over the last few years as a major diagnostic tool in Hypertrophic Cardiomyopathy (HCM). Recently, the presence o myocardial fibrosis (MF) visualized by CMR in HCM patients has been correlated with classical risk factors for sudden death. Although the association between hypertrophy and fibrosis has been suggested, the correlation between diastolic left ventricular (LV) wall thickness and MF has not been demonstrated.

Methods: Seventy-three of 600 outpatients with HCM were submitted to CMR in our facility (1.5-T Signa CV/I; GE Medical Systems). Myocardial hypertrophy was visualized with breath-hold cine SSFP MR images obtained in contiguous short-axis planes from the apex to the base of the heart with the patient in a resting state. Hypertrophy was defined as > 13 mm wall thickness and scored in a 17-segment model. Fibrosis was visualized using an inversion-recovery prepared gradient-echo for delayed enhancement (DE) 5 to 20min after intravenous bolus of 0.2 mmol/kg of gadolinium-based contrast. Fibrosis quantification was performed by planimetry on all short-axis slices from the base to apex, yielding quantified MF, expressed as a percent of total LV mass. The presence or absence of MF was also analyzed on a 17-segment model. LV mass was indexed to body surface area due to heterogeneity of the patients' age (3- to 69-years-old). Correlation between MF and indexed LV mass was performed by regression analysis. Agreement between the location of hypertrophy and fibrosis on a segment level was evaluated by Kappa test.

Results: Regression analysis showed no correlation between percent LV MF and LV mass index ($p = 0.47$; $r^2 = 0.007$) (Fig. 1). Moreover, there was a weak agreement between the location of LV wall hypertrophy and myocardial hyperenhancement (Kappa = 0.27) analyzed on 1241 segments. When analyzing the agreement within each patient, we observed a mean Kappa value of 0.30 ± 0.31. Therefore, the presence of MF on

HCM patients did not correlate with the indexed LV mass nor with the location of the LV wall hypertrophy (Fig. 2-HCM patient example with matched hypertrophy and myocardial fibrosis - Panel A; HCM patient with disagreement between the amount of MF and hypertrophy. One can note a massive MF with little or no increase in LV wall thickness - Panel B).

Conclusions: Our data on 73 patients did not support the previous observation, that MF in HCM patients occurs only in LV segments with hypertrophy. On the contrary, our study demonstrated a weak agreement between location of hypertrophy and MF and no correlation between indexed LV mass and percent MF. These findings suggest that additional mechanisms other than hypertrophy alone, possibly related to specific mutations and gene expression, may have an important role in the pathophysiology of MF in HCM patients.

161. HIGH PREVALENCE OF MYOCARDIAL FIBROSIS AND LEFT VENTRICULAR HYPERTROPHY IN
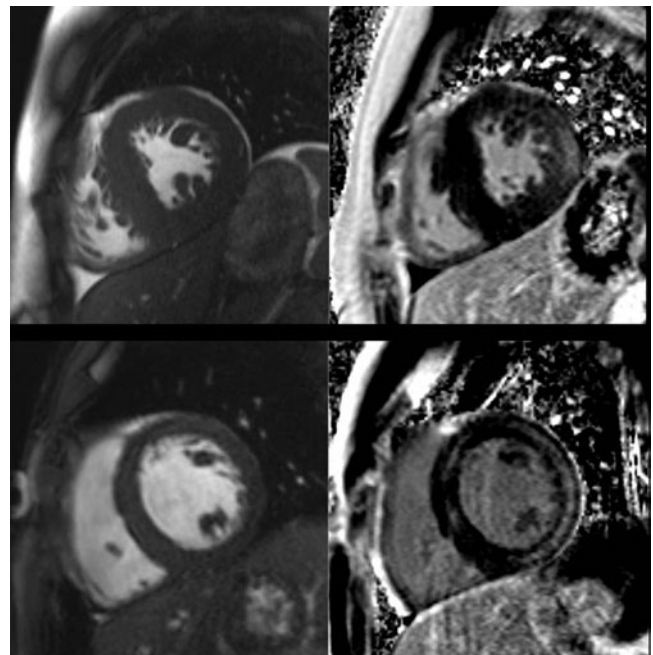
PEDIATRIC FRIEDREICH'S ATAXIA: A CARDIAC MAGNETIC RESONANCE IMAGING STUDY

Keren Hasbani, MD, Nicholas DiProspero, MD, PhD, Peter Kellman, PhD, Jonathan F. Plehn, MD, Marsha Block, RN, Pamela Vincent, Andrew E. Arai, MD. *National Institutes of Health, Bethesda, MD, USA.*

Introduction: Friedreich's Ataxia (FA), an autosomal recessive neurodegenerative disorder, is the most common cause of ataxia in the US (1 in 40,000 Caucasians). Cardiomyopathy is present in approximately 92% of patients and is the leading cause of death.

Purpose: To determine the prevalence of left ventricular hypertrophy (LVH) and myocardial fibrosis in pediatric patients with FA.

Methods: Forty-eight pediatric patients with FA were recruited for a double blind placebo controlled National Institutes of Health sponsored study of Idebenone. Prior to the investigational treatment, all of the patients were offered a cardiac MR cine study with the option to receive contrast. All patients were scanned on a Siemens 1.5 Tesla Avanto magnet using an 8-element phased array coil. Cine imaging was performed with steady state free precession (SSFP). Delayed enhancement (DE) imaging was performed using a single-shot phase-sensitive inversion-recovery SSFP sequence, 10 minutes post-administration of 0.15 mmol/kg gadolinium-DTPA. Additional higher resolution DE images were obtained in long and short axis views using a phase-sensitive inversion recovery gradient echo sequence to confirm abnormal regions. Left Ventricular Ejection Fraction (LVEF) and myocardial mass were

measured by planimetry, and DE was determined by consensus of two cardiologists.

Results: Forty-five of 48 patients completed the cine CMR, and 36/45 consneted to the gadolinium DE imaging. There were no complications. There were 24 males and 21 females. The average LVEF was 64.1% ± 7.1, 6/45 (13%) had an abnormal LVEF of less than 55%. The average myocardial mass in diastole was 73.7 ± 19.6 and in systole was 75.2 ± 20. The prevalence of LVH was 27% (12/45 patients) as defined by a myocardial mass > 80 g/m^2. The prevalence of atypical DE was 50% (18/36 patients). The DE pattern was similar to that seen in myocarditis and was predominately located in the mid wall, patchy, and did not follow the distribution of coronary arteries. Fig. 1 illustrates a sax cine and abnormal DE slice from 2 patients (cine on left, DE on right).

Conclusions: DE abnormalities are more common than either LVH, or decreased LVEF in patients with Friedrich's ataxia. This abnormal DE pattern likely represents myocardial fibrosis. Thus, myocardial fibrosis in these patients may be an early indicator of disease progression, and LVH may be secondary to the myocardial fibrosis.

162. MYOCARDIAL DELAYED CONTRAST ENHANCEMENT IN PULMONARY SARCOID PATIENTS, ASSOCIATION WITH SIGNIFICANT RIGHT AND LEFT CHAMBER REMODELING

Alexander B. Jehle, MD,[1] **Marcus Y. Chen, MD,**[1] **Mark Girzadas, MD,**[1] **E. Brigitte Gottschall, MD,**[2] **Howard D. Weinberger, MD,**[1] **Robert A. Quaife, MD.**[1] [1]*University of Colorado HSC, Denver, CO, USA,* [2]*National Jewish Medical Center, Denver, CO, USA.*

Background: Sarcoidosis is a systemic granulomatous disorder of unknown etiology. Clinical evidence of myocardial involvement is present in approximately 5% of patients with sarcoidosis, although autopsy studies suggest closer to 20–30% of patients have sub-clinical involvement. Cardiac involvement is associated with a poor prognosis, with mortality rates exceeding 40% at 5 yrs. While multiple modalities are employed, the diagnosis of cardiac sarcoid (CS) remains difficult. The ability of MRI to provide high-resolution anatomic information as well as cardiac function has made it an effective modality for direct visualization of the myocardium and pericardium. Furthermore, with the recent use of gadolinium delayed contrast enhanced imaging (DCE), small regions of injury, fibrosis and granulomas can be identified. Cardiac MRI is a promising, non-invasive method of diagnosing and following cardiac sarcoidosis.

Objective: To characterize bi-ventricular end-diastolic and end-systolic chamber sizes (LVEDV, LVESV, RVEDV, RVESV), myocardial masses, ejection fraction (EF) and the presence of (DCE) in 58 symptomatic pulmonary sarcoid patients (29 male, 29 female) referred for assessment of cardiac involvement by cardiovascular magnetic resonance (CMR).

Methods: All subjects underwent single breath-hold, gated cine true FISP cardiac magnetic resonance imaging at a 5 mm slice thickness, FOV 32–40 cm, and a minimum of 16 phase/cardiac cycle on a 1.5T Magnatom (Siemens Medical Imaging) scanner. Sequential MR images were acquired in the vertical, horizontal, and short axis planes. Cardiac chamber sizes and morphologic characteristics were measured applying a modified Simpon's technique and analyzed using Argus software (Siemens Medical Imaging). Delayed contrast enhanced imaging was performed following intravenous injection of 0.1 mmol/ kg of gadolinium DTPA contrast. Gated Turboflash IR images were obtained at 10 min after injection with the TI time (250–340 ms) adjusted to null the left ventricular myocardium. Data were analyzed using one-way ANOVA.

Results: Of the 58 (29 male, 29 female) patients studied, 23 (40%) displayed DCE on their initial scan. Table A represents data from each patient's baseline (first) MRI scan. Shown are the mean values ± SEE for each group and the p valve for comparison between those subjects with (+) and without (-) DCE. In Table A, significant morphologic differences were noted between the group displaying DCE and those without in regards to all parameters studied, except for LVEF, LV mass, RVEDV and RV mass. Table B represents data from all MRI studies performed over a three year period on 58 total patients, but a total of 80 studies. Of this group, 18 patients received multiple scans. The baseline MRI data from Table B illustrates

TABLE 1
Right and Left Ventricular Morphologic Characteristics

	A. + DCE	Baseline − DCE	Study p	B. + DCE	Multiple − DCE	Studies p
LVEDV (mL)	120.0 ± 6.5	97.9 ± 4.4	.006	119.4 ± 6.0	103.6 ± 3.9	.025
ESV (mL)	51.5 ± 4.2	39.0 ± 2.2	.005	51.5 ± 3.4	40.0 ± 1.8	.002
EF (%)	57.2 ± 2.0	60.4 ± 1.2	.15	57.5 ± 1.6	61.7 ± 1.0	.025
LV mass (g)	142.9 ± 8.1	125.9 ± 6.2	.099	146.3 ± 6.8	129.0 ± 5.2	.052
RVEDV (mL)	119.3 ± 6.7	104.6 ± 6.1	.118	127.0 ± 7.6	112.1 ± 5.0	.096
ESV (mL)	67.3 ± 4.9	55.7 ± 3.4	.048	71.8 ± 5.7	57.8 ± 3.0	.018
EF (%)	44.9 ± 1.9	45.4 ± 1.2	.813	45.7 ± 1.8	47.5 ± 1.1	.371
RV mass (g)	78.4 ± 6.0	62.7 ± 3.5	.019	78.6 ± 4.8	65.3 ± 2.9	.015

significant differences in all groups except RVEF. Note that the mean chamber volumes, mass and ejection fractions were larger in those with DCE compared to those without.

Conclusions: The application of the DCE technique is useful in the assessment of myocardial involvement in patients with known pulmonary sarcoidosis. This study shows that patients displaying DCE are likely to have significantly larger chamber sizes and reduced left ventricular ejection fractions. The lack of difference in the RVEF may suggest underlying RV systolic dysfunction in subjects with known pulmonary sarcoid involvement. Furthermore, this study suggests that the prevalence of undiagnosed cardiac sarcoid may be higher than previously reported. While a definitive gold standard for diagnosing this disease is lacking, our results likely reflect the high spatial resolution offered by CMR. We feel that CMR with DCE is a method to assess patients for cardiac sarcoid involvement and that it appears to correlate with ventricular chamber remodeling in the presence of known pulmonary sarcoid involvement.
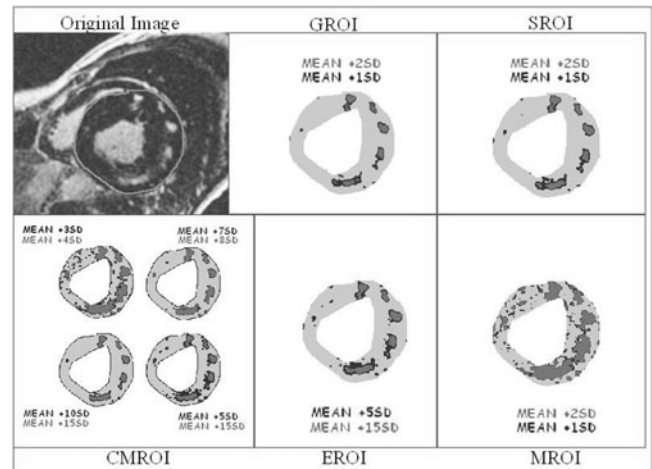
163. WHAT'S THE BETTER METHOD TO QUANTIFY FIBROSIS DETECTED BY DELAYED-ENHANCEMENT MAGNETIC RESONANCE IN HYPERTROPHIC CARDIOMYOPATHY?

Giovanni Donato Aquaro, MD,[1] Andrea Barison, MD,[2] Gianluca Di Bella, MD,[3] Elisabetta Strata, MD,[1] Alessandro Pingitore, MD, PhD,[1] Paolo Spirito, MD, PhD,[1] Massimo Lombardi, MD.[1] [1] Institute of Clinical Physiology, Pisa, Italy, [2] Cardiotoracic Department, Pisa, Italy, [3] University of Messina, Messina, Italy.

Introduction: Previous studies demonstrated that magnetic resonance (MR) with delayed enhancement (DE) technique allows to evaluate the presence of fibrosis in Hypertrofic Cardiomyopathy. The quantification of fibrosis could be clinically relevant in HCM but the method of analysis is not yet standardized.

Purpose: Aim of this study was to compare different methods of analysis of signal intensity of the myocardium in HCM patients

Methods: Forty patients (25 male, mean age 28 year) with a confirmed diagnosis of HCM underwent MR examination. MR protocol included acquisition of T1-weighted inversion recovery gradient echo pulse sequence images in short axis views with an inversion time to null signal from normal myocardium Using a dedicated software we compared 6 method for the quantification of normal myocardium, hyperenhanced myocardium and mild enhanced myocardium based to the detection of 2 cut-off derived from: 1) mean + 1 standard deviation (SD) (mild enhanced) and mean + 2SD (hyperenhanced) measured in a region of interest (ROI) in normal myocardium (MROI); 2) mean + 5 SD (mild enhanced) and mean +15 SD (hyperenhanced) from a ROI external to the thorax of patient (EROI); 3) mean + 1 SD (mild enhanced) and mean + 2 SD (hyperenhanced)from the entire ventricular myocardium in all the slices (GROI); 4) mean + 1

SD (mild enhanced) and mean + 2 SD (hyperenhanced) from the entire myocardium measured in each single image (SROI); 5) mean + custom SD chosen for mild enhanced and hyperenhanded region from ROI in normal myocardium (CMROI); 6) mean + custom SD chosen for mild enhanced and hyperenhanded region from external ROI (CEROI). Each image was transformed in a parametric image (Fig. 1) with the distinction of the 3 regions (normal, hyperenhanced and mild-enhanced myocardium) obtained using cut -off derived from the different methods. Three independent investigator, blinded each other, assigned a score (1 as not suitable to 4 as excellent) for each method comparing the parametric image to the original images using the visual assessment as gold standard. For CMROI and CEROI parametric images were obtained using progressive increment of SDs and a definitive cut-off was fixed when a score of 4 was assigned.

Results: Four hundred eighty-threeimages were analyzed. MROI was the better method in 1 patients (2.5%, mean score 1.45), EROI in 19 (47.5%, mean score 3.29), GROI in 16 (40%, mean score 3.38), SROI in 4 (10%, mean score 3.18). Mean difference in percentiles from the quantification of hyperenhanced region measured in the preferred technique assigned for each patients was 25.6 for MROI, 2.01 for EROI, 2.15 for SROI and 1.85 for GROI, 0.54 for CMROI and 0.48 for CEROI. MROI showed significantly higher difference than other methods (p < 0.00001), while CMROI and CEROI showed significantly lower difference from the preferred method in each patient (p < 0.0001) and high significant correlation with the preferred method (p < 0.0001, r 0.97).

Conclusions: Methods of DE quantification in HCM using myocardial or external ROI are the preferable if a custom determination of cut-off is performed. When a fixed cut-off of standard deviations is used, myocardial ROI is not suitable.

164. PREDICTION OF MORTALITY AND HEART FAILURE IN PATIENTS WITH SYSTEMIC AMYLOIDOSIS AND SUSPECTED CARDIAC INVOLVEMENT USING
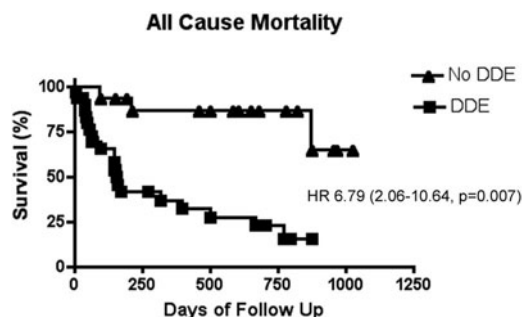
CARDIOVASCULAR MAGNETIC RESONANCE IMAGING

James White, MD,[1] Wael Al-Jaroudi, MD,[1] Han Kim, MD,[1] Manesh Patel, MD,[1] Dipan Shah, MD,[2] Michele Parker, MS,[1] Raymond Kim, MD.[1] [1]*Duke University Medical Center, Durham, NC, USA,* [2]*Nashville Cardiovascular MRI Institute, Nashville, TN, USA.*

Background: Cardiac involvement in patients with systemic amyloidosis is associated with high morbidity and mortality. We hypothesized that cardiovascular magnetic resonance (CMR) using delayed enhancement (DE) imaging would predict mortality and hospitalization for heart failure.

Methods: Forty-six consecutive patients with biopsy proven systemic amyloidosis and suspected cardiac involvement had CMR performed on a 1.5 Tesla scanner. Time from Inversion (TI) scout imaging was performed 10 minutes after injection of 0.1 mmol/kg gadolinium. The null point of both myocardium and blood pool was detected and the longest value used to perform standard segmented FLASH inversion recovery imaging. Studies were blindly interpreted for the presence of diffuse delayed enhancement (DDE) in addition to quantitative ventricular dimensions, wall thickness and function. Patients were followed for clinical events including the occurrence of death or hospitalization for heart failure (HF).

Results: The mean age was 63.0 Â ± 11.1 years (34 male, 12 female). Mean MRI ejection fraction was 52.9 Â ± 13.9% with a left ventricular mass of 196.6 Â ± 76.2 gand end-diastolic volume of 110.9 Â ± 46.2 mL. Thirty patients (65%) had evidence of DDE. At a mean follow up of 383 days, 24 patients (52%) had died, 5 (11%) were admitted for HF and 2 (4%) had heart transplantation (Txp). The presence of DDE identified 25 of 28 patients (89%) suffering from either death or admission for HF/Txp with a HR of 8.42 (2.48–11.32, p < 0.001). The HR for all-cause mortality was 6.79 (2.06–10.64, p = 0.007).

Conclusions: In patients with systemic amyloidosis DE-MR imaging identifies patients at a high risk of mortality and heart failure.

All Cause Mortality

165.   INCIDENCE OF CARDIAC COMPLICATIONS IN PATIENTS WITH CARDIAC SIDEROSIS DURING 1 YEAR FOLLOW UP

Paul Kirk, MRCP, Mark A. Tanner, MRCP, Diane Wu, Jane Taylor, Dudley J. Pennell, MD. *Royal Brompton Hospital, London, United Kingdom.*

Introduction: Myocardial siderosis is the main cause of morbidity and mortality in transfusion dependent anaemias such as thalassaemia major. In the United Kingdom, approximately 50% of patients die before reaching 35 years. The cardiomyopathy is reversible if chelation is commenced early, but diagnosis is often delayed due to the late onset of symptoms. T2* CMR can now assess cardiac iron directly, and this has profound implications for clinical management of iron overload and the assessment of chelation regimes.

Left ventricular ejection fraction falls with increasing myocardial iron (reduced myocardial T2*; normal value >20 ms), and accordingly iron overloaded patients with symptomatic heart failure have a low T2*. Although data is available on the level of T2* in patients developing heart failure, there is no published data on the incidence of heart failure and arrhythmia in patients during follow-up according to baseline myocardial T2*. The aim of this study, therefore, was to establish the risk of cardiac complications in patients with cardiac siderosis as measured by T2*.

Method: A database was produced containing clinical data and T2* values on 1098 patients with chronic transfusion dependent anaemias over a 6 year period. Of the 1098 patients scanned, 1039 were from the Royal Brompton Hospital and 59 patients were from Sardinia, Philadelphia, Thailand, Hong Kong or Singapore. The patients consisted of 872 thalassaemia patients (thalassaemia major and intermedia), 82 sickle cell disease patients and the remaining 144 patients were of miscellaneous transfusion related anaemias. The mean age of the patients was 34.6 ± 15.5 years.

Results: After 1 year of follow-up, there were 1018 patients who were asymptomatic, and their mean myocardial T2* was 30.4 ± 14.8 ms. Of the 59 patients with documented heart failure, 53 had thalassaemia major, 3 hereditary haemochromatosis and 3 had miscellaneous transfusion dependent anaemias. Their mean myocardial T2* was 6.4 ± 1.9 ms reflecting severe iron loading (p < 0.01 vs asymptomatic). Of the 40 patients with documented arrhythmia, the mean T2* was 14.3 ± 12.0 (p < 0.01 vs asymptomatic) Conversely, of the patients with a T2* < 10 ms (severe myocardial iron) at the baseline scan, in the year after the CMR scan, 38% developed heart failure, and 17 % developed arrhythmia, with a total of 51% of these patients having one or both of these conditions.

Of patients with a T2* of 10−20 ms (mild to moderate cardiac iron), 2% had an episode of heart failure, 5 % had a documented arrhythmia, with a total of 7% of these patients having one or both of these conditions.

Of patients with a T2* > 20 ms (normal myocardial iron), 0% had an episode of heart failure, 1% had a documented arrhythmia, with a total of 1% of these patients having one or both of these conditions.

Conclusion: This study demonstrates that 51% of patients with a T2* < 10 ms proceeded to heart failure or arrhythmia within one year of initial CMR scan, whilst the incidence of complications was 7% in mild to moderate myocardial siderosis and only 1% in patients with normal myocardial iron.

This data provides strong evidence that a myocardial T2* < 10 ms represents a high risk of developing cardiac complications. It is clear that these patients should be aggressively chelated to reduce their high morbidity and mortality from cardiac siderosis.

Saturday, February 3, 2007
Oral Abstracts: Basic-Session XIV

166. CAROTID PLAQUE MR IMAGING DURING POSSIBLE TIA/ISCHEMIC STROKE: A COMPREHENSIVE ANALYSIS OF PLAQUE INCIDENCE, OUTCOMES AND CARDIOVASCULAR RISK FACTORS
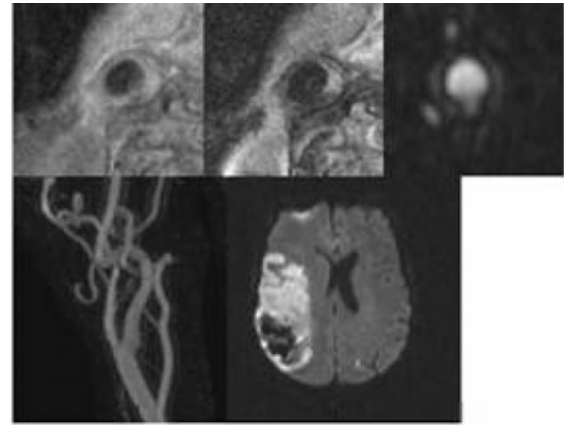
Jaywant P. Parmar, MD, Walter J. Rogers, PhD, Erol Baskurt, MD, Kiran Nandalur, MD, John P. Mugler, III, PhD, Christopher M. Kramer, MD. *University of Virginia, Charlottesville, VA, USA.*

Introduction: Atherosclerotic plaque structure is thought to be related to thromboembolic TIA and ischemic stroke (IS) risk. Furthermore, plaque rupture is felt to be an underlying event contributing to a large proportion of cerebral ischemic morbidity and mortality. Patients included in this study were acutely symptomatic of TIA/IS and referred for clinical stroke protocol MRI examination.

Purpose: We sought to assess (1) the relative incidence of plaque types as categorized by the MRI modified AHA system in the study population, (2) the relationship between type 6 (ruptured, hemorrhagic) carotid atherosclerotic plaque and patient outcome, and, (3) the relative predictive value of type 6 plaque observation in comparison to standard cardiovascular

TABLE 1
Relative Plaque Incidence

AHA Plaque Type	TIA	Ischemic Stroke	N observed
T 1/2	0	0	7
T 3	3	5	50
T 4/5	1	3	29
T 6	11	12	41
T 7	2	1	12
T 8	0	2	17
Totals	17	23	156

77 year old female smoker with a history of hypertension and hyperlipidemia presented with mental status change and left hemiparesis. Diffusion-weighted imaging (bottom right)

risk factors for identifying patients eventually discharged with the diagnosis of ipsilateral cerebral hemispheric TIA/IS.

Methods: Ninety-eight patients referred for an acute stroke protocol MRI/MRA examination underwent additional high resolution T1- and T2-weighted imaging of the carotid artery bifurcation using a single slab, 3D turbo spin echo sequence with double inversion recovery blood signal suppression (T1: TR/TE 800/24 ms; T2: TR/TE 2000/132 ms; true in plane resolution of 0.490 × 0.490 mm; 66 mm z axis coverage: 3.0 mm slice thickness reconstructed at 1.5 mm intervals).

Two blinded reviewers performed independent plaque gradings according to the MRI modified AHA system using T1- and T2-weighted axial images as well as contrast enhanced neck MRA data. Interobserver agreement between independent gradings was tested by kappa. Clinical outcome, brain MR results and cardiovascular risk factors were obtained by blinded chart review. A chi squared test was employed to ascertain the relationship between type 6 observation and outcome. A multiple logistic regression model was constructed using the risk factor data to assess the relative prognostic value of a type 6 plaque observation in the population.

Results: MR plaque characterization was technically feasible in 83/103 (81%) patients, of which 5 were excluded due to known source of TIA/IS. Seventy-eight patients were included (38 male, mean age 64 [24-93], SD 14.7), yielding 156 paired plaque-watershed observations. Quadratic kappa agreement among all plaque gradings was moderate, k = 0.66, and, agreement between the specific type 6 plaque observation was similarly moderate, k = 0.66. Twenty-three patients (23 hemispheres) received a diagnosis of IS with acute diffusion abnormality present on brain MR. Seventeen patients (17 hemispheres) had a discharge diagnosis of TIA with no diffusion abnormality on brain MR. The remaining 38 patients and non affected sides (total 76 hemispheres) had no diffusion abnormality and clinically were thought not to have a TIA/IS.

Plaque incidence is summarized in Table 1. There was a significant relationship between true TIA/IS outcomes and ipsilateral type 6 plaque observation, p < 0.001. A multiple logistic regression model was formulated including the presence

of ipsilateral MRI AHA type 6 plaques and the standard epidemiologically derived cardiovascular risk factors including: sex, age, insulin resistance, hypertension and hyperlipidemia. The observation of ipsilateral type 6 plaque was the dominant thromboembolic event associated risk factor, $p \leq 0.001$, OR 23.4 (8.6–65.2). The only other statistically associated risk factor was age, $p \leq 0.035$, OR 1.03 (1.002-1.060])

Conclusions: In the acutely symptomatic population that was studied, the presence of type 6 plaque correlated strongly with discharge diagnosis of cerebral ischemic event. Furthermore, this association was far stronger than any standard cardiovascular risk factor. The results support the pathological model of ruptured vulnerable plaque as a major source of thromboembolic morbidity and mortality. Further investigation of carotid atherosclerotic plaque with MRI is warranted.

167. MRI ASSESSMENT OF THE DEVELOPMENT OF ATHEROSCLEROSIS IN AORTIC ARCH AND MYOCARDIAL FUNCTION IN MICE HARBORING THREE DIFFERENT TNF GENOTYPES

Frank Kober, PhD,[1] Matthias Canault,[2] Franck Peiretti, PhD,[2] Christoph Mueller, PhD,[3] Patrick J. Cozzone, PhD,[1] Irène Juhan-Vague, PhD,[2] Gilles Nalbone, PhD,[2] Monique Bernard, PhD.[1] *[1]Centre de Résonance Magnétique Biologique et Médicale, Marseille, France, [2]INSERM-U626, Marseille, France, [3]Institute of Pathology, Bern, Switzerland.*

Purpose: The aim of this study was to evaluate the ability of MRI to follow the progression of atherosclerosis in the aortic arch of genetically induced atherosclerosis in mice harboring various TNF genotypes (1). In parallel, cardiac function and morphology was evaluated at one stage of the protocol in order to study possible modifications induced by TNF. The influence of TNF on plaque development is expected to be observable at stages up to 20 weeks of diet.

Materials and Methods: Six weeks-old ApoE−/− female mice harboring 3 different TNF phenotypes (i) wild type TNF (group ApoE−/−, n = 7), (ii) deficiency in TNF (group ApoE−/−/TNF−/−, n = 6), (iii) uncleavable transmembrane form of TNF (group ApoE−/−/TNFKI, n = 6) were submitted to an atherogenic diet (20% fat) for 20 weeks. In vivo MRI was performed in all groups at the beginning of the diet (T0), and

TABLE 1
Aortic wall thickness (micron) at different stages. #sign. vs T0, *progr. sign. vs ApoE

Group mean ±SD	T0	T5	T15	T20
ApoE−/−	130 ± 22	174 ± 21#	177 ± 27#	241 ± 24#
ApoE−/−TNF−/−	145 ± 23	150 ± 31	163 ± 15	208 ± 28*#
ApoE−/−TNF-KI	151 ± 19	160 ± 37	161 ± 25	216 ± 33#

TABLE 2
Left ventricular morphology and function at T15

Group mean ± SD	EDV (mL)	SV (mL)	LVEF (%)	LVW (mg)
ApoE−/−	98 ± 13	25 ± 4	73 ± 4	67 ± 8
ApoE−/−TNF−/−	103 ± 15	28 ± 6	77 ± 3	71 ± 9
ApoE−/− TNF-KI	98 ± 15	22 ± 3	69 ± 9	69 ± 9

then after 5 (T5), 15 (T15) and 20 (T20) weeks of diet on the same mice using a Bruker AVANCE 500 11.75 T vertical imaging system. Isoflurane-anesthetized animals were placed in a 30 mm radiofrequency coil in the magnet and maintained at 37°C. A cardiac- and respiratory-gated spin-echo sequence (TR/TE = 1500/8 ms) was used to gather morphologic information on the vessel wall and the aortic lumen of the aortic arch with an in-plane resolution of 117 μm and a slice thickness of 500 μm. The oblique slice was positioned perpendicular to the aorta using a cine MRI sequence in the plane of the aortic arch as reference. The aortic wall thickness was measured by comparing manually delineated luminal and outer areas using in-house developed software. Myocardial morphology and function was estimated using an ellipsoid model applied to three-axis cine MRI acquired within the protocol at stage T15.

Results: The tables summarize longitudinal data obtained on vessel wall thickness as well as cardiac morphology at stage T15.

Figures 1 and 2 show typical images for ApoE−/− and ApoE−/−TNF−/−, respectively.

Discussion/Conclusion: Aortic wall-thickening was significant at T20 for all groups compared with T0, but with a significantly higher progression in ApoE−/−. The lack of soluble TNF reduced the progression at early stages, because in ApoE−/−/TNF−/− and ApoE−/−/TNFKI mice, the wall thickness was not different at T5 and T15 compared with T0. Histological analysis at T20 (data not shown) showed similar results. Cardiac function and morphology estimation at T15 revealed no significant differences except a tendency to higher
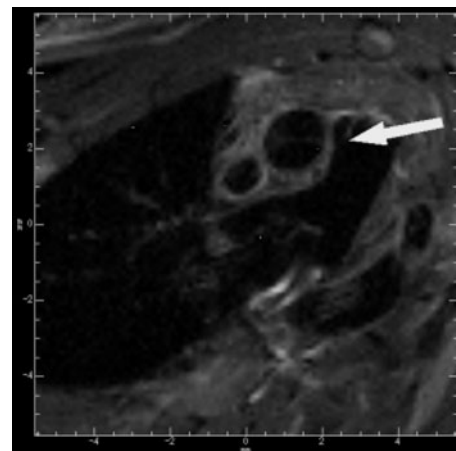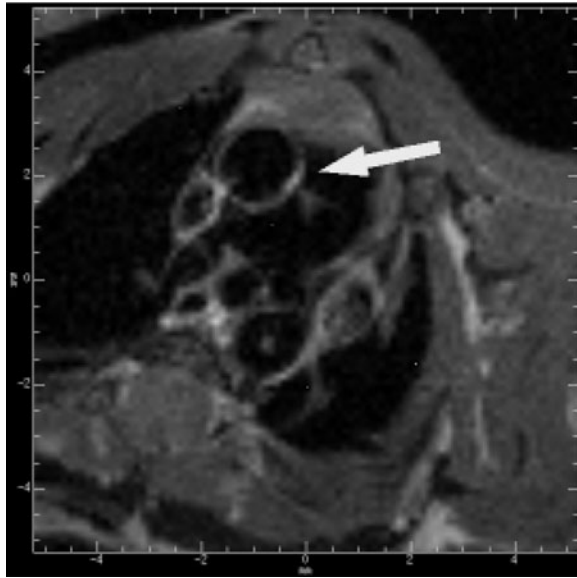

FIG. 1.   TNF wild type.

FIG. 2. TNF−/−.

ejection fraction in ApoE−/−/TNF−/− mice. Earlier mouse studies have evaluated plaque development in ApoE−/− mice at relatively advanced stages (after more than 40 weeks of diet [2]). Here we show that MRI allows the longitudinal follow-up of the development of atherosclerosis in the mouse aortic arch at earlier stages. MRI can be used to investigate the mechanisms implied in the pathogenesis of atherosclerosis using mouse models.

REFERENCES

1. Canault M, et al. Atherosclerosis 2004;172:211–218.
2. Itskovich VV, et al. Magn Reson Med 2003;49:381–5.

168. ASSOCIATION BETWEEN ADVENTITIAL VASA VASORUM AND ATHEROSCLEROSIS: A DYNAMIC CONTRAST-ENHANCED MAGNETIC RESONANCE IMAGING STUDY

Minako Oikawa,[1] William Kerwin,[1] Hunter Underhill,[1] Chun Yuan,[1] Thomas S. Hatsukami.[2] [1] University of Washington, Seattle, WA, USA, [2] VA Puget Sound HCS and University of Washington, Seattle, WA, USA.

Background: Vasa vasorum may play an important role in the pathogenesis of atherosclerosis. Previous animal studies have found not only an association between the vasa vasorum and plaque growth, but also that the direct inhibition of the vasa vasorum decreases plaque size (1). In humans, however, the role of the vasa vasorum during atherogenesis remains unclear. Although human autopsy studies have suggested that the vasa vasorum is associated with plaque progression (2), an inability to serially assess the vasa vasorum *in vivo* has prevented the identification of its relationship to the pathophysiology of human atherosclerotic disease.

Recently, dynamic contrast-enhanced (DCE) MRI has demonstrated a strong correlation between the rate of carotid plaque contrast enhancement and histological evidence of neovasculature and macrophage infiltration of the human atherosclerotic lesion (3). This technique has been recently modified to only capture the transfer constant, K^{trans}, of adventitial tissue to visualize and quantify the *in vivo* vasa vasorum of the carotid atherosclerotic lesion. In the present study, we tested the hypothesis that the extent of adventitial vasa vasorum as measured by K^{trans} is related to the severity of atherosclerosis.

Method: Seventy-three carotid arteries with 16–99% stenosis by duplex ultrasound were imaged at 1.5T with a high-resolution, multi-contrast MRI protocol that included a DCE-MRI sequence. Imaging parameters were TR = 100 ms, TE = 3.4 ms, flip = 60, matrix = 192 × 144, FOV = 16 × 12, and 0.1 mmol/kg of contrast agent (Omniscan, GE Healthcare) was injected coincident with the second of 12 images in the sequence. We performed kinetic modeling of the results to extract the partial plasma volume (v_p) and transfer constant (K^{trans}) for each pixel, using an automated procedure. Results were displayed as a two-color parametric image with v_p in red and K^{trans} in green.
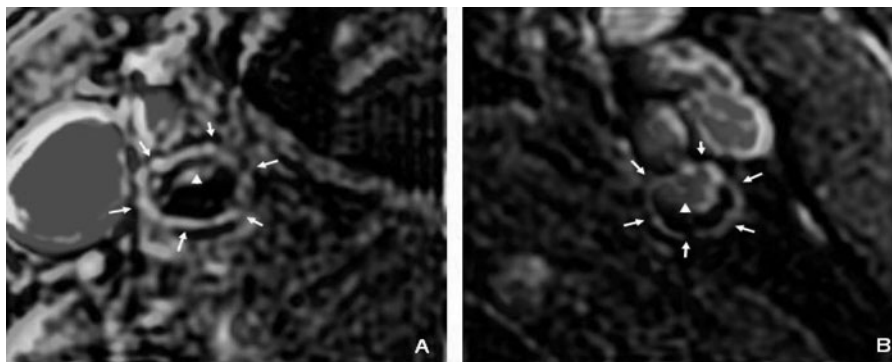

FIG. 1. Representative cases of the adventitial enhancement in both an advanced lesion (>80% stenosis, Image A) and a mild to moderate lesion (16–79%, Image B). The plasma volume v_p for the internal carotid artery is shown in red (arrowhead) and the transfer constant K^{trans} for the adventitial is in green (arrow).

An active contour technique was used to identify the adventitia in the parametric DCE-MRI image and average K^{trans} along this boundary was measured. An independent student's t-test was used for analysis.

Results: Of the 73 arteries evaluated, 40 arteries had mild to moderate atherosclerosis (16–79% stenosis), and 33 arteries had advanced atherosclerosis (80–99% stenosis). The average K^{trans} in the advanced group (Fig. 1A) was significantly higher than that in the mild to moderate group (Fig. 1B) (0.339 ± 0.081 vs. 0.288 ± 0.055 [mean $\pm$ SD], respectively; $p = 0.002$).

Conclusion: Extent of the adventitial vasa vasorum in the human carotid atherosclerotic lesion appears to be associated with the degree of carotid stenosis. DCE-MRI may be an effective technique for the *in vivo* evaluation and monitoring of the adventitial vasa vasorum in human atherosclerotic disease. Prospective studies are underway to assess whether the degree of adventitial enhancement is predicts more rapid atherosclerosis progression.

REFERENCES

1. Moulton KS, et al. Proc Natl Acad Sci USA 2003;100:4736–41.
2. Fleiner M, et al. Circulation 2004;110:2843–2850.
3. Kerwin W, et al. Radiology 2006 In Press.

169. CAROTID ARTERIAL VESSEL WALL THICKNESS MEAURED BY HIGH-RESOLUTION CAROTID CARDIOVASCULAR MR IS SIGNIFICANTLY HIGHER IN ASYMPTOMATIC SUBJECTS WITH CORONARY ARTERY CALCIFICATION: PRELIMINARY FINDINGS FROM THE ATLANTA FIREFIGHTERS COMPREHENSIVE CARDIOVASCULAR RISK ASSESSMENT PROGRAM

Robert E. O'Donnell, MD, Brenda Garrett, RN, Kim Christian, ASRT, Mary Harmon, PhD (C), H. Robert Superko, MD, FACC, Szilard Voros, MD. *Fuqua Heart Center of Atlanta, Atlanta, GA, USA.*

Introduction: Atherosclerosis (AS) remains the leading cause of mortality and morbidity in the United States. Thus, screening for asymptomatic disease is critical for early detection and intervention. Coronary artery calcium (CAC) scoring is an accepted method of screening for silent coronary AS. High-resolution carotid cardiovascular magnetic resonance (CMR) is an emerging technique to detect subclinical carotid AS. The relationship between CAC and carotid arterial wall thickness as measured by high-resolution carotid CMR has not been reported previously.

Purpose: To examine the relationship between carotid arterial wall thickness assessed by carotid CMR and CAC in a pilot phase of the Atlanta Firefighters Comprehensive Risk Assessment Program.

Methods: Eighteen subjects (15 male; average age 49) were enrolled in the pilot phase of the Atlanta Firefighters Comprehensive Risk Assessment Program. All subjects underwent history, physical, CAC, carotid CMR and advanced lipoprotein testing. High-resolution CMR of the carotid arteries was performed at 1.5T using a commercial neck coil. After careful localization, 22 axial, non-gated, high-resolution T1-weighted turbo spin echo images of the carotid arteries were obtained, centered on the bifurcation (TR 1500 ms, TE 10 ms, field-of-view 15 cm, voxel size $0.5 \times 0.5 \times 3.0$ mm, flip angle 180, number-of-averages 3). Total vessel area (TVA) and lumen area (LA) were manually planimetered and vessel wall area (VWA) was calculated (VWA = TVA-LA). Percent VWA (PVWA) was calculated as (VWA/TVA) $\times$ 100 and averaged over all slices for the right and left internal and common carotids (APVWA).

Demographic, Imaging and Lipoprotein Parameters

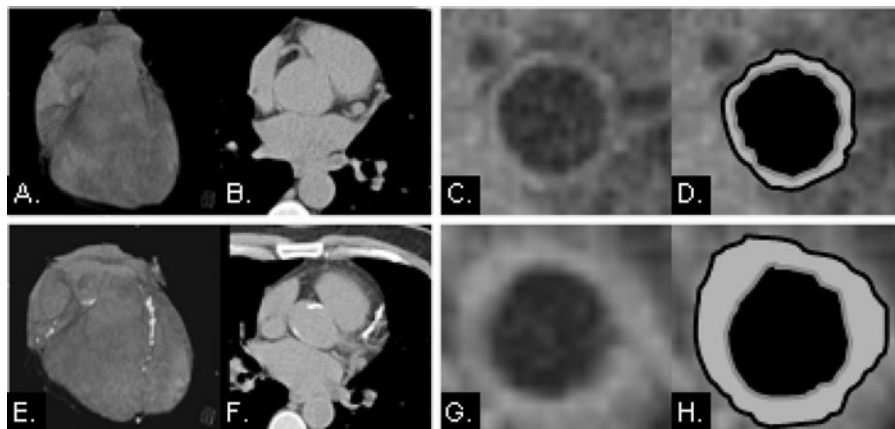|	Negative CAC (n = 8)	Positive CAC (n = 10)	p value
APVWA (%)	35.3 ± 0.7	38.6 ± 1.2	0.04
MPVWA (%)	47.2 ± 1.6	51.8 ± 2.2	0.11
Age	47.5 ± 1.8	50.7 ± 1.7	0.11
Total Cholesterol (mg/dL)	212 ± 10	205 ± 11	0.48
LDL-C (mg/dL)	140 ± 12	129 ± 10	0.35
HDL-C (mg/dL)	56.4 ± 5.3	53.7 ± 8.1	0.80
Triglycerides (mg/dL)	89.3 ± 18	100 ± 14	0.68
Homocysteine (uM/L)	8.7 ± 0.6	11.8 ± 0.8	0.03

FIG. 1.

Maximum PVWA in each patient was also recorded. A single blinded observer performed all carotid measurements. CAC was performed on a 64-slice computed tomography system (slices 32×2, detector width 0.6 mm, rotation time 370 ms, pitch 0.24 mm/rotation, tube voltage 120 kV). CAC was expressed as Agatston score. Advanced lipoprotein testing was performed using gradient gel electrophoresis. Statistical analyses of age, CAC, APVWA, Maximal PVWA, chemistry and lipid profiles were performed using the unpaired, two-tailed t-test. Results were expressed as mean ± SE. Statistical analyses of gender, history of HTN and smoking, and family history of smoking were performed using the Fisher exact test.

Results: Of the 18 subjects enrolled, none had symptoms consistent with coronary artery disease. Over half of the subjects (10; 56%) had subclinical atherosclerosis as determined by a positive CAC. The mean CAC was 160 ± 97, median value of 29. The traditional risk factors of age, gender, smoking, diabetes, hypertension and family history did not correlate with a positive CAC. Of the 18 patients in the current study, 4 had significantly thickened carotid arterial wall thickness, using a cutoff of 2SD from a previously established database of APVWA of $33.3 \pm 2.6\%$ in a normal, healthy population. All four patients with abnormal APVWA had a positive CAC. Importantly, APVWA was significantly greater in subjects with positive CAC, compared to subjects with negative CAC (APVWA: $38.6 \pm 1.2\%$ vs. $35.3 \pm 0.7\%$; $p = 0.04$) (Table) (Fig. 1.: Subject with negative CAC [A, B] with normal carotid wall thickness [C, D] and another subject with positive CAC [E, F] with thickened carotid artery wall [G, H]). Maximum PVWA was not different between CAC positive and CAC negative subjects (51.8 ± 2.2 vs. 47.2 ± 1.6; $p = 0.11$). There were no significant differences in LDL-C, HDL-C, triglycerides and Lp(a) between CAC positive and CAC negative patients (Table). However, homocysteine was significantly higher in CAC positive subjects (11.8 ± 2.3 vs. 8.7 ± 1.9 umol/L; $p = 0.03$).

Conclusions: In this pilot phase of the Atlanta Firefighters Comprehensive Risk Assessment Program, carotid arterial vessel wall thickness, as measured by high-resolution carotid CMR, was greater in patients with asymptomatic coronary disease, as determined by the presence of coronary calcium. High-resolution CMR of the carotid arteries is an emerging, important tool for the evaluation of subclinical carotid atherosclerosis.

170. AGE-RELATED CHANGES IN CAROTID ARTERY LUMEN AND WALL VOLUME IN A POPULATION FREE OF CARDIAC RISK FACTORS

Niall G. Keenan, BM BCh, MRCP, Peter D. Gatehouse, PhD, David N. Firmin, Dudley J. Pennell, MD, FRCP, FACC, FESC. *Royal Brompton Hospital, London, United Kingdom.*

Introduction: There has been much interest in carotid artery wall thickening as a marker of atherosclerosis, both by ultrasound and more recently by magnetic resonance (MR). Ultrasound measurements are limited by the presumption that the vessel is uniform. MR does not have this limitation. Most MR studies of atherosclerosis have focussed on late disease. Little attention has been paid to early disease, especially in the population without conventional cardiac risk factors, which still has a considerable incidence of cardiovascular events. In addition, age is the biggest single cardiac risk factor and yet there has been little imaging research into the effect of aging on arteries. The aim of this study was to study the carotid artery wall volume as a function of age in subjects of both sexes who were free from cardiovascular risk factors.
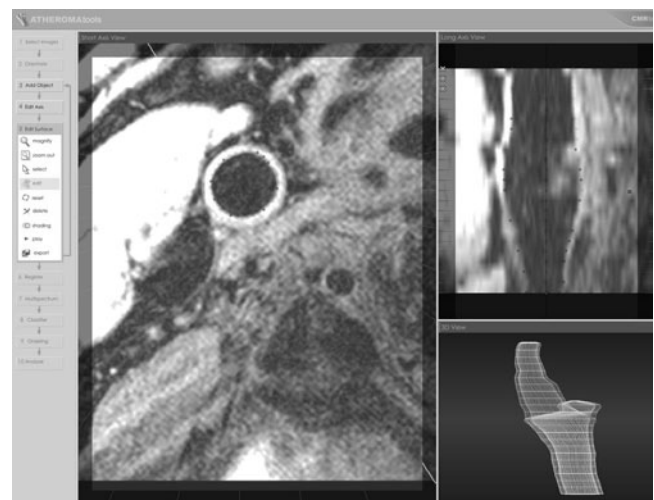
Methods: We recruited 89 healthy normal controls who we determined to be free of all conventional vascular risk factors (smoking, diabetes, hypertension, hyperlipidaemia, family history). There were 40 male subjects, with an average 18 subjects per decade between 20 and 70 years.

We performed a CMR study of their carotid arteries using a 1.5T Siemens Sonata scanner and purpose-built bilateral four channel phased-array surface carotid coils. We acquired a stack of high-resolution fast spin echo images centred on the carotid bifurcation and perpendicular to the carotid artery bilaterally. Slice thickness was 2 mm, and we acquired 20 contiguous slices for each side, giving 4 cm of longitudinal coverage per artery.

Using dedicated software (Atheroma Tools, Cardiovascular Imaging Solutions, London), we traced the internal and external carotid artery surfaces for each slice and hence measured the luminal area and the wall area for each slice. Then, by adding together the 20 slices, we were able to produce a 3D model of the carotid bifurcation, and to measure the lumen volume, wall volume and total vessel volume for the standardized 4 cm length.

Following Saam et al. (1), we divided the total wall volume by the total vessel volume to calculated the wall/outer wall (W/OW) index, enabling comparison between different subjects with varying sizes of carotid artery.

Results: Male and female results were analyzed separately (Table). In males, there was a strong and significant correlation

Correlation Coefficients Relating Carotid Arterial Parameters to Age

MALE	Lumen Volume v Age	Wall Volume v Age	Total Vessel Volume v Age	Wall/Outer Wall Ratio v Age
Pearson Correlation Coefficient (R)	0.352	0.756	0.524	0.701
p value	<0.01	<0.01	<0.01	<0.01
FEMALE				
Pearson Correlation Coefficient (R)	0.166	0.520	0.276	0.494
p value	0.10	<0.01	<0.01	<0.01

between age and the volume of the carotid artery wall (R 0.76), and this was also reflected in the W/OW ratio. The same was true for females, with a weaker but still significant correlation coefficient (R 0.52). Luminal volume was only weakly correlated with age in males (R 0.35) and not significantly in females. The mean wall/outer wall ratio for males was 32.6% and for females 31.7% (no significant difference).

Conclusions: We have demonstrated that in a normal population free from conventional vascular risk factors, there is a significant increase in carotid artery wall thickness with aging from 20 to 70 years. The more pronounced change in males is probably related to the protective effect of oestrogen on the female vasculature until the menopause.

This provides further evidence for the Glagov phenomenon of external remodelling of the artery to accommodate atherosclerotic burden which prevents encroachment of the lumen, at least in the early stages (2). Hence the wall volume was able to substantially increase in both sexes without a corresponding decrease in the luminal volume.

These results with a modest sample size show the power of carotid artery wall volume as measured by MR as a tool in vascular medicine. Reference normal data by age may enable MR carotid wall volume to become a risk stratification tool in at-risk populations.

REFERENCES

1. Saam et al. JCMR 2005;7:799–808.
2. Glagov et al. NEJM 1987;316:1371–1375.

171. LONGITUDINAL STRESSES IN CAROTID PLAQUES USING MRI-BASED FLUID STRUCTURE INTERACTION CFD MODELS
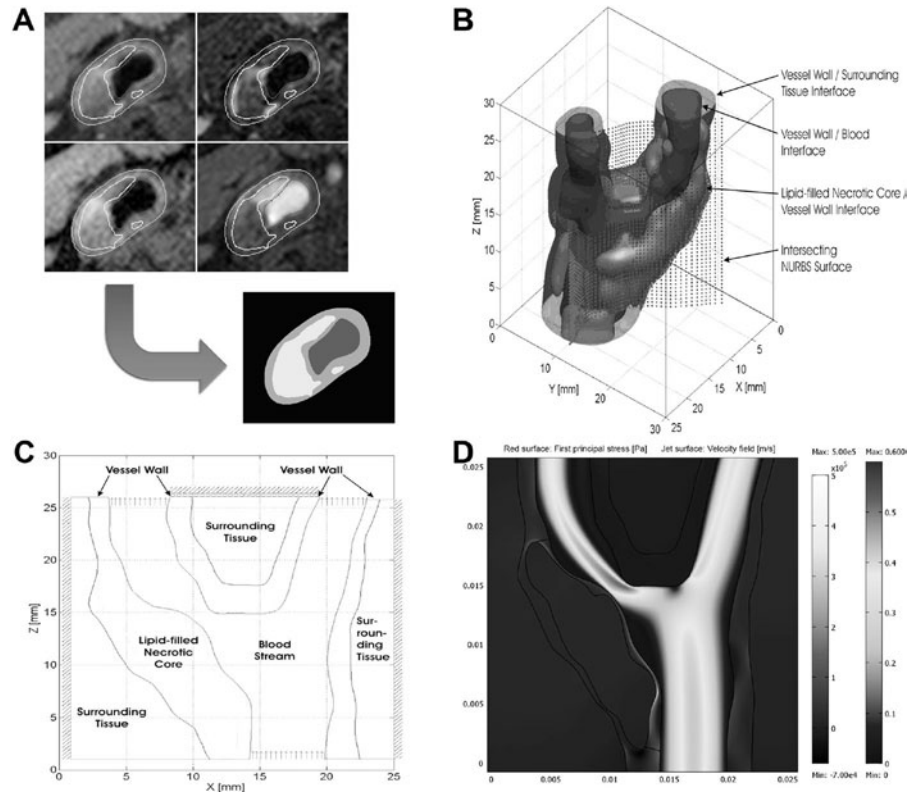
Samuel A. Kock, MSc,[1] Jens V. Nygaard, PhD,[2] Ernst T. Fründ, MSc,[3] Erling Falk, MD,[4] William Paaske, MD,[5] W. Yong Kim, MD.[4] *[1] Aarhus University Hospital, Aarhus, Denmark, [2] Interdisciplinary Nanoscience Center, Aarhus University, Aarhus, Denmark, [3] Department of Biomechanical Engineering, Aarhus, Denmark, [4] Department of Cardiology, Aarhus, Denmark, [5] Department of Vascular Surgery, Aarhus, Denmark.*

Introduction: Atherosclerosis is the main cause of death and severe disability in the world. The disease generates lipid cores covered by a protective fibrous cap—the atherosclerotic plaque. Plaque rupture in the carotid artery forms blood clots which may be carried down-stream to cause strokes. Currently the risk of cap rupture is assessed using the degree of luminal narrowing which fails to take the morphology of the plaque into account. Indeed, unstable or vulnerable plaques are known to possess large lipid cores and thin fibrous caps. A morphology such as this generates severe internal stresses in the fibrous cap. In vitro studies have shown that cap rupture predominantly occur when static stresses exceed 300 kPa. The ability to estimate stress magnitudes in the fibrous cap is thus expected to improve risk assessment.

Methods: Patients awaiting operation for severe carotid plaque were scanned using a well-validated MRI protocol designed by Yuan et al. (1). Sixteen slices were scanned using a T1-, T2-, PD-weighted and time-of-flight scan, each with a resolution of $0.61 \times 0.61 \times 2$ mm. The image intensities of each scan were combined allowing segmentation into lipid core, fibrous cap, vessel wall, and blood stream (Fig. 1A). Further, velocities were measured 2 cm up- and downstream from the flow divider using phase-contrast MRI scans. Each segmented slice was imported into Matlab to generate a 3D model using interpolation and smoothing between the slices (Fig. 1B). The 3D model was intersected using a NURBS surface to generate a 2D model (Fig. 1C). COMSOL multiphysics was used to simulate blood-flow as an incompressible homogenous Newtonian fluid ($\rho = 1050$, $v = 0.005$) and a parabolic inflow with a maximal central velocity of 42.3 cm/s. Pressure in the internal and external carotid outlets was set to 120 mmHg. A Neo-Hookean hyper-elastic model was used to specify the material properties of surrounding tissue ($\mu = 6.20$ e 6, $\kappa = 1.24$ e 8, $\rho = 960$) and vessel wall ($\mu = 7.20$ e 5, $\kappa = 1.44$ e 7, $\rho = 1200$). Lipid was treated as an isotropic materiel with Young's modulus set to 1/100 of that of the vessel wall (E = 1 e 5, $v = 0.45$, $\rho = 900$). Pressure was used to couple the fluid to the structural components along the vessel-wall/blood-stream interface (one-way coupling).

Results: First principal stress (red) and velocity field (jet) are depicted in Fig. 1D. The soft lipid pool deformed markedly generating severe stresses (max. 400 kPa) in the overlaying fibrous cap, most prominent in the inflow "shoulder region" i.e. the region of the fibrous cap adjacent to the vessel wall. A stagnation point is visible at the flow divider as well as a marked jet resulting from the severe luminal narrowing. Also present are

large areas of recirculating or slowly moving blood, a known progenitor of further plaque deposition.

Conclusions: The maximal stresses found in the fibrous cap exceed established criteria for caps at risk of rupture. Maximal stresses occurred in the inflow shoulder region, the preferential site of plaque rupture. Our results are thus in agreement with clinical findings of plaque physiology. Future comparisons of mechanical stresses matched to plaque histology may provide new insights into the etiology of vulnerable plaques and lead to improved risk stratification.

172.   MRI SIGNS OF CAROTID PLAQUE INFLAMMATION IN PATIENTS WITH UNSTABLE ANGINA

Luigi Natale, Antonio Bernardini, MD, Antonella Lombardo, MD, Agostino Meduri, MD, Filippo Crea, MD, Lorenzo Bonomo, MD. *Catholic University of Sacred Heart, Rome, Italy.*

Introduction: Inflammation may contribute to destabilize vulnerable plaques in acute coronary syndromes by promoting rupture and erosion. Systemic inflammatory factors could be related with widespread plaque activity in many vascular districts.

Purpose: We evaluated with contrast enhanced-MRI (CE-MRI) plaque inflammation signs in carotid arteries of pts with unstable angina (UA) and to relate them to serum levels of C-reactive protein (CRP), used as marker of systemic inflammation.

Methods: Thirty-two pts with carotid plaques, 19 with UA and 13 with stable angina underwent carotid arteries MRI (1.5 T GE scanner), with SE, FSE and bb-FSE sequences, before and 10 to 15 minutes after Gadolinium-DTPA (Gd) i.v. administration (0.2 mmol/Kg). We evaluated: wall thickening (arterial wall edema or infiltration); increased T2 or FSE-STIR signal intensity (SI), (arterial wall or plaque edema); arterial wall or plaque enhancement, (increased capillary permeability). A total of 44 plaques were evaluated (20 monolateral and 12 bilateral). CRP levels were determined with the ELISA essay.

Results: Twenty-four plaques showed wall thickening and/or increased T2 and/or FSE-STIR SI and Gd enhancement, 5 plaques showed only CE, whereas 15 plaques had no inflammation signs. CRP levels of patients with enhanced plaques were significantly higher than those of patients without enhancement (median values: 12.4 vs 3.4, $p < 0.05$).

Conclusions: Pts with UA showed plaque inflammation signs more frequently than controls; patients with UA and inflammation signs showed higher CRP levels than pts with UA and no inflammation signs. Our results suggest a widespread plaque activity, possibly mediated by systemic inflammation, in acute coronary syndromes.

173.   EVALUATION OF INFLAMMATION IN ATHEROSCLEROTIC PLAQUES: CORRELATION

BETWEEN 18F FLUORODEOXYGLUCOSE PET/CT AND DYNAMIC CONTRAST ENHANCED MRI PARAMETERS IN HUMAN PATIENTS

Claudia Calcagno,[1] James Rudd, MD, PhD,[1] Venkatesh Mani, PhD,[1] Kelly Myers, BS,[1] Silvia Aguiar, MD,[1] Josef Machac, MD,[1] Michael Farkouh, MD,[1] Valentin Fuster, MD, PhD,[1] William S. Kerwin, PhD,[2] Zahi A. Fayad, PhD.[1] [1]Mount Sinai School of Medicine, New York, NY, USA, [2]University of Washington, Seattle, WA, USA.

Introduction: Inflammation is crucial in the pathogenesis of high-risk atheroma (1). Important hallmarks of inflammation in plaques are the extent of neovascularization and the activation of inflammatory cells in the lesion: these cause increased glucose and oxygen uptake, which can be measured (together with neovascularization) as markers of inflammation. Fluorine 18 fluorodeoxyglucose (18F FDG) is a non-metabolized glucose analog which accumulates in the cell in proportion to metabolic activity. Recent reports have shown that FDG positron emission tomography (PET) can quantify plaque inflammation in rabbits

TABLE
Correlation parameters between Max FDG uptake and DCE-MRI parameters

	Blood Volume	Blood Flow	Mean Time of Transit
Max FDG uptake	RSQ = 0.1855 slope = -90892 intercept = 273060	RSQ = 0.308 slope = -546,96r intercept = 1483	RSQ = 0.3889 slope = 572.57 intercept = 1677.2

FIG. 1. Representative images of one patient are shown. In the upper panel the transaxial CT, PET and fised PET/CT images are shown. In the panel in the middle DCE-MRI images of the right internal carotid of the same patient are shown. The first image shows the natural MRI contrast before the injection of Gf-DTPA, while the second and third MR imgaes show the increased contrast between different components of the plaque which follows the injectin of the contrast agen. The bottom panel shows the corresponding blood volume, blood flow and mean time of transit parametric maps of the right internal carotid artery of the same patient.

and humans (2) . Furthermore it has been shown that plaque perfusion parameters evaluated by Dynamic Contrast Enhanced (DCE) MRI correlate with inflammation and neovascularization (3, 4) . Studies conducted in tumors (3) showed a negative correlation between FDG-PET uptake and kinetic parameters calculated by DCE-MRI, indicating that high FDG uptake may target hypoxic areas with low blood supply and increased glucose consumption. In this study we evaluate the correlation between 18F-FDG PET uptake and plaque perfusion parameters calculated from DCE-MRI in 6 patients with known 3 vessel disease.

Methods: PET data acquisition: Sixteen PET/CT slices of the internal carotid artery were obtained 1.5 hours after administration of 15 mCi FDG on a GE Adv LS scanner. After acquisition, images were manually traced on a Xeleris workstation. For each patient the evaluated parameters were: 1) maximum FDG vessel uptake 2) mean and maximum standardized uptake value (SUV) per slice 3) mean and maximum SUV per slice corrected for blood pool activity. *MR Imaging*: Patients were imaged in a 1.5 T clinical system (Siemens, Sonata). To allow for plaque characterization we performed DCE-MRI protocol with a black blood TSE sequence (TE = 5.6 ms, TR = 250 ms, slice thickness = 3 mm, time resolution = 4.8 s, number of images = 100). After the 5th image, 0.2 mmol/Kg of Gd-DTPA were injected at a rate of 2mL/s followed by saline flush. *DCE MRI Parameters*: Semi-quantitative pixel-by-pixel maps of blood volume (BV), blood flow (BF) and mean time of transit (MTT) were calculated. BV was calculated as the area under the signal intensity versus time curve (AUC), while BF was calculated as the first moment of the AUC and MTT as the ratio between the two. A region of interest covering the whole plaque was placed in the carotid arteries and average values of BV, BF and MTT were extracted. PET/CT and DCE-MRI slices were matched using fiducial markers. DCE-MRI parameters were correlated with maximum corrected FDG uptake in the matching slice using Pearson's test.

Results: Statistical analyses showed negative correlation between FDG-PET uptake and plaque perfusion parameters BV (R square = 0.1855) and BF (R square = 0.308). A positive and more robust correlation was found between FDG-PET uptake and MTT (R square = 0.3889). Correlation parameters R square, slope and intercept are shown in Table 1. Figure 1 shows representative images of one patient: 1) PET/CT transaxial images 2) right carotid artery during DCE-MRI 3) BV, BF and MTT maps (right carotid artery).

Conclusions: As previously found by others while studying the correlation between DCE-MRI parameters and FDG uptake in tumors (5), our results indicate a negative correlation between plaque blood supply and FDG uptake. This result may indicate that FDG uptake in the atherosclerotic plaque could be able to indentify not only areas of high inflammatory activity, but also hypoxic areas where neovessel distribution and plaque perfusion are low. Therefore multimodality imaging combining DCE-MRI and FDG-PET may be useful to non-invasively assess high-risk atherosclerotic plaques.

REFERENCES
1. Moreno, et al. Curr Mol Med 2006;6:457–77.
2. van Laarhoven, et al. Radiology 2005;237:181–8.
3. Kerwin, et al. Circulation 2003;107:851–6.
4. Kerwin, et al. Radiology 2006.

Saturday, February 3, 2007
Oral Abstracts: Clinical-Session XV

174. TROPONIN POSITIVE CHEST PAIN WITH UNOBSTRUCTED CORONARY ARTERIES: A ROLE FOR DELAYED ENHANCED CARDIOVASCULAR MAGNETIC RESONANCE IN THE DIAGNOSIS OF NON-ST ELEVATION MYOCARDIAL INFARCTION?

Nick G. Bellenger, MD, BSc, MRCP,[1] Charles Peebles,[2] Steve Harden,[2] Keith Dawkins,[2] Nick Curzen.[2] [1]*Royal Devon and Exeter NHS Foundation Trust, Exeter, United Kingdom,* [2]*Wessex Cardiothoracic Centre, Southampton, United Kingdom.*

Introduction: International guidelines recommend early coronary angiography and revascularisation for all patients diagnosed as having a non-ST elevation myocardial infarction (NSTEMI). This diagnosis is based on at least two out of the variables, typical ischaemic symptoms, ECG changes and elevated cardiac troponin. Many of these patients, however, are found to have normal or unobstructed coronary arteries at coronary angiography. Under such circumstances the presenting diagnosis may be unclear, but the patient often retains the label of NSTEMI. Such a diagnosis carries important implications for the patient in terms of prognosis, the need for secondary prevention, their psychological well-being, and subsequent occupational and health insurance assessment.

Purpose: This study examined the incidence and extent of DE-CMR defined myocardial necrosis in patients with clinical evidence of NSTEMI but angiographically normal coronary arteries.

Methods: Twenty-five consecutive patients diagnosed as having a NSTEMI (defined as a combination of: (i) typical cardiac-sounding chest pain, and (ii) a significant rise in troponin with no clear alternative cause with (iii) ST segment depression, non-specific T wave changes or an unremarkable ECG) who underwent in patient coronary angiography with a view to percutaneous intervention, and who were found to have normal coronary arteries underwent DE-CMR. Images were acquired 10 minutes after intravenous administration of gadolinium (0.1 mmol per kg) using a 1.5T Siemens Sonata.

Results: All patients had typical cardiac sounding chest pain, ST segment depression or non-specific T wave changes on ECG. The mean troponin I level was 7 ± 11 μg/L (range 0.18 to 28 μg/L). Only 16% had hyper-enhancement consistent with
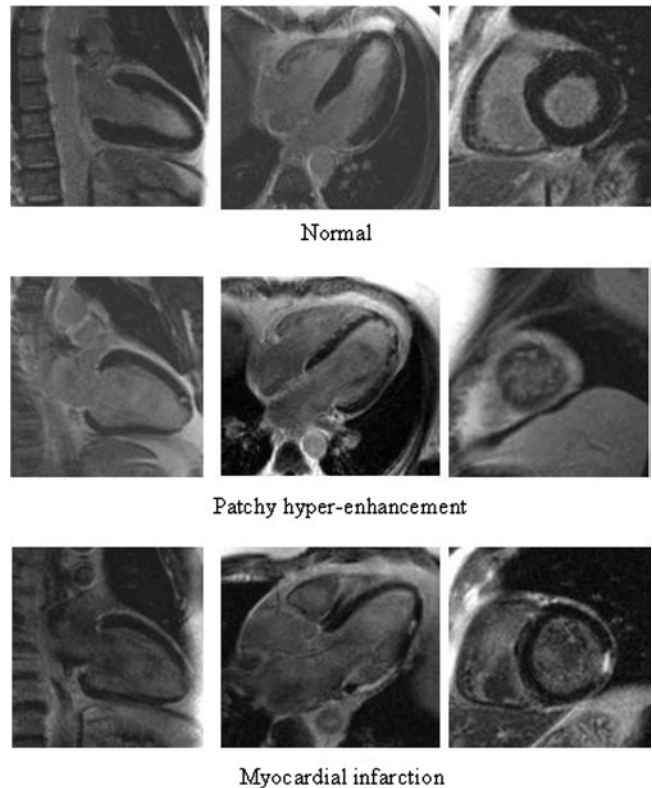
myocardial infarction (sub-endocardial hyper-enhancement in coronary artery distribution with a regional wall motion abnormality. The mean MI mass was 4.9 ± 2 g/cm2). 32% had patchy areas of hyperenhancement consistent with myocarditis and 52% had no areas of hyperenhancement.

Conclusions: This study confirms that the diagnostic conundrum provided by patients presenting with cardiac chest pain with Troponin elevation but unobstructed coronaries is relatively common and that DE-CMR has the potential to improve diagnostic accuracy in such patients. In only 16% of patients was there clear evidence of myocardial infarction. We assume that such a patient would continue to benefit prognostically from aggressive secondary prevention therapy and that they should declare the diagnosis of heart attack during insurance enquiries in the future. By contrast, 84% of these patients who would otherwise be diagnosed clinically as having NSTEMI had no evidence of myocardial necrosis. Given the published sensitivity of DE-CMR in detecting even small areas of myocardial damage, it may be reasonable to suggest that such patients can be told that they did not, after all, experience a heart attack on this presentation and that their secondary prevention therapy may be both inappropriate and potentially hazardous. In terms of insurance applications, this would clearly not be served well by the diagnostic label of NSTEMI. This study, therefore, illustrates the difficulty in defining a diagnosis of NSTEMI in some patients with troponin positive chest pain, and suggests that DE-CMR may well be useful in determining which patients have indeed suffered myocardial necrosis, thereby directing their further management appropriately. The findings demand further investigation of this potentially management-altering tool in larger cohorts of patients. For example, the long term follow up of a large cohort of patients with troponin positive NSTEMI but normal coronary arteries and normal DE-CMR may well reveal no greater risk of future cardiac events and strengthen the case for the routine use of CMR in the diagnosis of myocardial infarction.

175. CORRELATION OF DELAYED ENHANCEMENT AND NO REFLOW AREA MEASURED BY CARDIAC MRI AND N-TERMINAL-PRO-B-TYPE-NATRIURETIC-PEPTIDE IN PATIENTS WITH FIRST ACUTE ST SEGMENT ELEVATION MYOCARDIAL INFARCTION

Markus Jochims,[1] Mani Farazandeh,[1] Christoph J. Jensen,[1] Peter Hunold,[2] Georg V. Sabin,[1] Oliver Bruder,[1] Jörg Barkhausen.[2] **[1]** *Department of Cardiology and Angiology, Elisabeth-Hospital-Essen, Essen, Germany,* **[2]** *Department of Diagnostic and Interventional Radiology and Neuroradiology, University Hospital Essen, Essen, Germany.*

Introduction: Following acute myocardial infarction coronary artery disease (CAD) patients are at increased risk for cardiac failure, arrhythmias and sudden cardiac death. Several attempts

Normal

Patchy hyper-enhancement

Myocardial infarction

have been made to identify high-risk patients and to guide therapy. Among others N-terminal-pro-B-type-natriuretic-peptide (NTproBNP) emerged as a potential marker of LV dysfunction and prognosis after ST segment elevation myocardial infarction (STEMI). On the other hand contrast enhanced MRI allows measuring the infarct size and the no-reflow area, which also predict patient prognosis. However, the correlation between these parameters has not been investigated so far in a larger patient cohort.

Purpose: Our study aimed to evaluate the relationship between quantitative parameters obtained from contrast enhanced MRI and the plasma level of NTproBNP in patients with first STEMI who underwent rescue percutaneous coronary interventions.

Methods: Sixty-two consecutive patients with acute STEMI were included into this prospective study. Patients with previous myocardial infarction, known congestive heart failure (e.g., caused by cardiomyopathy or valvular heart disease) and contraindication to MRI were excluded, resulting in a study cohort of 37 patients (25 males and 12 females, median age 56 years [37/76]). All patients were successfully treated by percutaneous coronary intervention (PCI) resulting in TIMI flow grade 3. Plasma levels of NTproBNP were determined 24 to 72 hours after admission in all patients. MRI was performed using a standard 1.5 Tesla MR Scanner (Magnetom Sonata, Siemens Medical Solutions, Erlangen, Germany) within 5 ± 1.2 days after acute MI. Left ventricular ejection fraction (LVEF) was calculated from cine short axis views using SSFP sequences (TR 3 ms,

TE 1.5 ms, FA 60°). Delayed myocardial contrast enhancement imaging was performed in all patients following injection of 0.2 mmol/KG body weight gadodiamide (GE Healthcare Buchler, Munich, Germany) using a IR-FLASH sequence (TR 8 ms,TE 4 ms, FA 25°) at different time points after injection. All examinations were evaluated by an experienced cardiologist and an experienced radiologist in consensus. The extent of delayed enhancement (DE) and the extent of the no reflow area (NRA) were determined in percent of left ventricular myocardial mass.

Results: After acute STEMI NTproBNT plasma levels were elevated in all patients (median 1818 pg/mL [332/11580]). A positive correlation between NTproBNT plasma level and DE (r = 0.70, p = 0.01), NTproBNP plasma level and NRA (r = 0.65, p = 0.01) as well as LVEF and DE (r = 0.60, p = 0.01) were observed. However, the correlation between the LVEF and plasma levels of NTproBNP was only moderate (r = −0.44, p = 0.01).
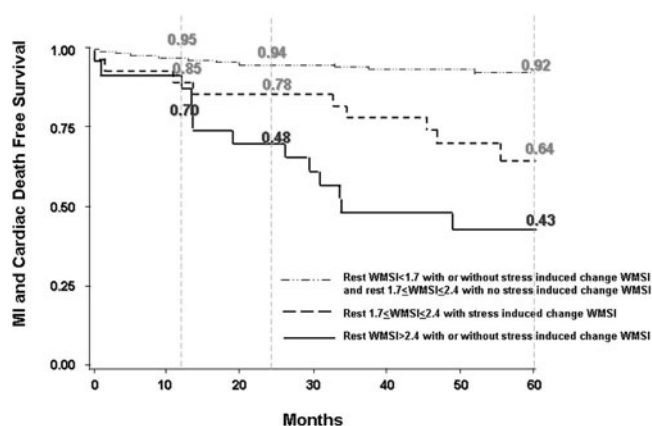
Conclusion: NTproBNP plasma levels correlate well with the extent of damaged myocardium defined by late enhancement imaging, whereas NTproBNP plasma levels and the LVEF showed a moderate correlation only. However, long term follow-up of these patients is mandatory to investigate which parameter at best predicts patients prognosis.

176. DOBUTAMINE CMR STRESS INDUCED CHANGE IN WALL MOTION SCORE INDEX PREDICTS MYOCARDIAL INFARCTION AND CARDIAC DEATH IN INDIVIDUALS WITH REDUCED LEFT VENTRICULAR EJECTION FRACTION

Erica Dall'Armellina, MD, Timothy M. Morgan, PhD, Hollins Clark, MD, Paige Clark, MD, J. Jeffrey Carr, MD, William Ntim, MD, Craig A. Hamilton, PhD, John Hoyle, MD, Kerry M. Link, MD, W. Gregory Hundley, MD. *Wake Forest University School of Medicine, Winston Salem, NC, USA.*

Introduction: Dobutamine cardiovascular magnetic resonance (DCMR) results predict a poor cardiac prognosis in patients with normal resting LVEF and prior studies have shown an elevated wall motion score index (WMSI) and a low left ventricular ejection fraction (LVEF) are poor prognostic factors in patients with coronary artery disease (CAD). We measured the predictive value of DCMR for myocardial infarction (MI) and cardiac death based on change in WMSI during dobutamine infusion in patients with reduced LVEF.

Methods: Between April 1997 and May 2005, 240 consecutive patients with a LVEF ≤55% that were poorly suited for stress echocardiography were recruited and underwent DCMR to diagnose inducible ischemia. Wall motion score index (WMSI) was obtained by physician review using cine white blood imaging techniques at rest, with low dose and after peak intravenous infusion of dobutamine/atropine. Follow up was obtained by

Kaplan-Meyer MI and cardiac death event-free survival curves in patients with stress induced change in WMSI for strata defined by the WMSI at rest. Risk of future cardiac events depending on resting WMSI combined with stress induced change in WMSI are reported at 2, 3 or 5 years.

personnel unaware of the study design or stress testing results an average of 5 ± 1 years after DCMR. The occurrence of MI and cardiac death were determined and verified thorough record review.

Results: Increase in WMSI after the infusion of dobutamine was associated with a reduced event-free survival (MI and cardiac death) (p < 0.03), independent of risk factors associated with coronary arteriosclerosis or myocardial infarction, and resting LVEF. The prognostic ability of DCMR for events was greatest for stress induced change in WMSI occurring when the resting WMSI was 1.7 ≤ WMSI ≤ 2.4 (p = 0.012).

Conclusions: In patients with a reduced LVEF, a stress induced increase in WMSI during dobutamine CMR identifies individuals with a high risk of sustaining myocardial infarction or cardiac death. The predictive value of the stress induced change in WMSI is highest when resting WMSI is ≤ to 2.4.

Kaplan-Meyer MI and cardiac death event-free survival curves in patients with stress induced change in WMSI for strata defined by the WMSI at rest. Risk of future cardiac events depending on resting WMSI combined with stress induced change in WMSI are reported at 2, 3 or years.

177. RELATIONSHIP BETWEEN MICROVASCULAR OBSTRUCTION ASSESSED WITH FIRST-PASS PERFUSION OR DELAYED CONTRAST-ENHANCED MRI AND LEFT VENTRICULAR REMODELING IN PATIENTS AFTER ACUTE MYOCARDIAL INFARCTION

Stijntje D. Roes, MD, Theodorus A. M. Kaandorp, MD, Hildo J. Lamb, MD, PhD, Jeroen J. Bax, MD, PhD, Ernst E. van der Wall, MD, PhD, Albert de Roos, MD, PhD. *Leiden University Medical Center, Leiden, The Netherlands.*

Introduction: Microvascular obstruction (MO) occurs after acute myocardial infarction (AMI) and is associated with poor clinical outcome and adverse left ventricular (LV) remodeling.

MO can be assessed with first-pass perfusion (FP) and de-layed contrast-enhanced (DE) magnetic resonance imaging (MRI).

Purpose: The purpose of this study was to investigate the value of MO assessed with either FP or DE imaging, in predicting LV remodeling at follow-up in patients after AMI.

Methods: We studied 28 patients at a mean of 5.9 ± 1.6 days after AMI with FP and DE imaging to assess MO and infarct size. Furthermore, LV volumes and function were assessed at initial presentation and 8.7 ± 5.5 months later.

Results: MO assessed with FP imaging was present in 18 of the 28 patients (64%). In 12 of these 18 patients (67%), MO was observed at DE images as well. End-diastolic volume increased in patients with MO determined at FP images, but not in those patients without MO ($5.0 \pm 4.7\%$ vs. $-1.5 \pm 3.7\%, p = 0.001$). No significant difference in change in end-diastolic volume was observed between patients with and without MO assessed at DE images ($4.3 \pm 5.4\%$ vs. $1.2 \pm 5.1\%$, $p = 0.139$). Univariate regression analysis showed that MO assessed with FP imaging ($R^2 = 0.354, p = 0.001$) and infarct size ($R^2 = 0.450$, $p < 0.001$) predict LV remodeling, but not when MO was assessed at DE images ($R^2 = 0.086$, $p = 0.139$). Multiple regression analysis showed that the combination of infarct size and MO assessed with FP imaging is the best predictor of LV remodeling ($R^2 = 0.528$, $p < 0.001$).

Conclusions: MO assessed with FP imaging is a stronger predictor of adverse LV remodeling in patients after AMI, than MO determined with DE imaging.

178. AUGMENTATION OF RIGHT VENTRICULAR FUNCTION BY DOBUTAMINE STRESS CARDIAC MAGNETIC RESONANCE PROVIDES INDEPENDENT CARDIAC PROGNOSTICATION BEYOND LEFT VENTRICULAR REGIONAL ISCHEMIA AND LEFT VENTRICULAR GLOBAL DYSFUNCTION

Maung M. Khin, MD,[1] Vijay Gandla, MD,[1] Frank Rybicki, MD, PhD,[1] Zelmira Curillova, MD,[1] Sui Tsang, BSc,[2] Raymond Y. Kwong, MD, MPH.[1] [1]*Brigham and Women's Hospital, Boston, MA, USA,* [2]*Yale University School of Medicine, New Haven, CT, USA.*

Introduction: The prognostic significance of global right ventricular (RV) systolic function in response to high-dose dobutamine stress has not been well characterized in patients with suspected or known coronary artery disease (CAD). Cardiac MRI (CMR) can assess and accurately quantify global RV function in this setting.

Purpose: We, therefore, tested the hypothesis that reduced augmentation of RV systolic function during dobutamine stress is associated with major adverse cardiac events (MACE) in patients with suspected or known CAD.
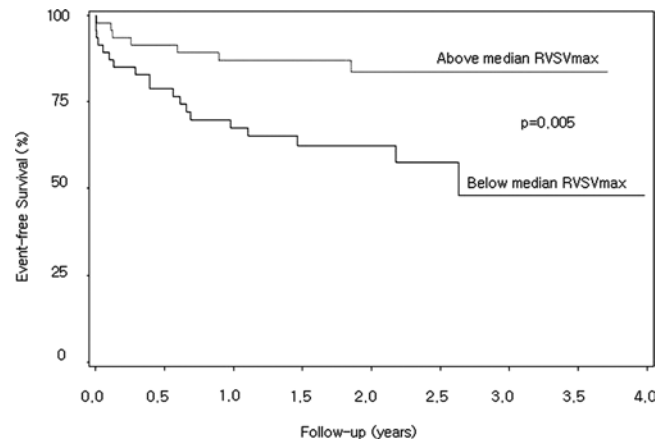

FIG. 1. Event-free survival of dobutamine CMR study cohort during follow-up period

Methods: We studied 95 patients (60 males, age 61 ± 12 years) who underwent dobutamine stress CMR. Assessment of global RV systolic function during dobutamine stress CMR was done using cine steady-state free precession imaging. Maximal increase in RV stroke volume ($RVSV_{max}$) during dobutamine infusion was derived from 3 short-axis locations of the RV acquired at rest and at peak dobutamine stress. We assessed the prognostic association of clinical information and $RVSV_{max}$ (above and below median value) with MACE by Cox proportional hazards regression.

Results: During a median follow-up of 1.6 years (6 months–4 years) after CMR, 27 patients experienced MACE (16 deaths and 11 non-fatal cardiac events). Patients with below median $RVSV_{max}$ in response to dobutamine stress (N = 48) experienced a more than 3-fold increase in hazard to MACE (hazard ratio [HR], 3.19; 95% confidence interval [CI], 1.34–7.63; $p = 0.008$). Kaplan Meier analysis illustrates reduced event-free survival in patients with reduced $RVSV_{max}$ (Fig. 1). There is a significant correlation between $RVSV_{max}$ and basal left ventricular ejection fraction (LVEF) (R = 0.35; $p \leq 0.001$). Reduced $RVSV_{max}$ on dobutamine stress has significant association with diabetes mellitus ($p \leq 0.0001$), history of CAD ($p = 0.01$), coronary artery bypass surgery ($p = 0.02$), right bundle branch block ($p = 0.01$), and LV wall motion abnormalities ($p = 0.01$). While deterioration of regional left ventricular function indicating induced LV myocardial ischemia during increasing myocardial oxygen demand was associated with worsened clinical outcome (HR, 2.52; 95% CI, 1.13–5.65; $p = 0.02$), reduced $RVSV_{max}$ maintained significant prognostic association with MACE adjusted to deterioration of regional LV function (adjusted HR, 1.25; 95% CI, 1.04–1.49; $p = 0.01$), and to basal LVEF (adjusted HR, 1.18; 95% CI, 0.99–1.41; $p = 0.06$).

Conclusion: Reduced $RVSV_{max}$ on dobutamine stress CMR portends an increased hazard in MACE, independent of deterioration in regional LV function or basal LVEF. Assessment of RV function during progressive dobutamine stress may provide

additional prognostic information to the current patient risk stratification.

179.   CHANGES IN LV TORSION FOLLOWING SURGICAL VENTRICULAR RECONSTRUCTION IN PATIENTS WITH ISCHEMIC HEART FAILURE

Randolph M. Setser, DSc,[1] **Nicholas G. Smedira, MD,**[1] **Richard D. White, MD.**[2] [1]*Cleveland Clinic, Cleveland, OH, USA,* [2]*University of Florida College of Medicine—Jacksonville, Jacksonville, FL, USA.*

Introduction: Patients with heart failure related to severe myocardial scarring, with or without left ventricular (LV) aneurysm formation, may benefit from surgical ventricular reconstruction (SVR) (1), in which the scarred or aneurysmal region is anatomically and functionally excluded from the LV. Rotation of the LV apex relative to the base (torsion) is related to myocardial contractility and structure, and is a sensitive indicator of cardiac function. Because SVR restores the LV to a more "normal" elliptical shape, it has been postulated that torsion will improve post-SVR (2). However, this hypothesis has not been tested.
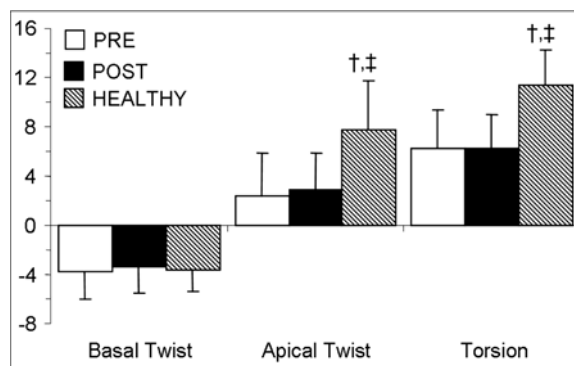
Purpose: We have computed LV torsion in patients before and 4–18 months after SVR to determine the effects of surgery on global and regional LV twist mechanics.

Methods: SPAMM tagged MR images (TE 4 ms, TR 90 ms, α 15°, FOV 300–360 mm, RFOV 75–100%) were acquired in 26 patients (62 ± 11 years, 19 M/7 F) (mean ± s.d.) referred for clinical assessment of myocardial viability by CMRI (Siemens Sonata), before and 233 ± 111 days after SVR[1]. SVR was accompanied by bypass grafting in 22 patients and/or mitral valve repair in 9. SPAMM tagged images were also acquired in 7 healthy volunteers (34 ± 7 years, 5 M/2 F). LV twist was computed using harmonic phase (HARP)[3] analysis software (Diagnosoft, CA) at basal and apical short-axis levels; torsion was defined as the difference between apical and basal twist. Analysis required manual delineation of the LV myocardium in end-systolic images at each level; LV twist was then computed automatically at all time points. Cardiac volumes (end diastolic volume, EDV; ejection fraction, EF) were computed using cine SSFP images also acquired in each patient/volunteer. The statistical significance of comparisons between time points was made by paired t-test, between patients and volunteers by two-sample t-test.

Results: Pre-SVR, LVs were dilated with impaired function (EDV 277 ± 86 mL, EF 29 ± 8%, p < 0.001 vs healthy); maximal basal twist was not significantly different from that of healthy volunteers (p = 0.84), but maximal apical twist and torsion were diminished (p < 0.001) (Fig.). Post-SVR, both LV size and EF improved (EDV 212 ± 55 mL, EF 37 ± 10%, p < 0.001 vs Pre-SVR), although both remained abnormal relative to healthy volunteers (p < 0.001). On average, maximal LV twist did not change significantly at either the base or apex post-SVR, nor did maximal LV torsion (Fig.). However, patients with relatively worse torsion before SVR showed more improved function afterwards: patients with torsion <6° before surgery had significantly worse EDV (203 mL vs 306 mL, p = 0.03), EF (25% vs 35%, p = 0.002), apical twist (0.9° vs 4.7°, p = 0.004) and torsion (4.2° vs 9.4°, p < 0.001) than patients with torsion ≥ 6°. Although all patients had improved EDV and EF post-SVR (p < 0.001 for each), only patients with pre-surgical torsion < 6° showed significant improvements in apical twist (0.4° vs 1.9°, p = 0.03) and torsion (3.5° vs 4.7°, p = 0.004). Furthermore, these patients showed significantly greater improvement in EF (15% vs 6%, p = 0.005) and torsion (1.2° vs -0.8°, p = 0.01) post-SVR than patients with torsion ≥6°.

Conclusions: Indices of LV function based on volume measurements (e.g. EF, CO) can be misleading following surgery which grossly modifies LV shape. It has been postulated that LV torsion should improve following SVR due to "restoration of the normal elliptical architecture" of the LV (2). Our results indicate that although torsion is unchanged following surgery on average, patients with relatively worse torsion pre-SVR do show improvement, while those with relatively better torsion before surgery actually worsen, on average, following SVR. Thus, using pre-surgical torsion as a metric, these results indicate that it might be possible to predict which patients will show functional improvement following SVR.

† p<0.05 vs Pre-SVR, ‡ p<0.05 vs Post-SVR

REFERENCES

1. Dor V, et al. Sem Thorac Cardiovasc Surg 1997;2:123.
2. Buckberg GD, et al. Sem Thorac Cardiovasc Surg 2001;13:386–401.
3. Osman NF, et al. MRM 1999;42:1048.

180.   LEFT VENTRICULAR REMODELING AFTER INTRACORONARY BONE MARROW CELL THERAPY FOR ACUTE MYOCARDIAL INFARCTION. EIGHTEEN MONTHS' MRI FOLLOW-UP DATA FROM THE RANDOMIZED, CONTROLLED BOOST-TRIAL

Gerd P. Meyer, MD, Kai C. Wollert, Joachim Lotz, Jan Steffens, Peter Lippolt, Stephanie Fichtner, Hartmut Hecker,

Lubomir Arseniev, Bernd Hertenstein, Arnold Ganser, Helmut Drexler. *Medical School, Hannover, Germany.*

Introduction: Intracoronary transfer of autologous bone marrow cells (BMCs) may enhance recovery of left ventricular (LV) function and limit the remodeling process in patients after acute myocardial infarction (AMI). However, clinical studies addressing the effects of BMCs after AMI have covered only limited time frames ranging from 3 to 6 months.

Purpose: To answer the critical question of whether BMC transfer can have a sustained impact on LV function, volumes, mass and infarct size.

Methods: After percutaneous coronary intervention with stent implantation (PCI) of the infarct-related artery, 60 patients were randomized 1:1 to a control group with optimal postinfarction therapy and a BMC transfer group that also received an intracoronary BMC infusion 4.8 ± 1.3 days after PCI (***BO**ne marr**O**w transfer to enhance **ST**-elevation infarct regeneration, BOOST-trial*). Cardiac MRI was performed 3.5 ± 1.5 days, 6 ± 1 months, 18 ± 6 months after PCI and analysed in a blinded fashion by observers not involved in the clinical care of the patients.

Results: In the control group, mean global LV ejection fraction (LVEF) increased by 0.7 and 3.1 percentage points after 6 and 18 months, respectively. LVEF in the BMC transfer group increased by 6.7 and 5.9 percentage points. The difference in LVEF improvement between groups was significant after 6 months but not after 18 months ($p = 0.27$). The speed of LVEF recovery over the course of 18 months was higher in the BMC transfer group ($p = 0.001$). LV mass and infarct size decreased in both groups until the 6 month follow up, but not thereafter ($p = $ N.S. between group*s*). Left ventricular enddiastolic volumes tended to increase in both groups, left ventricular endystolic volumes did not change ($p = $ N.S. between groups).

Conclusions: In this first randomized-controlled study, a single dose of intracoronary BMCs did not provide long-term benefit on LV systolic function after AMI; however, the study suggests an acceleration of LV ejection fraction recovery after AMI by BMC therapy. There was no effect of BMC therapy on left ventricular volumes, mass and infarct sizes, suggesting a limited or no influence of BMC therapy on the postinfarct remodeling process. These MRI-data from the BOOST trial underline the strong need for optimizing the technique of intracoronary BMC therapy after AMI.

Abstract Session XVII

Sunday, February 4, 2007
Oral Abstracts: Clinical/Basic-Session XVII

181.   RIGHT HEART MRI, AS A NEW MODALITY FOR ASSESSMENT OF COR PULMONALE: EFFECTS OF

BOSENTAN ON SERIOUS PULMONARY HYPERTENSIVE PATIENTS

Atsushi Yamauchi,[1] Naka Sakamoto,[1] Syunsuke Natori,[2] Yuichiro Kawamura,[1] Naoyuki Hasebe,[1] Yoshinobu Osaki,[1] Kenjiro Kikuchi.[1] [1]*Asahikawa Medical College, Asahikawa City, Japan,* [2]*Furano kyokai Hospital, Furano City, Japan.*

Introduction: Recent progress of magnetic resonance imaging (MRI) enabled to assess the structural and functional abnormality of heart, even of right heart system of pulmonary hypertention (PH).

Purpose: To elucidate the effects of bosentan on exercise capacity, right cardiac function and morphometry of patients with marked PH and right ventricular (RV) hypertrophy using cardiac MRI.

Methods: Six patients with severe PH (WHO functional class III, age 47.5 ± 13 yrs), were treated with bosentan (125–250 mg/day) for four weeks. The 6-minute walking distance (6MD), tricuspid pressure gradient (TPG) on echocardiography, and cardiac MRI findings of right ventricular (RV) end-diastolic volume (RVEDV), RV ejection fraction (RVEF) and RV myocardial mass (RVM) were compared before and after bosentan therapy.

Results: Exercise capacity in 6MD was significantly improved by bosentan, 242.5 ± 49.7 to 320 ± 51.1 m ($p < 0.05$). The degree of PH in TPG was significantly reduced by bosentan, 97.5 ± 15.4 to 77.8 ± 12.9 mmHg ($p < 0.05$). RVEF of MRI showed a modest improvement (14.5 ± 6.4 to 18.72 ± 7.2%). RV hypertrophy assessed by MRI showed a significant reduction in RVM (74.2 ± 10.4 to 68.5 ± 13.9 g ($p < 0.05$)) by bosentan.

Conclusions: Bosentan effectively improved cardiac function and exercise capacity, and unexpectedly reduced RV hypertrophy in patients with severe PH. Right heart MRI is a promising strategy for functional as well as a morphometrical assessment of cor pulmonale.

182.   IS THE B-TYPE NATRIURETIC PEPTIDE CORRELATED WITH THE MYOCARDIAL PCR/ATP RATIO DETERMINED BY RAPID ^{31}P-MRS IN DCM PATIENTS?*

Koichi Chida, PhD,[1] Hiroki Otani, MD,[2] Masahiro Kohzuki, MD,[3] Haruo Saito, MD,[4] Yutaka Kagaya, MD,[2] Yoshihiro Takai, MD,[1] Shoki Takahashi, MD,[4] Shogo Yamada, MD,[4] Masayuki Zuguchi, MD.[1] [1]*Department of Radiological Technology, Tohoku University School of Health Sciences, Sendai, Japan,* [2]*Department of Cardiovascular Medicine, Tohoku University School of Medicine, Sendai, Japan,* [3]*Department of Internal Medicine and Rehabilitation Science, Tohoku University School of Medicine,*

Sendai, Japan, [4]*Department of Radiology, Tohoku University School of Medicine, Sendai, Japan.*

Introduction: Dilated cardiomyopathy (DCM) is characterized by progressive dilatation of the heart with loss of contractile function. Its etiology is unclear in many cases. B-type natriuretic peptide (BNP) is released from the cardiac ventricles in response to volume expansion and pressure overload. The plasma BNP levels are elevated in patients with left ventricular dysfunction. Furthermore, the plasma BNP level is the single most accurate predictor of the presence or absence of congestive heart failure. Phosphorus-31 magnetic resonance spectroscopy (^{31}P-MRS) of the heart is unique in its ability to noninvasively quantify myocardial levels of high-energy phosphate compounds such as adenosine triphosphate (ATP) and phosphocreatine (PCr), which fuel contractile function and are critical to viability. Hence, the myocardial PCr/ATP ratio determined using ^{31}P-MRS has been used to evaluate patients with cardiac disease. Nevertheless, the relationship between the BNP and the myocardial PCr/ATP ratio is not clear.

Purpose: This study describes the correlation between the plasma BNP level and the myocardial PCr/ATP ratio determined using rapid ^{31}P-MRS in patients with DCM.

Methods: In patients with DCM, who had slight or moderate heart failure, in the Department of Cardiovascular Medicine of Tohoku University Hospital were selected at random. The DCM diagnoses were made from the clinical histories, ECG, and plasma creatine kinase (CK) levels, and all patients underwent echocardiography and either cardiac catheterization (including angiocardiography) or radionuclide scanning. Coronary artery disease was ruled out in all patients. DCM patients who had a pacemaker, severe arrhythmia, implants, vascular clips, unstable angina pectoris, or claustrophobia were excluded. The plasma BNP levels were measured using a commercial specific immunoradiometric assay kit for human BNP. The plasma BNP was measured on a day close to the rapid ^{31}P-MRS study.

^{31}P-MRS measurements were conducted with a 1.5-T MR instrument. Using a 2D-CSI in combination with 30 mm axial slice-selective excitation, complete three-dimensional localization was performed. The rapid-sequence ^{31}P-MRS procedure was phase encoded in arrays of 8 × 8 steps with an average of four acquisitions. K-space zero-filling (similar to matrix interpolation) was used.

A set of ECG-triggered proton images was obtained in the transverse, coronal, and sagittal orientations using a modified gradient-echo technique. TR was set to one R-R interval for the phosphorus 2D-CSI measurements. The acquisition time was 3–5 minutes, and the total examination time, including proton imaging and shimming, for the rapid ^{31}P-MRS procedure was 10–15 minutes, depending on the heart rate. The volume element for each 2D-CSI sequence was positioned on the interventricular septum of the anterior wall of the left ventricle. The correlations (BNP vs. PCr/ATP, log of BNP vs. PCr/ATP) were analyzed using a linear regression. The p value was obtained from an analysis of variance.

Results: The mean plasma BNP level and mean PCr/ATP determined by rapid ^{31}P-MRS of DCM patients were 192 ± 240 pg/mL and 1.8 ± 0.3, respectively. The plasma BNP levels tended to be correlated negatively with the myocardial PCr/ATP, although the correlation did not reach statistical significance. By contrast, the log of the plasma BNP levels was correlated negatively with the myocardial PCr/ATP.

Conclusions: Our results indicate that the myocardial energy metabolism evaluated using ^{31}P-MRS tends to be correlated with the severity of heart failure and left ventricular dysfunction estimated using the plasma BNP levels in DCM patients. This presentation provides additional information regarding the relationship between the BNP and myocardial energy metabolism in DCM patients.

This abstract will be displayed during Saturday Poster Session.

183. METABOLIC AND FUNCTIONAL IMAGING OF THE HUMAN HEART: EFFECTS OF A VERY LOW CALORIE DIET

**Rutger vd Meer,[1] Sebastiaan Hammer,[1] Jan W. A. Smit,[1] Sebastian Kozerke,[2] Michael Schaer,[3] Michaela Diamant,[4] Luuk J. Rijzewijk,[4] Albert De Roos,[1] Johannes A. Romijn,[1] Hildo J. Lamb.[1] [1]*Leiden University Medical Center, Leiden, The Netherlands, [2]Institute for Biomedical Engineering, University of Zurich and Swiss Federal Institute of Technology, Zurich, Switzerland, [3]Johns Hopkins University School of Medicine, Baltimore, MD, USA, [4]VU University Medical Center, Amsterdam, The Netherlands.*

Introduction: During fasting, adipose tissue releases fatty acids which can be used by non-adipose tissues as alternative fuel supply. An increase of myocardial triglyceride (TG) content after fasting has recently been shown in the human heart. However, lipid accumulation can be a pathological event also, especially in diabetes and obesity and can lead to lipo-apoptosis or diastolic dysfunction. However, it is unknown whether myocardial TG
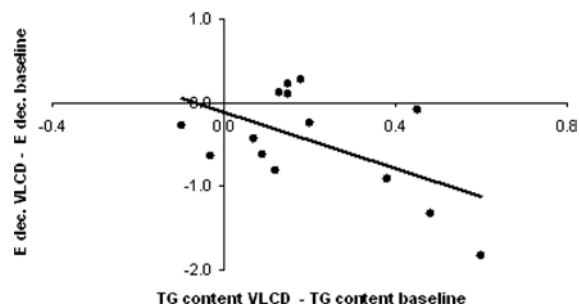

FIG. 1. Correlation between the decrease in E deceleration and the increase in myocardial triglyceride caused by a very low calorie, low fat diet. Pearson r = −0.55, p < 0.05. VCD = Very Low Calorie Diet, dec = deceleration.

TABLE
Effects of a Very Low Calorie Diet on myocardial triglyceride content and function

	Baseline	Very Low Calorie Diet
Myocardial Triglyceride (%)	0.38 (0.19)	0.59 (0.24)*
LVEF (%)	60 (5)	60 (5)
E/A	2.14 (0.39)	2.03 (0.40)
E deceleration (mL/s$^2 \times 10^{-3}$)	3.37 (0.74)	2.91 (0.58)*

Values are mean (SD).
*p < 0.05 (paired T-test).

accumulation following fasting results in a change of myocardial function.

Purpose: To determine the effect of dietary fat content on myocardial TG accumulation and myocardial function in healthy subjects, using MRI and ^{1}H-MR spectroscopy (MRS).

Materials and Methods: ^{1}H-MRS of the interventricular septum was performed at 1.5T (Gyroscan ACS/NT15; Philips, Best, the Netherlands) in 14 healthy non-obese men (Mean [SD] age: 22.5 [3.1], BMI 23.1 [1.7]) to determine TG content at baseline and after a 3-day period of a very low-caloric, low-fat diet. Furthermore, the entire heart was imaged in short-axis orientation to assess left ventricular ejection fraction (EF). An ECG-gated gradient-echo sequence with velocity encoding was performed to measure bloodflow across the mitral valve for the determination of left ventricular diastolic function. Flow velocities in early diastole (E) and at atrial contraction (A) were measured. Their peak flow ratios (E/A) and mean E deceleration were calculated.

Between group differences were calculated using a two-tailed dependent sample T-test. P < 0.05 was considered statistically significant.

Results: During the low fat diet, mean (SD) myocardial TG content (expressed as a percentage relative to myocardial water content) increased significantly when compared to baseline (0.59% [0.24%] vs. 0.38% [0.19%], p < 0.05) (Table 1). Myocardial systolic function (EF) did not change (Table 1). E deceleration decreased significantly after the very low calorie diet (Table 1). The increase in myocardial TG correlated significantly with a decrease in E deceleration (Fig. 1).

Conclusion: Myocardial triglyceride content increases after a short-term very low calorie diet in healthy subjects, while diastolic function decreases. In addition, the change in myocardial triglyceride content correlates with the change in left ventricular diastolic function after a very low calorie diet. Therefore, dietary fat content influences myocardial triglyceride content and heart function.

184. DOSE DEPENDENT EFFECTS OF CALORIC RESTRICTION ON MYOCARDIAL TG ACCUMULATION, ASSESSED WITH ^{1}H-MRS

Sebastiaan Hammer,[1] Rutger W. van der Meer, MD,[1] Jan W. A. Smit, MD,[1] Sebastian Kozerke, PhD,[2] M. Schaer, PhD,[2] Michaela Diamant, MD,[3] Luuk J. Rijzewijk, MD,[3] Albert de Roos, MD,[1] Johannes A. Romijn, MD,[1] Hildo J. Lamb, MD.[1] [1]*Leiden University Medical Center, Leiden, The Netherlands,* [2]*Institute for Biomedical Engineering, Zurich, Switzerland,* [3]*Free University Medical Center, Amsterdam, The Netherlands.*

Background: Myocardial accumulation of triglycerides (TG) is involved in the pathogenesis of insulin resistance and in type 2 diabetes mellitus (DM) in animal models. Short-term dietary interventions have proven to influence myocardial TG content in healthy subjects, which may be explained by changing fluxes of plasma Free Fatty Acids (FFA).

Purpose: To determine in humans whether diet induced changes in FFA levels induce a dose dependent response on myocardial TG accumulation.

Materials and Methods: We measured myocardial TG content in 5 healthy men (mean age ± SD: 23.2 ± 2.2 yrs, BMI 23.9 ± 2.6 kg/m^2) before and after 3 days of a very low calorie diet (VLCD, 473 kcal/day) and after 3 days of complete starvation (0 kcal/day). ^{1}H-MRS of the myocardium was performed at 1.5T (Gyroscan ACS/NT15, Philips) on all occasions. Breathing artefacts were minimized by using respiratory motion compensation. To detect lipid signals, single-voxel spectra (2 × 4 × 1 cm) were recorded by using a point resolved spectroscopy sequence after water suppression. Also spectra without water suppression were recorded to quantify the myocardial TG ratio: TG/water × 100. Differences were calculated using a Wilcoxon matched pair test.

Results: Mean (SD) myocardial TG ratio at baseline was 0.44 (0.16) % and increased to 0.67 (0.34) % after the VLCD (p = 0.08), and to 1.29 (0.65) % after complete starvation (p = 0.043) (Fig. 1).

Mean (SD) plasma FFA at baseline was 0.61 (0.36) mmol/L and increased to 1.32 (0.41) mmol/L after the VLCD (p = 0.043) and to 2.31 (0.87) mmol/L after complete starvation (p = 0.043) (Fig. 2).

Conclusions: Increased caloric restriction leads to increased myocardial TG accumulation in healthy subjects. Changes in myocardial TG content are paralleled by changes in plasma FFA. ^{1}H-MRS of TG content may help understanding the pathophysiological significance of elevated plasma FFA levels and myocardial TG accumulation in type 2 DM.

185. MYOCARDIAL IRON OVERLOAD AND MYOCARDIAL FIBROSIS IN THALASSEMIA INTERMEDIA PATIENTS: A COMPARATIVE MULTICENTER STUDY VERSUS THALASSEMIA MAJOR PATIENTS

Alessia Pepe, MD,[1] Anna Ramazzotti, PhD,[1] Barbara Scattini, MS,[1] Vincenzo Positano, MS,[1] Maria Eliana Lai, MD,[2] Luciano Prossomariti, MD,[3] Marcello Capra,

MD,[4] **Lorella Pitrolo, MD,[5] Gianluca Forni, MD,[6] Caterina Borgna-Pignatti, MD,[7] Paolo Cianciulli, MD,[8] Massimo Midiri, MD,[9] Aurelio Maggio, MD,[10] Massimo Lombardi, MD.[1]** [1]*MRI Laboratory, Institute of Clinical Physiology-CNR of Pisa, Pisa, Italy,* [2]*Microcitemico Hospital, Cagliari, Italy,* [3]*Centro per la Cura delle Microcitemie, Cardarelli Hospital, Napoli, Italy,* [4]*Pediatria per le Emopatie Ereditarie, G. Di Cristina Hospital ARNAS, Palermo, Italy,* [5]*Pediatria II per le Emopatie Ereditarie, Villa Sofia-CTO Hospital, Palermo, Italy,* [6]*Centro microcitemia ed anemie congenite, Galliera Hospital, Genova, Italy,* [7]*Department of Pediatrics, University of Ferrara, Ferrara, Italy,* [8]*Centro Talassemie, "Sant'Eugenio" Hospital, Roma, Italy,* [9]*Department of Radiology, University of Palermo, Palermo, Italy,* [10]*Ematologia II con Talassemia, "V. Cervello" Hospital, Palermo, Italy.*

Introduction: It is reasonable to expect a cardiac involvement in thlassemia intermedia (TI) patients due to chronic anemia, resulting in a high cardiac output state and iron overload, mainly related to the increased gastro-intestinal iron absorption. Little is known about cardiac involvement in TI using cardiovascular magnetic resonance (CMR), which is the unique tecnique for the non invasive evaluation of miocardial iron overload and fibrosis.

Purpose: Aim of our study was to investigate in TI myocardial iron overload and fibrosis correlating with morfological and functional cardiac parameters using CMR and to compare the data with that of thalassemia major (TM) patients, matched for age and sex.

Methods: The study population was sent to our MRI laboratory from 8 different thalassemia centers. In 60 TI and 60 TM patients, myocardial iron overload (MIO) was assessed using a multislice multiecho T2* approach. Liver iron overload was evaluated by T2* multiecho sequences. Cine sequences were obtained to measure quantitatively atrial areas and biventricular function parameters. Myocardial fibrosis was evaluated by late gadolinium enhanced acquisitions.

Results: MIO was present in the 23% of TI patients, more frequently (92%) with an heterogeneous distribution. Abnormal liver T2* values were detected in the 72% of the TI cases. TI patients with myocardial fibrosis (32%) showed significantly reduced or borderline left ventricular ejection fraction (LVEF) (p = 0.01). There was no correlation between the global heart T2* values and the biventricular EF, the myocardial fibrosis or the liver T2*. LV and right ventricular (RV) dilatations with increased stroke volumes were present in the 32% and in the 13% of TI patients, respectively. TI patients showed normal or increased LVEF and RVEF in the 71% and in the 98% of the cases, respectively. The 60% of TI patients showed bi-atrial enlargement. Mean Hb-levels were significantly lower in the TI patients (p < 0.0001). MIO was significantly lower in TI than in TM patients (p < 0.0001). The proportion of TI patients with homogeneous MIO was tendentially lower than TM patients (TI group 9% versus TM group 40%; p = 0.11). TI patients showed

heterogeneous MIO with normal T2* global value more frequently (p = 0.01). Conversely, TM patients showed heterogeneous MIO with abnormal T2* global value more frequently (p = 0.0001). Liver T2* values were comparable in the 2 groups (p = 0.17). End-diastolic volume indexes, stroke volumes, EF and bi-atrial areas were significantly higher in TI. The presence of myocardial fibrosis was not significantly difference in TI and in the TM patients (p = 0.9).

Conclusions: CMR confirms its role as fitted guide to cardiac managements also in TI. TI patients showed lower myocardial iron burden and more pronounced high cardiac output findings. The high cardiac output state seems to increase the relative risk of further dilatation, myocardial fibrosis, and decreased systolic function. On this basis, could be reconsider protocol for blood transfusions and chelation therapy in this disease.

186. ECG CHANGES IN THALASSEMIA MAJOR PATIENTS: CORRELATIONS WITH MYOCARDIAL IRON OVERLOAD AND MYOCARDIAL FIBROSIS

Alessia Pepe,[1] Barbara Scattini,[1] Anna Ramazzotti,[1] Marcello Pili,[2] Giorgio Derchi,[3] Francesco Formisano,[3] Vincenzo Positano,[1] Maria Eliana Lai,[4] Gianluca Forni,[5] Massimo Lombardi.[1] [1]*MRI Laboratory, Institute of Clinical Physiology-CNR, Pisa, Italy,* [2]*Servizio di Cardiologia, Microcitemico Hospital, Cagliari, Italy,* [3]*Dipartimento di Cardiologia, Galliera Hospital, Genova, Italy,* [4]*Centro Talassemici Adulti, Microcitemico Hospital, Cagliari, Italy,* [5]*Centro microcitemia ed anemie congenite, Galliera Hospital, Genova, Italy.*

Introduction: Nonspecific twelve lead Electrocardiogram (ECG) changes have been frequently reported in thalassemia major (TM). However, relationships between ECG changes and pathologic subst rates of cardiac involvement in TM, such as myocardial iron overload (MIO) and myocardial fibrosis were not investigated. To date, Cardiovascular Magnetic Resonance (CMR) is the only noninvasive technique for the evaluation of MIO and myocardial fibrosis, although its availability is often problematic in the countries where TM is prevalent.

Purpose: Aim of our study was to correlate Cardiovascular Magnetic Resonance (CMR) changes with MIO and with myocardial fibrosis, evaluated by CMR, in TM patients.

Methods: We studied 104 TM patients (32 male; 27 ± 8 years) consecutively sent to our Laboratory, using a 1.5 T scanner (GE, USA). MIO was assessed using a multislice multiecho T2* approach. Three short-axis views of the left ventricle were obtained and analyzed with a custom-written software: the global T2* value of the myocardium was calculated, as well as each T2* values of the standardized 16-segments of the heart model. Myocardial fibrosis was evaluated by late gadolinium enhanced acquisitions after the intravenously administration of Gadobutrol (1.0 mol/L) (0.2 mmol/Kg). ECG was performed

within one month from CMR, in absence of clinical cardiovascular events. ECG was read blindly by 2 cardiologists who were unaware of the results of the CMR.

Results: We found 21% of TM patients had normal T2* values for all 16 segments (>20 ms). Of the patients with abnormal segmental T2* values, 29 % showed an homogeneous MIO (all segments with T2* values <20 ms). Twenty-one percent of TM patients showed myocardial fibrosis. We found ECG changes in the 45% of cases. The most common findings in TM patients were T wave inversion (27%), right bundle-branch block (12%) and flat T wave (7%). The inter-rate (K) agreement between the 2 cardiologists was 0.8. A significant correlation was found between the abnormal T2* global value and changes in ECG (chi-square 3.9; p = 0.04). Patients with abnormal ECG showed significantly lower T2* global values and segments with normal T2* values *versus* the patients with normal ECG (19 $\pm$ 11 ms *versus* 27 $\pm$ 13 ms, $p = 0.001$; 6 $\pm$ 6 segments *versus* 10 $\pm$ 6 segments, p = 0.003). Sensitivity, specificity, negative predictive value (NPV) and positive predictive value (PPV) of ECG in detecting an abnormal T2* global values were 54%, 67%, 51% and 70%, respectively. A significant correlation was found between the presence of myocardial fibrosis and changes in ECG (chi-square 3.6; $p = 0.05$). Sensitivity, specificity, NPV and PPV of ECG in detecting myocardial fibrosis were 66%, 60%, 87% and 31%, respectively. Sensitivity, specificity, NPV and PPV of ECG in detecting MIO and/or myocardial fibrosis were 61%, 72%, 42% and 81%, respectively (chi-square 5.2; p = 0.002).

Conclusions: ECG changes found in TM patients showed significant correlation with MIO, myocardial fibrosis and CMR pathological findings (MIO and/or myocardial fibrosis). ECG could be a suitable guide for performing a CMR exam in TM, due to its high PPV and low cost, in particular in countries where CMR is uneasily available.

187.   COMPARISON OF STRESS MR IMAGING WITH STRESS NUCLEAR PERFUSION FOR THE ASSESSMENT OF CORONARY ARTERY DISEASE

John Heitner. *DCMRC, Durham, NC, USA.*

Background: Single positron emission scintigraphy (SPECT) imaging is the most utilized outpatient procedure in the United States. The diagnostic accuracy of SPECT can be limited by soft tissue attenuation and low resolution. Cardiac magnetic resonance imaging (CMR) can also assess myocardial perfusion with a much higher spatial resolution without the susceptibility to soft tissue attenuation.

Objectives: To compare stress CMR to stress SPECT in the assessment of coronary artery disease (CAD) in patients who present with chest pain.

Methods: We prospectively enrolled 65 patients with chest pain who were at intermediate risk for CAD. Exclusion criteria included; pregnancy, age <35, prior CAD, caffeine within 16 hours, pacemaker or defibrillator, aneurysm clips, morbid obesity and claustrophobia. Patients who met entry criteria for the study had a comprehensive evaluation including: physical exam, serum lipid profile, C-reactive protein (CRP), ECG, and a chemistry profile. All patients underwent both a stress CMR and stress SPECT. CMR included cine, adenosine- stress and rest perfusion, and delayed enhancement. If either of the two stress tests were positive patients were referred for coronary angiography. Patients were followed for myocardial infarction (MI), revascularization, or cardiac death.

Results: There were two patients excluded from the study due to technical issues in retrieving the SPECT images from archive. Of the remaining 63 patients, 37 patients were referred for cardiac angiography. There were 13 patients who had significant CAD ($\geq$70%). The mean follow up was 30 months. Two patients had a myocardial infarction/cardiac death and one patient had non-cardiac death (metastatic prostate cancer) on follow-up. The sensitivity, specificity, positive predictive value (PPV) and negative predictive value (NPV) of CMR are 71%, 83%, 56%, and 91%, respectively. The sensitivity, specificity, PPV, and NPV of stress SPECT are 64%, 87%, 60%, and 89%, respectively.

Conclusion: In patients being evaluated for the presence of CAD, stress CMR has similar diagnostic accuracy as stress SPECT.